University of Zurich[UZH]

Surges and Glacial Lakes of the Nevado del Plomo Glacier (Argentina): Historical Events, Present Situation and Potential Future Developments

GEO 511 Master's Thesis

Author
Valerie Widmer
16-708-372

Supervised by
Dr. Samuel Nussbaumer
Dr. Holger Frey

Faculty representative
Prof. Dr. Andreas Vieli

30.09.2022
Department of Geography, University of Zurich

University of Zurich[UZH]

Surges and Glacial Lakes of the Nevado del Plomo Glacier (Argentina)

Historical Events, Present Situation and Potential Future Developments

GEO 511 Master's Thesis

Valerie Widmer
valerie.widmer2@uzh.ch

Supervised by
Dr. Samuel Nussbaumer
Dr. Holger Frey

Faculty Representative
Prof. Dr. Andreas Vieli

Department of Geography

September 30, 2022

Abstract

Surging glaciers are characterized by an abrupt advance of the glacier front in a relatively short time. This fast advance can cause a variety of problems, such as the damming of a river. The Nevado del Plomo glacier is a surging glacier (at 33° S, 70° W) in the Central Andes of Argentina. During the surge in 1933, the advancing ice masses of the glacier dammed the Río del Plomo and a lake was formed. This lake drained later in January 1934 in a disastrous GLOF event. At least two other surge events occurred in 1984-1985 and 2006-2007, which both dammed the Río del Plomo but the lakes drained gradually. In this thesis, the historical surge events of the Nevado del Plomo glacier of 1933, 1984 and 2006 are analyzed.

In comparison to existing studies about the Nevado del Plomo glacier, the glaciological conditions of the glacier before the 1933 surge could be additionally investigated, based on a historical map of 1912 created by Robert Helbling. To survey the ice transfer during the last surge event of 2006-2007, several ASTER DEMs were subtracted from each other to visualize and quantify the elevation changes. The results of the DEM differencing revealed an accumulation of ice from 2000 to 2006, and the mass transfer from the accumulation area to the glacier tongue during the surge, which was approximately 54 x 10^6 m^3. With the GlabTop model, the ice thickness distribution of the Nevado del Plomo glacier of several years, as well as potential future glacial lakes were modelled. The ice volume of the glacier decreased by 66.2% since 1912, from 0.269 km^3 to 0.091 km^3 in 2020. Shortly before the last surge in 2006, the ice volume was 0.152 km^3. A 2-D numerical glacier flow model was applied to reconstruct the surge of 2006-2007 and to model a potential future surge with the 2020 glacier extent and volume. According to the modelling, the Nevado del Plomo glacier would not reach and dam the Río del Plomo during a potential surge under current conditions, since the advance would be too short. A surge could only be initiated in the model by changing the ice rheology and not due to a climate cooling, which was simulated by decreasing the ELA.

Besides the study of the Nevado del Plomo glacier, a total ice volume decline of 15.9% of the glaciers in the Plomo catchment area between the years 2010 and 2020 was calculated. Some small glacial lakes can be expected in consideration of continued future glacier retreat, but the volume of the lakes is negligible in comparison with the temporary lakes formed in the past due to the damming of the Río del Plomo. According to the results, it is very unlikely that a future surge will dam a lake again, as the volume of the glacier is too small. However, future glacial lakes and the potential of landslides damming the Río del Plomo must be considered.

Resumen

Los glaciares galopantes se caracterizan por un avance abrupto del frente glaciar en un tiempo relativamente corto. Este rápido avance puede causar diversos problemas, como el embalsamiento de un río. El glaciar Nevado del Plomo es un glaciar galopante situado en los Andes Centrales de Argentina (33° S, 70° W). Durante el surge de 1933 el avance de las masas de hielo del glaciar embalsó el Río del Plomo y se formó un lago. Este lago se descargó más tarde, en enero de 1934, en un evento GLOF desastroso.

En esta tesis se analizan los eventos históricos del surge del glaciar del Nevado del Plomo ocurridos en 1933, 1984 y 2006. Las condiciones glaciológicas del glaciar antes del surge de 1933 podrían ser investigadas en base a un mapa histórico excepcional de 1912 creado por Robert Helbling y colegas. Para estudiar la transferencia de hielo durante el último evento de surge de 2006-2007, se sustrajeron varios modelos digitales de terreno (de la misión ASTER) entre sí para visualizar y cuantificar los cambios de elevación. Finalmente, para estimar cuánto avanzaría actualmente el glaciar durante un surge potencial, se modela un posible surge con la extensión del glaciar en 2020.

Los resultados mostraron la acumulación de hielo entre 2000 y 2006, y la transferencia de masa durante el surge, que fue de aproximadamente 54 x 10^6 m^3. Con el modelo GlabTop, un método rápido y robusto para modelar la distribución del espesor y la topografía de la base de glaciares utilizando un Sistema de Información Geográfica, se modeló la distribución del espesor del hielo del glaciar Nevado del Plomo y los posibles lagos glaciares futuros. El volumen de hielo del glaciar disminuyó un 66,2% desde 1912, pasando de 0,269 km^3 a 0,091 km^3 en 2020. Poco antes del último surge, en 2006, el volumen de hielo era de 0,152 km^3. Además del estudio del glaciar del Nevado del Plomo, se calculó un descenso total del volumen de hielo del 15.9% de los glaciares de la cuenca del Plomo entre los años 2010 y 2020.

Se aplicó un modelo numérico de flujo glaciar en 2-D para reconstruir el surge de 2006-2007 y para modelar un posible surge futuro con la extensión y el volumen del glaciar en 2020. Según la modelización, el glaciar del Nevado del Plomo no alcanzaría a llegar hasta y embolsar el Río del Plomo durante un surge glaciar potencial bajo las condiciones actuales, ya que el avance es demasiado corto. Un surge sólo podría iniciarse en el modelo por un cambio en la reología del hielo y no por un enfriamiento climático, que se simuló mediante la disminución de la línea de equilibrio glaciar (ELA).

En futuro, se pueden esperar algunos pequeños lagos glaciares considerando la continuación del retroceso del glaciar, pero el volumen de los lagos es insignificante en comparación con los lagos temporales formados en el pasado debido al embalsamiento del Río del Plomo.

Table of Contents

List of Figures

List of Tables

List of Abbreviations

ASTER	Advanced Spaceborne Thermal Emission
DEM	Digital Elevation Model
DoD	DEM of Difference
ELA	Equilibrium Line Altitude
GlabTop	Glacier Bed Topography
GLOF	Glacial Lake Outburst Flood
MODIS	Moderate Resolution Imaging Spectroradiometer
MST	Mean Summer Temperature
MWP	Mean Winter Precipitation
NGI	National Glacier Inventory
SAR	Synthetic Aperture Radar
SRTM	Shuttle Radar Topography Mission
Tan-DEM-X	TerraSAR-X add-on for Digital Elevation Measurement

1 Introduction

1.1 Motivation

In the last years an ongoing drought and the retreat of the big ice masses in the Central Andes of Argentina have raised concern (Masiokas et al., 2020; Rivera et al., 2021). An unusual small amount of snowfall during the wintertime causes that the melt water runoff during the summer is lower and moreover, the continued and accelerated retreat of the world's glaciers due to climate warming is also evident in this region (Espizúa, 1986; Braun et al., 2019; Ferri et al., 2020).

However, in the year 1933 the opposite was the problem when all of a sudden, the Río Mendoza turned into a wild stream that flowed down in the direction of the city of Mendoza in Argentina. The flood destroyed several bridges, railway infrastructure, and the hydropower station (King, 1934). The reason for this catastrophe was a so called glacial lake outburst flood (GLOF) of a lake that nobody was aware of beforehand, because it was formed after an unusually fast glacier advance of the Nevado del Plomo glacier within a few months (Helbling, 1940).

To examine this phenomenon of surging glaciers, which had been barely explored at that time, the Swiss explorer Robert Helbling was called to analyze the event as it was known that he is familiar with the backcountry of Mendoza and the glaciers. He and his German friend Friedrich Reichert visited the remote and barely known Plomo valley during an expedition from 1909 to 1912. They climbed several peaks and generated a precise map of the area (Ruetz, 2022). According to this map, it was visible that the glacier had drastically advanced from 1910 until the flood event in 1934 (Helbling, 1940).

The mentioned map of the Plomo valley created by Helbling with the help of Reichert and collaborators (Helbling, 1919) is the base of this master's thesis as it allows to examine the surge event of 1933 with the historical map and the technical possibilities and knowledge of today. Even though the two known surge events of the Nevado del Plomo which occurred later on have been less hazardous, the question remains whether another surge could happen with the current ice masses, which would once again pose the danger of a GLOF.

In addition to the analysis of the surges of the Nevado del Plomo glacier, the modelling of the ice thickness distribution plays a central part in this thesis. The glaciers of the Central Andes of Argentina are crucial for the environment since they store water in the form of ice during the winter and release it as melt water during the dry months in the austral summer (Rivera et al., 2017). The decreasing ice masses are therefore of great concern as people and agriculture are dependent on the meltwater especially in times of a drought (Masiokas et al., 2016; Dussaillant et al., 2019). Hence, it is important to know how much ice has already been lost since the beginning of the drought and how much is still remaining.

1.2 State of Research

The Rio Mendoza basin had been unexplored for a long time and only the region around the Cerro Aconcagua and the Volcán Tupungato aroused interest in the end of the nineteenth century when Fitz Gerald published a map of the expedition routes in the southern region of the Aconcagua (Helbling, 1919). Due to the border conflict between Argentina and Chile concerning the watershed, the border agencies surveyed and mapped the region between the Aconcagua and Tupun-

gato, however, the Juncal range was drawn as a white spot. In 1909, Helbling and Reichert decided to map the region with its widespread glaciation (Helbling, 1919). Furthermore, Helbling (1935 and 1940) analyzed the catastrophic GLOF event of 1934 by the obtained data of King (1934). Another surge event in 1984 was examined by Bruce et al. (1986) and Espizúa (1986). Moreover, the satellite images enabled Espizúa et al. (1990) to examine the lake formation from a new perspective. The surge event in 2005, as well as the former surges were mentioned by Pitte et al. (2016) who investigated the surge of the Horcones inferior glacier in 2002-2006 and compared it with the Nevado del Plomo glacier. Falaschi et al. (2018) analyzed the glaciers of the whole Central Andes to locate new surge-type glaciers. The newest publication about the Nevado del Plomo surges was launched by Correas-Gonzalez et al. (2020), who analyzed the historical events and generated a risk map.

The remoteness of the glaciers may have caused that long-term direct mass-balance measurements are scarce in the Central Andes. Only the Echaurren Norte glacier in Chile has been observed for more than 45 years (since 1975/76), which is also the longest recording for the whole southern hemisphere (WGMS, 2020). To fully understand the temporal and spatial patterns of the high-elevation temperatures, more records of different areas are still needed (Masiokas et al., 2016).

The mechanism of surging glaciers and the key driver of the temporal variability of surging events are still not precisely known, even though such abnormally fast advances of glaciers have been observed at least since the sixteenth century (Jiskoot, 2011b). In the beginning of the twentieth century, the first scientific studies about surging glaciers in Svalbard and Alaska were published (De Geer, 1910; Tarr and Martin, 1914). Since then, many theories about the mechanism of surging glaciers had been proposed and were summarized by Benn et al. (2019). The classification of surge-type glaciers into hydrologically controlled surges and thermally controlled surges is commonly accepted (Lv et al., 2020). However, Benn et al. (2019) came up with a general theory of surging glaciers which applies for both types and considers the mass and enthalpy budgets. Recently, Paul *et al.* (2022) observed three surging glaciers in the same climatic setting in the Karakorum, which differ in the surge behaviour.

1.3 Research Questions

The objective of this master thesis is to find out more about the historical surges of the Nevado del Plomo glacier and to assess the current situation of the glacier using the obtained results. The superior aim is to determine if the ice masses of the Nevado del Plomo glacier still reach the Río del Plomo during a future surge event. To answer this question, the glaciological conditions before and during the surge events will be analyzed by determining the ice thickness distribution before the surge events and the ice mass transfer during the surging phase. Since glaciers are affected by the climate, the analysis of the climatic conditions before the surges will complete the thesis. With the obtained results, it is then the goal to assess the potential for a future damming of the Río del Plomo related to a surge event of the Nevado del Plomo glacier.

The objectives of this thesis are addressed in the following two main research questions and the three subordinate questions:

1. **Which are the glaciological and environmental conditions before and after the past surge events in the Plomo valley?**

   a) What is the ice volume of the Nevado del Plomo glacier in its quiescent phase?

   b) How much ice volume is moved around by a surge?

   c) What were the climatic conditions before the surge events? Can we deduce some characteristics for glacier surging in general?

2. **Can these results give insight to expect a future damming of the Plomo valley related to a surge of the Nevado del Plomo glacier?**

1.4 Approach and Structure of the Thesis

For the understanding of this thesis, a theoretical part about glacier surges and glacial lake outburst floods (GLOFs) is given in the next chapter prior to more detailed information about the study area and the Nevado del Plomo glacier. Subsequently, in chapter four the used data and the corresponding sources are explained.

In chapter five, the description of the methods follows. In the beginning of this chapter the digitising process of the historical map of Helbling (1919) is explained, followed by the digital elevation model (DEM) differencing, which is used to examine the mass transfer before, during, and after the surge. For this DEMs of different dates are subtracted from each other. The third method is the Glacier Bed Topography (GlabTop) model which is applied to investigate the ice thickness distribution and to assess the ice volume of the Nevado del Plomo glacier and the neighboring glaciers of different dates. The glacier flow model is the last method that is implemented, since it enables to reconstruct the last surge of the Nevado del Plomo glacier and is used to model a potential future surge.

The obtained results of the GlabTop model runs, the DEM differencing, and the reconstruction and modelling of a surge are presented in chapter six. In the discussion part the results are combined and explained in more detail in consideration of the research questions. Eventually the crucial points are summarized and an outlook is given.

2 Theoretical Background

2.1 Surge-Type Glaciers

2.1.1 Characteristics of a Surging Glacier

The glacier flow velocity differs from glacier to glacier and can show seasonal, weekly or diurnal variations depending on the thermal regime (Dunse et al., 2015). Cold-based glaciers flow usually relatively slowly as the glacier masses are frozen to the bed, whereas the flow speed of thermal and polythermal glaciers are faster due to the enhanced ice deformation and the occurrence of water at the glacier bed that reduces the friction (Jiskoot, 2011a). Principally, each glacier has a balance flux whereby the steady-state glacier profile is maintained by transferring ice from the accumulation area down to the ablation area with the corresponding balance velocity. However, if the measured flux velocity is lower than the actual balance flux for a longer time, a flow instability can emerge resulting in an abrupt switch from slow to fast flow (Clarke, 1987).

Only approximately one percent of the Earth's glaciers show quasiperiodic oscillations between very fast and slow flow velocities (Jiskoot et al., 1998; Sevestre and Benn, 2015). Those glaciers are called *surge glaciers, surge-type glacier*s, *galloping glaciers* or *pulsating glaciers* (Jiskoot, 2011b). The range of glacier types, where surges could have been observed, varies from valley glaciers, cirque glaciers, tidewater glaciers to ice streams with different sizes and climatic settings (Harrison et al., 2015; Herreid and Truffer, 2016). Apart from the glacier types, also the length of the surging phase and extent of the surge differ from glacier to glacier. Typically, the period of fast flow is relatively short compared to the long quiescence period of slow flow (Herreid and Truffer, 2016).

A glacier surge period can be described using a three-phase system:

During the *quiescent phase* or *build-up phase,* which can last from decades to centuries, the glacier ice flow is restricted and the glacier accumulates ice and builds a reservoir in the upper part while the remaining ice of the last surge in the receiving area diminishes progressively (Lv et al., 2020). As the reservoir zone gains mass, the glacier profile gets steeper and a *surge bulge* can be formed at the border between the reservoir and the receiving zone (Murray and Drewry, 1998). Eventually, towards the end of the quiescent phase, the basal shear stress is high and the glacier is therefore prone to flow instabilities (Jiskoot, 2011b).

Following this, a comparatively short (months to years) *active* or also called *surge phase* occurs, during which the ice masses from the reservoir zone are transferred downwards to a receiving area which is mostly associated with an unusual long terminus advance. The advance speed can reach meters to more than hundred meters per day and the flow velocity increases 10-1000 times (Jiskoot, 2011b). The glacier gets flatter during the surge as the accumulated ice of the upper part is transferred to the receiving zone where consequently the ice thickness is increased (Benn and Evans, 2010). A surge does not have to include the whole glacier and it is also possible that only a tributary glacier surges while the rest of the glacier does not show any uncommon mass transfer (Harrison et al., 2015). Sometimes the active phase can be interrupted by short periods of quiescence (Clarke, 1987).

When the surge phase is over, the *depletion phase* follows. The glacier front retreats and the ice thickness in the receiving area shrinks. Depending on the length of the advance, the lower part of

the glacier can detach and remains as dead ice (Weidick, 1988). The transition to the next circle build-up phase is gradually.

To detect and classify a glacier advance as a surge, it is recommended to examine the mass distribution pattern by subtracting DEMs of different years. During a normal glacier advance, the upper part of the glacier usually does not show a significant surface lowering contrary to the strong surface lowering of a surging glacier during the active phase (Lv et al., 2020). Another occurrence that indicates a possible surging glacier is an advancing glacier, whose neighboring glaciers show a retreating behaviour (Sevestre and Benn, 2015). Additionally, the surface of surge-type glaciers looks very chaotic as there are crevasses distributed all over the surface due to the fast advance (Figure 1A). The chaotic surface of a glacier that surged enables the formation of potholes and small lakes (Meier and Post, 1969). Furthermore, looped moraines, which occur when supraglacial debris exists and a tributary flows into the considered glacier, are a signifier of a surge-type glacier as shown in Figure 1B and 1C (Jiskoot, 2011b). However, up to now there exists no official threshold value for the advance rate or time period, which clearly states that a glacier belongs to the surge-type category or not (Falaschi et al., 2018).

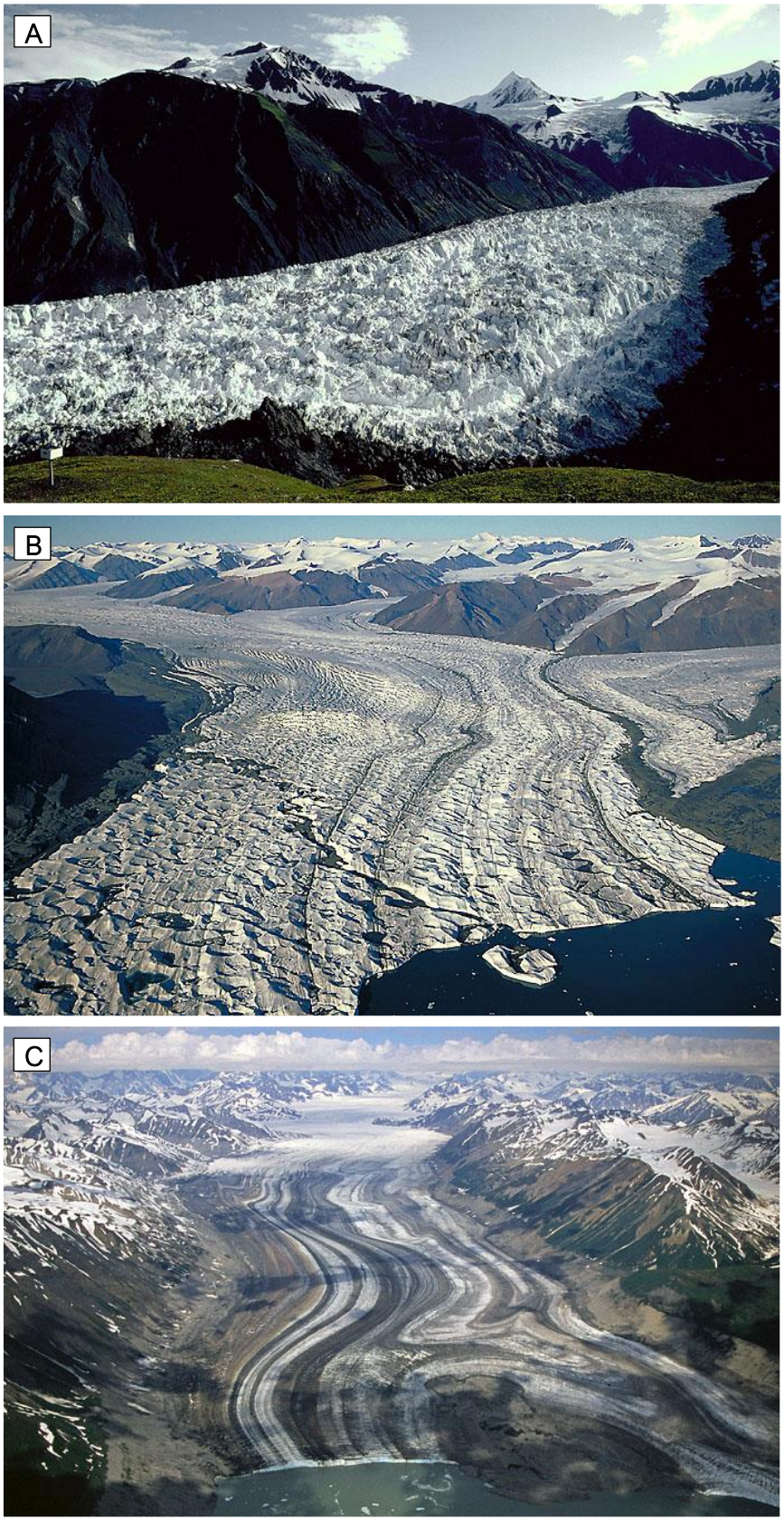

Figure 1: A. Crevassed surface of the Variegated Glacier, southern Alaska; photo by J. Akeab, 1983. B. Looped moraines and irregular surface of the Iceberg Glacier, Axel Heiberg Island; photo by J. Alean, 1977. C. Looped moraines of the Lowell Glacier, Icefield Ranges, Yukon, Canada; photo by M. J. Hambrey, 2006. All images downloaded from swisseduc.ch.

2.1.2 Surge Mechanism Theories

Even though the interest in surge-type glaciers is high, the knowledge about the surge mechanism is still limited (Paul et al., 2022). Nonetheless, it has been observed that some surging glaciers have shown an abrupt switch from the quiescent to the surging phase, whereas others have a three-phase surge cycle with the active phase additionally separated into an accelerating and deceleration phase as the velocities change gradually over years (Kamb et al., 1985; Murray et al., 2003). Therefore, it is generally distinguished between two surging-types: the *Alaska-type* and the *Svalbard-type.*

Alaska-type glaciers exhibit an abrupt change of slow to fast flow at the beginning of the active phase and therefore show relatively short active (1-3 years) and build-up phases (decades) (Jiskoot, 2011b). The surge initiation is supposably triggered due to englacially stored water that flows downwards into the till and reduces the shear strength of the till. This can lead to a collapse of the drainage system that results in a widespread enhanced glacier bed deformation and thereby fast flow (Jiskoot, 2011b). For this surge type, the surge initiation usually starts in winter and ends in summer when finally the basal shear stress is reduced and melt water intake re-establishes the efficient conduit system (Eisen et al., 2005).

On the other hand, the active phase of *Svalbard-type* glaciers lasts at least three years and the quiescent phase could last over a century (Murray et al., 2003). The surge mechanism for this type of glaciers (polythermal) is supposed to be thermally regulated. During the build-up phase the glacier is cold-based or polythermal, but as soon as the ice thickness is big enough to reach the pressure melting point, basal melt water evolves, which reduces the stability of the underlying till and enables further water storage. The basal motion increases and does not stop until the ice pressure is lower and the ice at the bed freezes again (Jiskoot, 2011b).

The division into these two types is used in most studies, Paul et al. (2022), however, analyzed three surging glaciers in the central Karakoram and found out that even though the glaciers are situated in the same climatic setting, the surge mechanisms are different and may also switch from one mechanism to the other. Additionally, the presence of both mechanisms in one region was also observed in East Greenland (Jiskoot and Juhlin, 2009). This points out that a clear classification of surging glaciers into *Alaska-type* or *Svalbard-type* does not work for all surge-type glaciers.

Benn et al. (2019) observed that for both surging types the water accumulation at the glacier bed is a crucial common factor. Therefore, they introduced an enthalpy balance theory which states that the basic principle of all surges is an imbalance of the internal enthalpy budget. This imbalance occurs when the heat gained by the flow friction and geothermal heating accumulates and cannot leave the glacier system via meltwater or heat conduction. According to them, a steady state flow can only be apparent when the mass budget and enthalpy budget are balanced, otherwise, if a surplus of enthalpy exists, a variation in flow can occur as an increase in enthalpy raises the ice creep and sliding rates.

The results of the enthalpy model reflect the observation of the spatial distribution and geometry characteristics of surge-type glaciers (Benn et al., 2019). In cold, dry climates, where the enthalpy of glaciers is generally low, glaciers need to be very large in order to surge, because then the heat conduction is less efficient, while small glaciers are not observed surging as the heat conduction through the thin ice prohibits an enthalpy imbalance (Benn, 2021). In a more temperate climate, long and relatively flat glaciers are more prone for an imbalance due to the big ice thickness which reduces the efficiency of heat conduction and simultaneously increases the frictional heating as

the balance velocity is higher which results in the production of more meltwater. Additionally, the relatively flat glacier bed does not promote an efficient drainage system. Glaciers in the European Alps and other temperate or warm and humid regions are not prone to surging as due to the high meltwater penetration down to the glacier bed, the drainage system changes to an efficient channelized system before an enthalpy excess can occur (Benn, 2021).

The glacier bed is another crucial factor that must be considered when analysing the surge mechanism. The bed or parts of the bed of surge-type glaciers commonly consist of deformable sediments. However, it is not a sufficient condition for surging, as also non-surging glaciers can have a sedimentary bed. Harrison et al. (2015) state that "[…] surging is a basal phenomenon, involving not the enhanced flow of ice, but of the basal motion over or within the underlying till." Most surge-type glacier models deal with the hydrological system or the thermal change, but according to Minchew and Meyer (2020) it would be valuable to amplify the models with the mechanical properties of the underlying sediments. Apart from the exact surge mechanisms, it is widely recognized that the surge is initiated when the reservoir zone reaches a critical slope and ice thickness, since those two factors have an influence on the shear stress at the glacier bed (Kienholz et al., 2017).

2.1.3 Global Distribution of Surge-Type Glaciers

Surge-type glaciers appear mostly in geographical clusters (Figure 2) and are reported in Alaska, the Karakorum, Pamir, Arctic Canada, West- and East Greenland, Iceland, Novaya Zemlya (archipelago in the north of Russia), parts of the Andes, Svalbard, and in the Tian Shan mountain range in central Asia (Sevestre and Benn, 2015; Benn *et al.*, 2019; and references therein).

According to the analysis of the climatic setting of surge-type glaciers, Sevestre and Benn (2015) defined an upper and lower threshold consisting of the mean summer temperature (MST in °C) and the mean winter precipitation (MWP in mm a^{-1}) where surge-type glaciers occur. In areas where the mean summer temperature is higher than $0.001MWP + 8.4$ no surge-type glaciers are

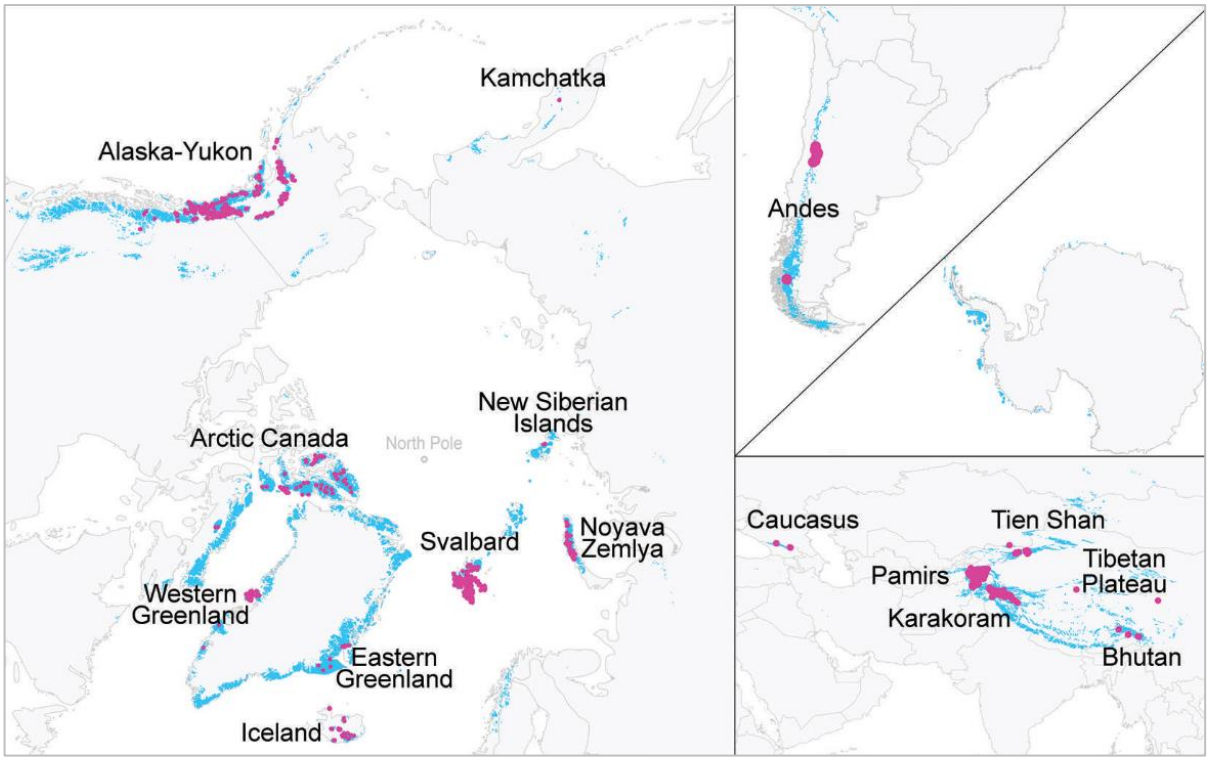

Figure 2: Worldwide distribution of surge-type glaciers (pink dots) and the Randolph Glacier Inventory (RGI) outlines of the non-surge-type glaciers (blue). The map on the right middle depicts Antarctica. Figure by Sevestre and Benn (2015: 647).

present. The lower threshold is defined as *MST= 0.0014MWP – 0.97*. In between those boundary values surge-type glaciers are observed. The climatic range where most surge-type glaciers are located is defined by an annual average temperature of -10°C to 0° and annual mean precipitation values of 165 to 2250 mm. Therefore, the density of surge-type glaciers in colder and drier climates such as Arctic Canada is relatively low (Sevestre and Benn, 2015).

The comparison of surge-type glaciers with normal glaciers in the clusters showed that surge-type glaciers are mostly longer and have a bigger area, especially in the cold, arid zone. Surge-type glaciers in the Yukon seem to have more branches than the normal neighboring glaciers (Sevestre and Benn, 2015). By comparing the surge-type glaciers of several clusters, it could be observed that the advances of the surging front of the glaciers in the Central Andes are on average shorter and slower than the advances of surge-type glaciers in other clusters. Additionally, the area of the glaciers are comparatively smaller in the Central Andes and the surge cycles of the surging glaciers of the Karakorum and the Central Andes seem more irregular compared to the other clusters (Falaschi et al., 2018).

Surging glaciers can cause a variety of problems. One of the most dreaded scenarios occurs, when the fast and far advancing ice masses dam a river of a side valley. Owing to the damming, a lake can evolve which is prone to a discharge in a glacial lake outburst flood (GLOF). The detection of surge-type glaciers is therefore essential to be prepared for a possible glacial lake (Harrison et al., 2015). An interesting case in this context is the Vernagtferner in the Eastern Alps, which in historical times has periodically advanced (Hoinkes, 1969).

2.2 Glacial Lake Outburst Floods

A glacial lake outburst flood (GLOF) is defined as the abrupt discharge of a moraine-dammed lake or a lake that is dammed by a glacier or by (bed)rock, which can lead to an increased river discharge below the failed dam. The islandic term *jökulhlaup* is sometimes used as a synonym for GLOFs (mainly with lake drainage through subglacial channels), but originally refers to a flood that is triggered by a subglacial volcanic eruption (Thorarinsson, 1969). The runoff of a GLOF can be very high and is not comparable with peak flows of a strong rainfall event. The flood can also entrain debris and depending on the settings, the flood increases its magnitude while flowing down a valley. Determined by the lake outburst mechanism, the water discharge can happen in hours or a few days (Clague and Evans, 2000; Iturrizaga, 2011).

It is distinguished between several types of glacial lakes. *Moraine-dammed lakes* can arise when the glacier is in retreat and the past end moraine impounds the meltwater or when the side moraines of the trunk glacier act as a barrier for the melt water of the side valley glacier (Figure 3) (Clague and Evans, 2000). The stability of the moraine depends on the compaction of the moraine sediment and increases with a lower porosity. Such moraine dams, which mostly originate from the Little Ice Age or Neoglacial, can reach up to 200 m and are mostly characterized by a steep slope in the direction of the glacier tongue and a less steep slope in the direction down the valley (Clague and Evans, 2000). Ice-cored moraines and moraines including permafrost lenses have a

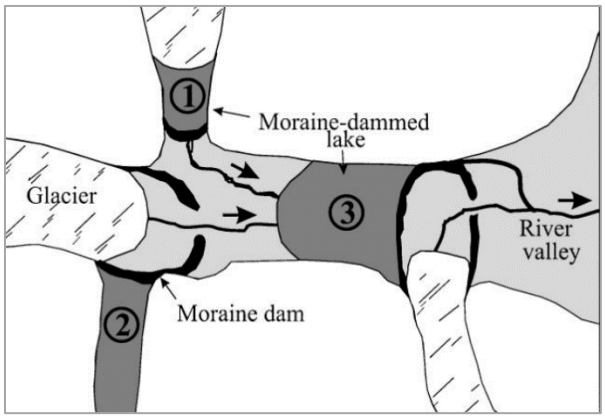

Figure 3: Overview of the formation processes of a moraine dammed lake. A lake can be formed 1) in between the end moraine and the glacier front, 2) in between the moraine of a main valley glacier and a side valley glacier and 3) due to a side moraine dam which dams the river in the main valley. Sketch by Clague and Evans (2000).

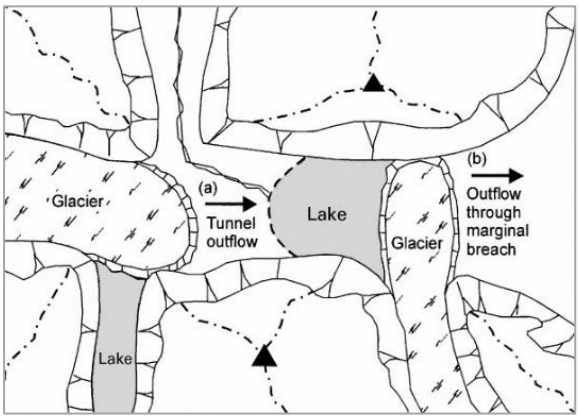

Figure 4: Scenarios which can result in glacier-dammed lakes. Firstly, the fast advance of a side valley glacier leads to a dam and impounds the meltwater of the main glacier. Second, the advance of the trunk glacier dams the meltwater runoff of a former tributary glacier. Sketch by Walder and Costa (1996).

reduced stability and are therefore prone to subsidence of the dam due to melting or a dam failure (Richardson and Reynolds, 2000b). Independent of the dam properties, outbursts can be triggered by ice avalanches or rocks falling into the lake producing a displacement wave or earthquakes. High water levels due to meltwater input, heavy rainfall or a GLOF from an adjacent lake can also lead to an overspilling of the lake (Westoby et al., 2014). As soon as water overtops the dam, it can erode a channel whereby more water can drain, which additionally enhances the erosion until the lake drains very rapidly (Clague and Evans, 2000). The stability of moraine dams can also decrease through processes like increased seepage and piping (Westoby et al., 2014).

Glacier-dammed lakes can develop when a tributary glacier advances into the main valley and therefore creates a barrier with its ice masses and impounds the river in the valley. Such lakes often arise spontaneously, e.g. due to a big advance of a surging glacier (Iturrizaga, 2011). Another possibility is that the main glacier in the valley blocks the discharge of the receding tributary glaciers (Figure 4). Lakes impounded by an ice-dam (or ice-debris-dam) can discharge rapidly due to several mechanisms, such as hydrostatic flotation of the glacier dam, overspilling, widening of the drainage channels (Iribarren Anacona et al., 2015), ice-dam weakening by sub-glacial volcanic activity (Björnsson et al., 2003) and seismic activity (Iturrizaga, 2011). Ice-dams created by advancing tributary glaciers often fail due to subaerial breach-widening, for example between the ice-masses and the adjacent valley wall where the dam ruptures abruptly and releases a short, but intense flood (Walder and Costa, 1996; Richardson and Reynolds, 2000a). *Ice-marginal lakes* form at the fringe of glaciers or ice sheets at places where the outflow is dammed (How et al., 2021). The Gornersee is an example of such a lake in the Swiss Alps. It forms annually at the confluence of the Gornergletscher and Grenzgletscher in spring and drains between July and August through a temporary flotation of the ice dam or a classical channel enlargement (Huss et al., 2009).

Bedrock-dammed lakes form in glacier bed depressions after the glacier has retreated and the depression fills with meltwater. Since the damming structure consist not of ice or unconsolidated sediments such as a moraine dam, the damming structure is very stable and GLOF events mainly occur due to avalanches or rocks falling into the lake (Tweed and Carrivick, 2015).

Lakes can also develop on the glacier surface such as supraglacial lakes. However, they usually form in depressions of debris-covered glaciers where the surface inclination is smaller or equal to 2° and meltwater or rain can accumulate (Reynolds, 2006).

GLOFs can cause severe damage up to tens to hundreds of kilometers down the valley depending on the peak discharge volume, the dam failure mechanism, the height and texture of the dam, the downstream topography and the occurrence of sediments (Clague and Evans, 2000; Iribarren et al., 2015). Due to the entrainment of available debris, the discharge can increase and turn into a debris flow (Clague and Evans, 2000). One of the best known and most disastrous GLOF event of the Andes was caused in 1941 by the Lake Palcacocha (Stuart-Smith et al., 2021). The lake is located in the Cordillera Blanca, close to the city Huaraz, Peru. Up to now it is not clear whether the failure of the moraine dam was triggered by an ice avalanche or due to internal erosion through piping, however, the flood destructed one third of the Peruvian town Huaraz and killed around 1800 people (Mergili *et al.*, 2020). In the last years, the lake has increased and is again a serious threat to the city Huaraz (Stuart-Smith et al., 2021).

Since the 19th century, glaciers are generally retreating and due to global warming the melting of the ice masses is enhanced since the last decades, which has also enabled the formation of new glacial lakes behind moraine ridges and in glacier-bed depressions (Zemp et al., 2015; Wilson et al., 2018; Shugar et al., 2020). In the Central Andes of Chile and Argentina a rise in the number of glacial lakes has been observed and the frequency of GLOF events increased as well. Apart from climate warming, the increase in discovered glacial lakes can also be attributed to the improvement of available data and examination possibilities (Harrison et al., 2018; Wilson et al., 2018; Emmer et al., 2020).

3 Study Area

3.1 Location

The Nevado del Plomo glacier is a surging valley glacier situated in the Central Andes of Argentina. The Central Andes are situated between the Arid Andes (north of 31° S) and the Northern Patagonian Andes (35-45° S). The glacierized area of the Central Andes of Argentina and Chile is relatively large (1767 km^2) in comparison with the Arid Andes (271 km^2) further north and the Northern Patagonian Andes (289 km^2) (Secretaría de Ambiente y Desarrollo Sustentable de la Nación, 2019). Reasons for this are the scarce precipitation in the Arid Andes and the lower elevation of the Northern Patagonian Andes (Falaschi et al., 2018). The variety of glaciers is wide in the Central Andes and nowhere else in the Andes exist more rock glaciers (Barcaza et al., 2017). Additionally, the glaciers are very complex and often turn from glaciers with clean ice in the upper part into debris-covered glaciers on lower altitude and sometimes even end as rock glaciers the furthest down (Zalazar et al., 2017).

The Nevado del Plomo glacier belongs to the Río del Plomo sub-basin, which contains the most glacierized area of the Río Mendoza basin (32° 57'-33°12' S and 69°57'-70°60' W). The Río Mendoza basin (Figure 5) runs along the mountain range border to Chile from north to south. On the other side of the mountain range, the capital of Chile, Santiago del Chile, is situated to the southwest of the Plomo valley. The Río del Plomo originates from the Plomo glacier and flows firstly south-east, then to the north where it joins the Río Tupungato. At Punta de Vacas, the Río de la Cuevas, Río de la Vacas, and Río Tupungato confluence and flow to the east to the city of Mendoza. Mendoza is located at 746 meters above sea level (m a.s.l.) and is famous for its wine and olive oil production. Apart from many high peaks above 6000 m a.s.l., the highest mountain of the Americas, the Cerro Aconcagua (6961 m a.s.l.), is also situated in the Mendoza basin north to the

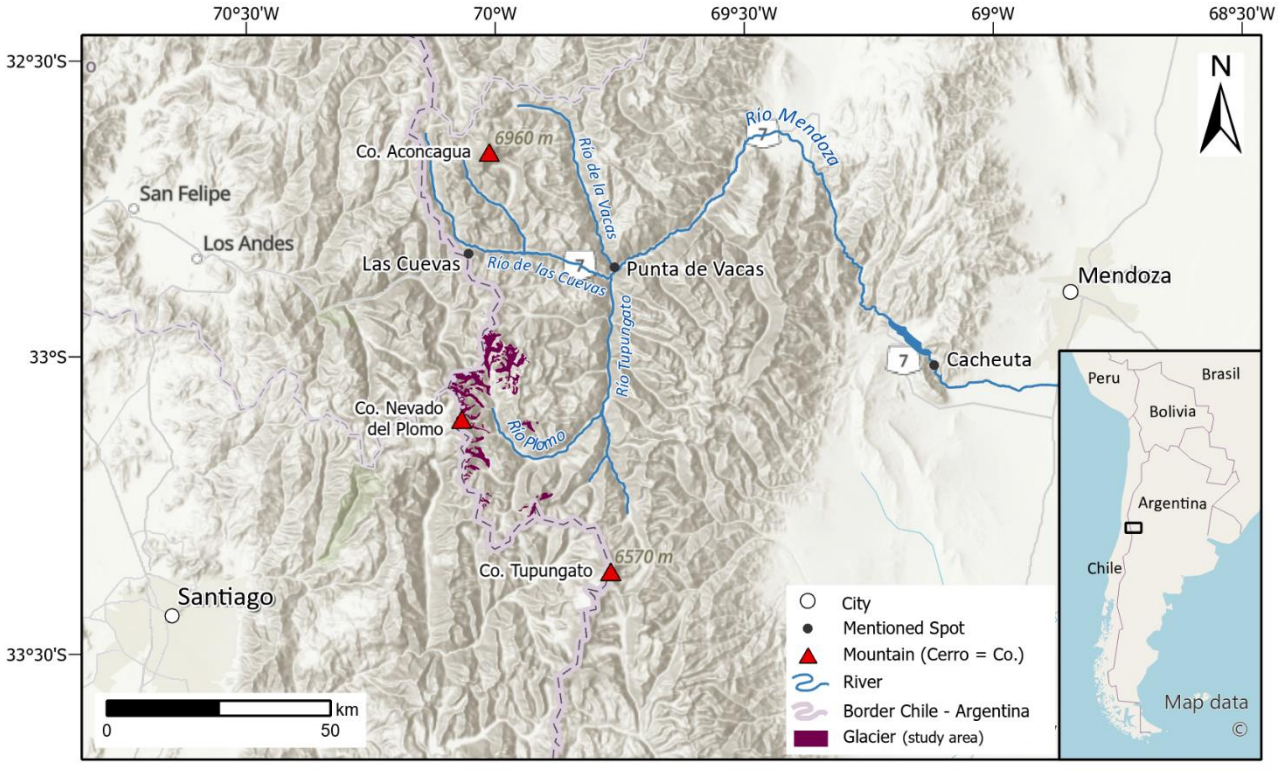

Figure 5: Overview of the study region of the Mendoza River basin situated at the border to Chile. Adjusted topographic map of Esri, overview map of Open Street Map.

Nevado del Plomo glacier. Forty kilometers to the south-east of the Cerro Nevado del Plomo there is the extinct Volcán Tupungato (6570 m), which marks the southern border of the Río Mendoza basin. There had been a mule track from Argentina to Chile via the Cumbre de las Cuevas in the past, but it was replaced in 1910 by the first railway track between the Pacific and the Atlantic oceans. The railway line passed the Cumbre de las Cuevas via a 3 km long tunnel at an altitude of 3179 m a.s.l. (Helbling, 1919). Due to political tensions and an avalanche, the railway has been out of service since 1984. Today, the international road *Ruta Nacional 7* runs across the Río Mendoza basin and connects Buenos Aires with Chile as part of the *Pan-American Highway* (Fellmann and Studer, 2020).

3.2 Climate of the Central Andes of Argentina

The climate of the central Andes of Argentina is characterized by semi-arid conditions, which is also described as Mediterranean (Masiokas et al., 2016; Ferri et al., 2020). The precipitation peak usually occurs during the austral winter from June to August as snow until the melt season begins in October or November. During the warmer months (November to March) the amount of precipitation is significantly lower. The population of this region highly depends on the seasonal melting of the snow and therefore on the snowfall during winter, as it is the main source of the river runoff that is used for agriculture, industries, hydroelectric power stations, and human consumption (Masikoas et al., 2010). This zone of South America is influenced by the midlatitude westerly Pacific frontal systems, which causes rainfall at the Chilean coast and lowlands as well as snow in the Andes (Garreaud, 2009). The position of the South Pacific High determines the intensity of the westerlies and is the reason for the seasonal differences in precipitation. During the winter the South Pacific High moves closer to the equator, which enables the westerly winds to blow more to the north and eventually causes an increase in precipitation (Masiokas et al., 2020).

The Central Andes of Argentina are influenced by the El Niño Southern Oscillation (ENSO), which is an irregularly recurring variation of the oceanic and atmospheric circulation system in the Pacific Ocean (Moreiras, 2005). The ENSO phenomenon consists of a warm and cold phase. The warm phase, called *El Niño* is associated with above-average precipitation anomalies in the Central Andes due to positive sea surface temperature anomalies on the west coast of South America. In contrast, during the cold phase called *La Niña,* mostly below-average snowfall anomalies are observed in the Central Andes (Prieto et al., 2001; Masiokas et al., 2006).

Past climate analyses between 31° S and 35° S resulted in a mean annual precipitation above 950 mm in heights higher than 2000 m a.s.l (Masiokas et al., 2016). In general, precipitation increases from the north towards the south in this area, as the influence of the westerlies becomes increasingly pervasive (Garreaud, 2009). According to Sagredo and Lowell (2012) the average temperatures in the Central Andes are +5.5°C during summer and -5.3°C during the colder winter months. January is the warmest month in the research area, with temperatures varying between 0°C and 5°C at altitudes ranging from 1550 to 3200 (Correas-Gonzalez et al., 2020).

Since 2010 the region of the Central Andes is experiencing a severe drought, also called *the Mega Drought* (Garreaud et al., 2019). The reason for this drought is the South Pacific Subtropical High, which is positioned more to the south than usual and therefore causes that the storm tracks of the westerlies do not or only partly reach the Central Andes during the winter. This results in reduced snow fall and accordingly less melt water in the rivers (Boisier et al., 2018; Flores-Aqueveque et al., 2020). As visible in Figure 6, droughts occurred already in earlier times, however, the length

and spatial extent of the Mega Drought is exceptionally. Only between 2015-2017 the amount of snowfall was close to normal and the streams could partly recover. However, from July to December 2019, all observed rivers in Central-Western Andes showed again extreme hydrological drought conditions (Rivera et al., 2021).

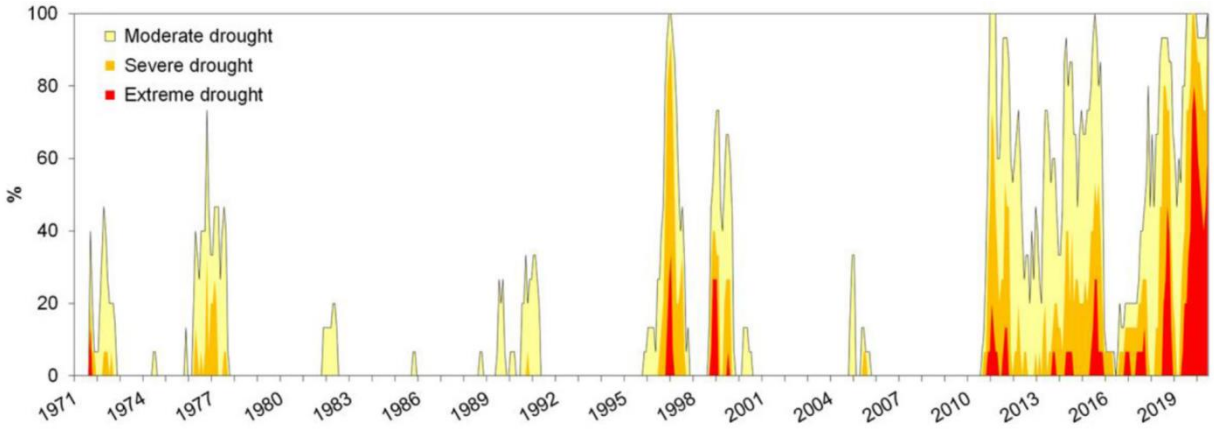

Figure 6: Drought conditions from 1971 to 2020 in the Central-Western Andes (CWA). The percentage of the affected stations of the CWA with drought is shown on the y-axis and the colours indicate the intensity of the hydrological drought. Figure by Rivera et al. (2021:11).

3.3 Nevado del Plomo Glacier

The Glaciar Grande del Nevado del Plomo or *Ventisquero Grande del Nevado del Plomo* is, to simplify matters, referred to in this thesis as *Nevado del Plomo glacier*. It is important, not to mistake it with the Plomo glacier which is the main glacier in the Plomo valley. The Nevado del Plomo glacier is situated at 33.10° S and 70.06° W below the *Cerro Nevado del Plomo* (6'070 m a.s.l.) at the border of Argentina and Chile (Figure 8). It flows roughly in west-east direction down the slopes of the Cerro Nevado del Plomo into a side valley of the Plomo valley. In contrast to a common valley glacier, this glacier is largely fed by avalanches from the steep slopes around the glacier and there does not exist a proper accumulation area (King, 1935). Additionally, it is a surge-type glacier which is especially known for the catastrophic GLOF event of 1934. The glacier has an elevation range of 1500 m and flows from 5200 m a.s.l. down to 3700 m a. s. l. After the last surges, the ice masses reached the valley bottom at 3190 m a.s.l. The area of the Nevado del Plomo glacier in 2020 was approximately 2.54 km^2 according to the analysis of satellite images which was conducted within the scope of this thesis. However, area determinations are difficult for the Nevado del Plomo glacier because each surge event has left behind a lot of ice in the ablation area, and it is therefore difficult to distinguish the glacier front from the dead-ice. Moreover, the extensive debris cover of at least 60% impedes the determination of the outlines and glacier front as well (Ferri et al., 2020). The surface of the glacier is very chaotic with many crevasses during and shortly after the surge stopped as a result of the forces acting during a surge (Figure 7) (Harrison et al., 2015). As for most of the Central Andean glaciers, there are no data available on the mass balance or the accurate elevation of the equilibrium line. The closest glacier, of which long recordings and modelling of the mass balance exists, is the Echaurren Norte which is situated south-west of the Nevado del Plomo glacier at 33.5° S in the Central Andes of Chile (Masiokas et al., 2016).

The Nevado del Plomo glacier is situated very remotely, and it takes a long time to reach it apart from using a helicopter. It is possible to drive up to Punta de Vacas from Mendoza, but then the road has to be left and the remaining 55 km must be completed on foot or by horse along the Tupungato river and further along the Río del Plomo through stony areas with nearly no vegetation (Bruce et al., 1986).

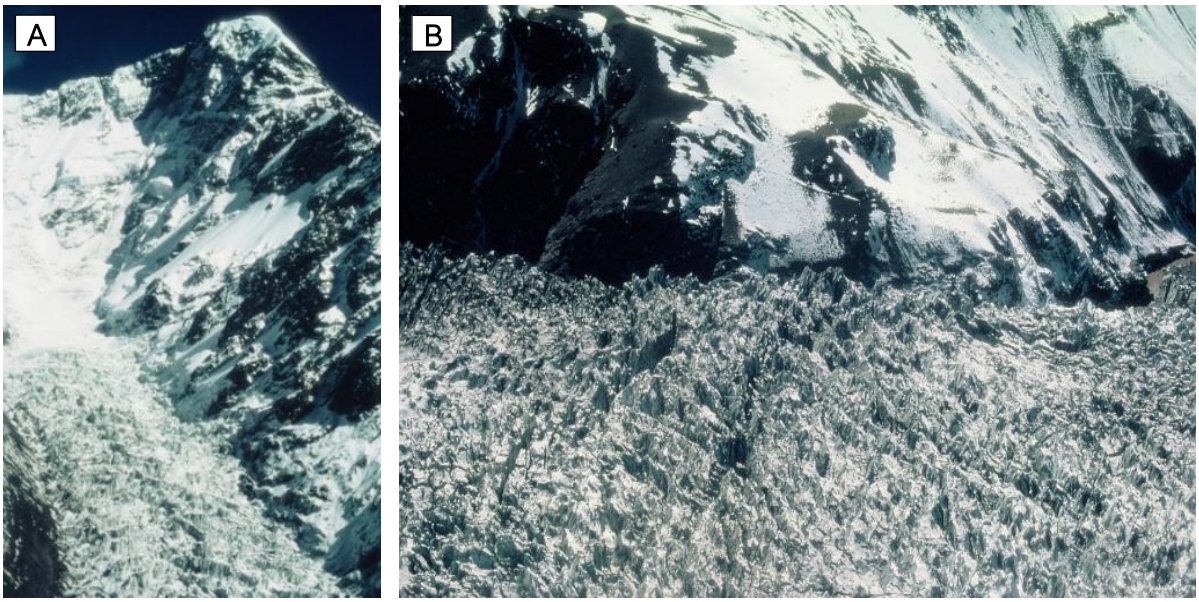

Figure 7: A. Cerro Nevado del Plomo and the glacier B. Chaotic glacier surface of the Nevado del Plomo glacier. Images by W. Haeberli, 1985.

3.4 Neighboring Glaciers

As previously mentioned, the Rio Plomo sub-basin contains many glaciers (Figure 8). The Nevado del Plomo glacier itself has a small neighbor glacier called *Glaciar Pequeño del Nevado,* which in the past converged with the Nevado del Plomo glacier (Espizúa, 1986). To the north the *Grande del Juncal* glacier with its side branches *Glaciar Alfa, Beta, and Gama* are situated. The eponym of the Plomo valley is the *Alto del Plomo* glacier which formerly coalesced with the *Oriental del Juncal* glacier. In this region, the occurrence of glaciers is highly dependent on the exposure due to the strong westerly winds. Snow accumulates mostly on the east-facing slopes as they are sheltered from the wind and the snow is not blown away (Helbling, 1935). Most glaciers are widely covered with debris, especially on the glacier snout as the rough climatic conditions and the high incoming solar radiation promote the weathering of the mountain crest (Helbling, 1919).

During the expedition of Helbling and Reichert, they found traces of glacial erosion such as glacial striations 150 m above the Plomo valley bottom which indicates former extents of the glacierized area (Helbling, 1919). However, since the studying of the glaciers in the Plomo valley in the beginning of the twentieth century, the glaciers have undergone a general retreat apart from some time spans (1940s, 1980s-1990s, 2003, and 2007) where the mass balance of the Echaurren Norte glacier was positive and glacier advances could be observed in the Central Andes (Masiokas et al., 2016). Nonetheless, the overall retreating behaviour has caused that many glaciers and its tributaries have lost their connection. In the beginning of the 21st century the glaciers in the Central Andes showed on average a slight ice thickening rate of 0.17 ± 0.23 m w.e. yr^{-1} (period between 2001 and 2008). However, between 2009 and 2017 the rate became negative with -0.40 ± 0.21 m w.e. per year. The ice loss in the second decade coincides with the beginning

of the drought in the Central Andes (Dussaillant et al., 2019). According to Masiokas et al. (2016), the main force to affect the mass balance of the Echaurren Norte is the precipitation and not the temperature as observed in other regions.

Already Helbling (1919) detected that it is difficult to determine a clear snowline for the glaciers in the Plomo area since the snow cover is hardly closed due to the wind. Nonetheless, he placed it to 4200 m a.s.l. for the time of his expedition in 1909-1912. Later in 1986 Espizúa (1986) reported a snowline of 4550 m a.s.l. for the neighboring Oriental del Juncal glacier.

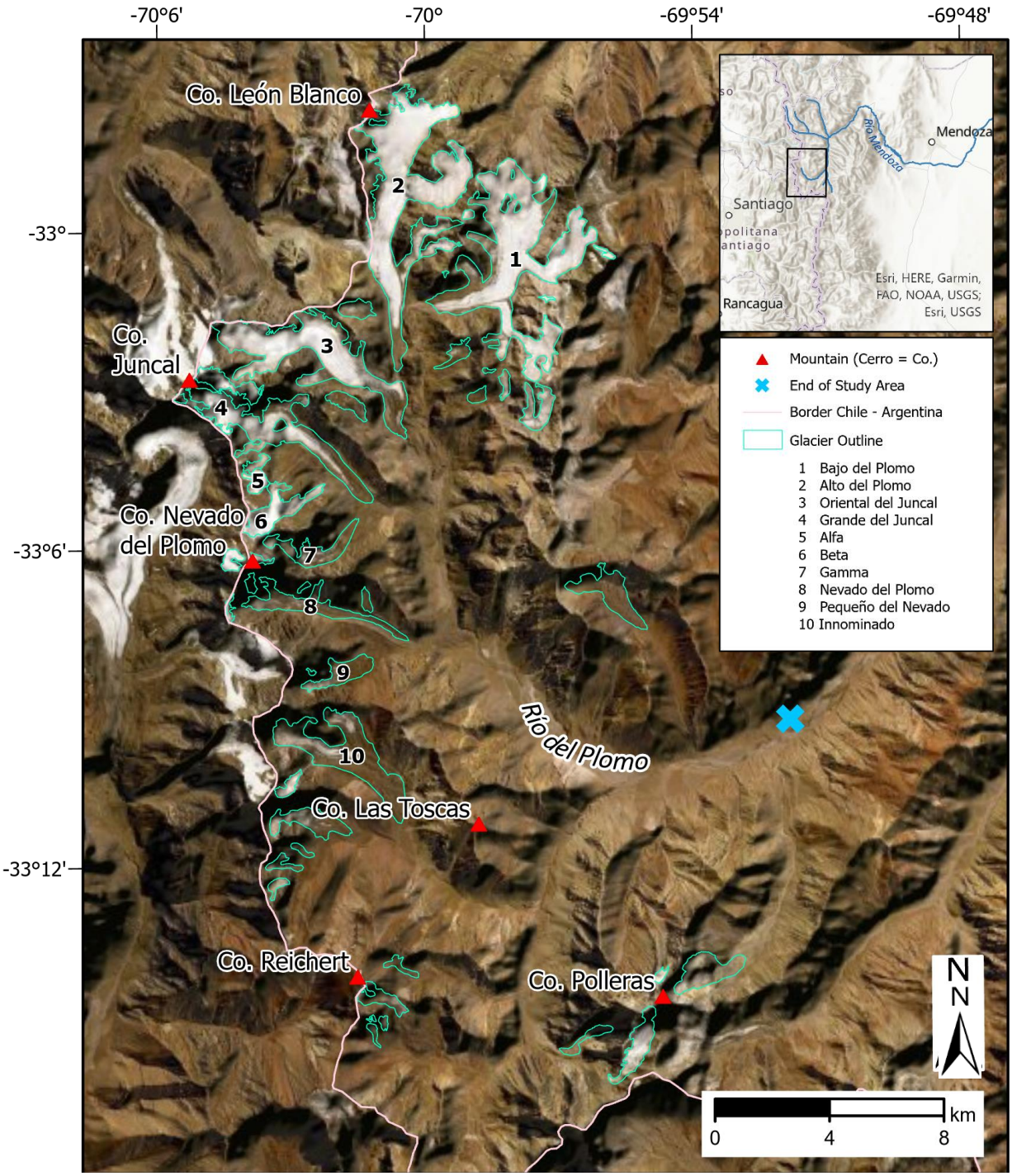

Figure 8: Overview of the Plomo valley showing the glacier outlines, some mountains, the border to Chile and the extent of the catchment area that is considered in this study for the ice volume estimations (blue cross). Map created with ArcGIS Pro (Esri).

3.5 Historical Surge and GLOF Events at Nevado del Plomo Glacier

Up to now there exist knowledge and assumptions about five surging events of the Nevado del Plomo glacier. During the last century, the possibilities to examine such a natural phenomenon have improved drastically and the technological tools sometimes can even partly replace a field trip. Nevertheless, explicit descriptions, maps and sketches from a time where satellites were not yet circling around the world, still allow to draw conclusions for the historical events. Following, the knowledge of the five surging events is summarised for each surge.

3.5.1 Surge of 1786

On January 22, 1788, the level of the Río Mendoza increased extraordinary according to different written sources (Carvallo y Goyeneche, 1889; Darwin, 1916; Haenke, 1943). The flood damaged the town hall and the slaughter house of Mendoza but more importantly, landslides partly buried the road to Chile and destroyed bridges (Del Rosario Prieto, 1986). Two years earlier, in 1786, a group of people, who were looking for a new route to cross the mountains to Chile, reported a proglacial lake at a position, which could coincide with today's Río Plomo basin. Therefore, it is assumed that this lake was the origin of the flood. The sudden flood, without any knowledge of intense rainfall at this time, the abrupt stop and the noise during the flood supports the assumption that the dam of this lake was broken (Del Rosario Prieto, 1986). During the mapping process of Helbling and Reichert from 1909 to 1912, they observed ancient moraines that ranged up to the rock wall Roca Pulida on the eastern side of the Río del Plomo and traces which they attributed to a former greater glaciation in the Quaternary. However, they did not mention a assumption about a previous advance (Helbling, 1935). Del Rosario Prieto (1886) was the first who described the possible advance and GLOF event in the 18th century. After the 1984 surge of the Nevado del Plomo glacier she looked for historical sources to find pieces of evidence for a similar advance before the 1933 and 1984 events to determine whether those surges happen in a regular time interval.

3.5.2 Surge and GLOF Event of 1933-1934

The following years, no flood or uncommon behavior of the Nevado del Plomo glacier were documented, which could also be due to the remoteness of the area. Later, in the 20th century the photographs taken during the expedition years of Helbling and Reichert in 1909-1912 indicated a retreating behaviour of the Nevado del Plomo glacier (Helbling, 1935).

However, all of a sudden on January 10, 1934, approximately at 3 pm the runoff of the Río Mendoza was increasing abnormally to 2890 $m^3 s^{-1}$ at Punta de Vacas (King, 1934). Shortly after midnight the flood arrived at the Luján de Cuyo dam near Mendoza and 120 km down the valley of Punta de Vacas and eventually broke the dam at 2 am. It was estimated that about 60'000'000 m^3 water flowed through the dam with a maximum runoff of 3000 $m^3 s^{-1}$. According to the distance covered, the flood velocity was approximately 4 m s^{-1} and it lasted less than 5 hours. In comparison, the usual runoff of the Río Mendoza during the peak melting season was 130 to 250 m^3 s^{-1} and in very rare cases up to 500 $m^3 s^{-1}$(King, 1934). The reported floods of earlier years (1888, 1900 and 1915) never reached runoff values close to this flood. The flood propagated through the valley with a height of 5-6 m and in the narrow part near Cacheuta even 12 m (Diario Los Andes, 1934). Thus, the damage of the flood was extensive. On its way down the valley, the flood wave destroyed seven bridges, 12.6 km of the Transandio Railway track (Figure 9), a hydropower station and a hotel in Cacheuta, and 19 km of the power supply line were demolished and 75 km

badly damaged. The flood caused some fatalities, however, the exact number is not known and differs in reports (King, 1935; Helbling, 1940; Harrison et al., 2015).

A flight over the valley showed a collapsed ice dam on the valley bottom in front of the Nevado del Plomo glacier. According to King (1934), a mass of ice and snow dammed the Río del Plomo, with a width of 200 m where the Nevado del Plomo glacier enters the Plomo valley, and a width of 600 m where the ice masses reached Roca Pulida (Figures 10 and 11). The ice masses dammed the Río del Plomo with a maximum dam height of 75 m and an average of approximately 30 m. With a dam length of 1100 m it was estimated that the total ice masses were approximately 60 x 10^6 m^3. In northern direction of the ice dam, traces of a recent lake were found with a length of 3 km, a maximum depth of 70 m and an average depth of approximately 30 m (Figure 12). The amount of dammed water was estimated to be 30-55 million m^3 (Helbling, 1940). With the help of field reports and images of the two engineers King and Yorke, the railway company commissioned Robert Helbling to analyze the event (Helbling, 1940). Helbling noticed an ice surface lowering in the upper part of the glacier and therefore rejected the assumption of King (1934) that the ice

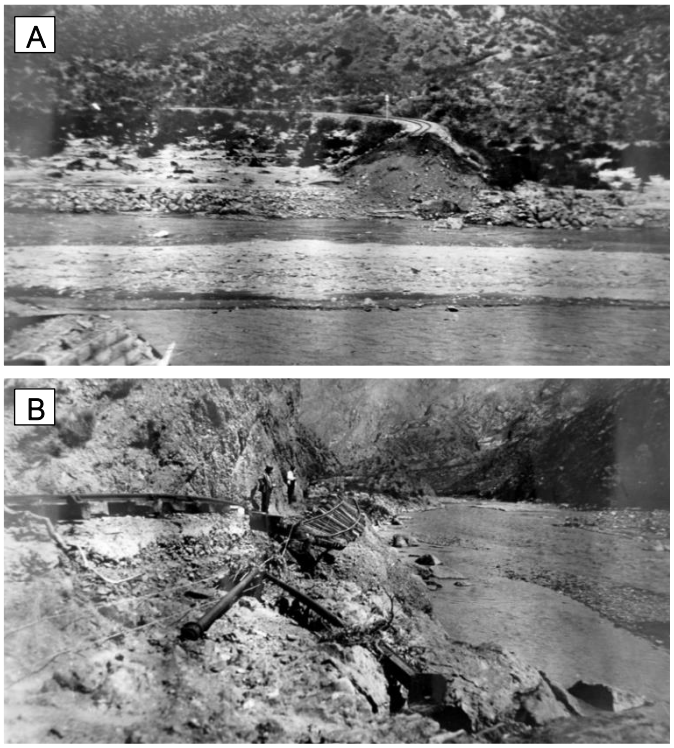

Figure 9: Images showing the destructive force of the flood. A. The flood washed away a railway bridge in the Mendoza valley. B. The railway tracks were washed away or severely damaged. Images taken in February 1935, by W.D.O. King (1935).

Figure 10: Nevado del Plomo glacier (looking direction to the West) shortly after the surge in 1934, Image by R. Helbling, January 1934 (Helbling, 1935:50).

dam possibly originated from an avalanche. Images of 1930 showed that no ice masses were present at this part of the valley and after the surge, remains of living vegetation were detected on the east side of the Río del Plomo below the ice masses. Therefore, Helbling inferred that the 4.5 km advance (Pitte et al., 2016) had taken place in a range of few weeks to months. Since the neighboring glaciers were retreating at the same time, he categorized the ice movement as an *extraordinary glacier fluctuation* which had at this time already been reported in the Karakorum, Greenland, and Alaska. According to the glaciers in the Karakorum, Mason (1935) already suspected that the extraordinary advances occur within a certain periodicity.

The process of the dam creation and failure is not clear. The filling of the lake could have been completed in about 30 days (Helbling, 1940). Field observations indicated that the water of the lake did not flow over the dam and King (1934) assumed that in the beginning, when the ice masses reached the Río del Plomo, it was still flowing through a tunnel until the high temperatures let to the collapse of the tunnel and thus to the damming of the river. The flood occurred as soon as the pressure was high enough to push out the ice masses. Helbling (1935) assumed, that the river was dammed as additional ice was pushed into the ice-tunnel and Harrison et al., (2015: 457) describe "a collapse structure in the central part of the heavily fractured ice dam directly above the subglacial drainage tunnel". Thus, the exact damming and breaking mechanism is still not defined but as images taken after the outburst showed, the dam still existed but with a tunnel where the Río del Plomo was flowing through (Figure 11).

Therefore, the fear remained that another damming could occur. However, the ice masses slowly melted and no further damming could be observed (King, 1935). In the following years, the Nevado del Plomo glacier was retreating (Espizúa, 1986; Alean, 1987). Until 1955, the glacier lost approximately 3180 m in length and between 1955-1963 the glacier retreated additional 950 m. On aerial images it could then be observed that the Nevado del Plomo glacier advanced 1050 m between 1963-1973 while the other glaciers in the valley were still retreating (Espizúa, 1986). This untypical advance, compared to the other glaciers, led to the assumption that another surge occurred. Falaschi et al. (2018) described it as a minor surge. However, in the literature this advance is hardly mentioned.

Figure 11: Dimension of the ice masses damming the Rio Plomo after the surge. The image is north-facing (valley up). In the east the ice masses are arched upwards at the Roca Pulida. Image of the Argentine Transandino Railway Company taken in 1934 by A.T.R. (Helbling, 1940:124).

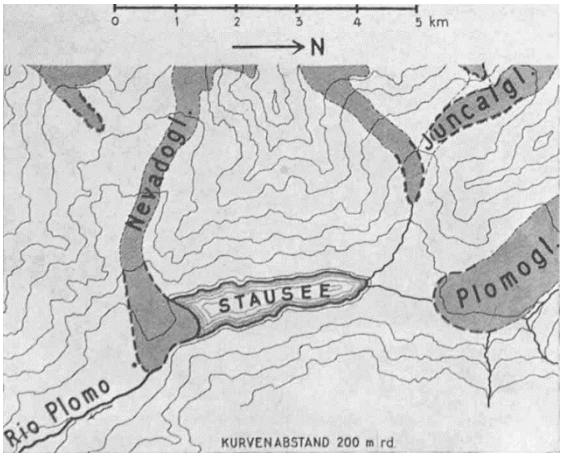

Figure 12: Sketch sowing the advanced glacier tongue and the dammed glacial lake in the year 1934. Sketch by R. Helbling (1940).

3.5.3 Surge and Glacial Lake of 1984-1985

Between February 16, 1984 and April 4, 1984, the Nevado del Plomo glacier started surging, as in between those dates an advance of 500 m could be recognized on satellite images. Later, on November 14, 1984, the glacier front already reached the rock wall Roca Pulida and consequently advanced 2.7 km in total (Figure 13). The ice masses dammed the Rio Plomo again and already nine days later a 1.65 km long and 600 m wide lake was formed (Espizúa and Bengochea, 1990). Pitte *et al.* (2016) calculated a maximum advance rate of 16 m per day between April 4 and August 26, 1984. The biggest dimensions of the lake were measured on January 9, 1985, when it was 2.8 km long with a width of 1.1 km. Already on February 28, 1985, Bruce *et al.* (1986) measured an obvious reduction of the dimensions of the lake (1.49 km long and 703 m wide) with an estimated lake volume of 12.1 x 10^6 m^3 and an ice dam volume of 27 x 10^6 m^3 (Figure 14). Eventually the lake disappeared on March 30, 1985 (Espizúa and Bengochea, 1990). There are no indications of damage in the literature.

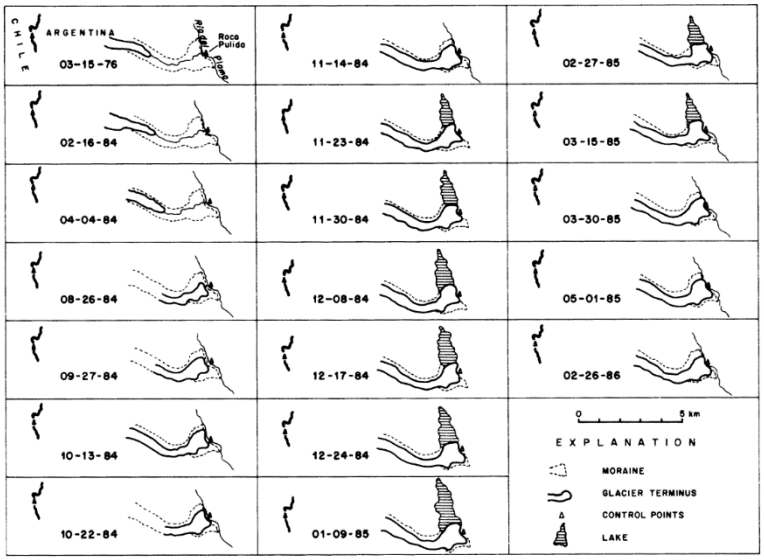

Figure 13: Sketches according to the satellite images showing the propagation of the surge and the formation and discharge of the lake. Figure by Espizua and Bengochea, 1990:257).

Figure 14: Image of the ice dam after the lake discharging (south-facing). Photograph taken by J. Suarez (May 1986) in: Espizua and Bengochea (1990:259).

The lake drainage was noticeable in the form of three runoff peaks of the Río Tupungato. The first and also the highest runoff peak occurred on February 14, 1985 with a maximum runoff of 293 m^3s^{-1} followed by two weaker, but still striking runoff peaks on February 22 and March 13, 1985 (Harrison et al., 2015). According to estimations of Bruce et al, the lake stored 55 x 10^6 m^3 water shortly before the first peak runoff occurred in February. Even though the runoff peaks were high, it was not comparable to the flood of the event in 1934 where the lake drained in an outburst flood since this time the drainage occurred gradually through a subglacial tunnel (Espizúa and Bengochea, 1990) or a glacier mill (Bruce et al., 1986) in March 1985. The hydrographs of all three dates showed an immediate steep ascent and a flatter, slower descent (Harrison et al., 2015). According to Haeberli (1983) this is characteristic for an abrupt mechanical rupture and not for a lake outburst where subglacial channels progressive enlarge. Therefore Harrison et al., (2015) assume that at least some mechanical breaking mechanism was part of the initiation of the floods.

3.5.4 Surge of 2006-2007

Following the surge in 1984 the Nevado del Plomo glacier showed a 22-year quiescence phase until in the beginning of the year 2006 a new advance was noted (Ferri Hidalgo et al., 2012; Pitte et al., 2016). According to Pitte et al. (2016) the surge started February 5, 2006 and ended September 26, 2007. During this surge event the glacier front progressed 3.0 km. Through the examination of satellite images it was determined that the fastest advance of the glacier was happening between May 7 and May 23, 2007 with a rate of 35 m per day (Pitte et al., 2016). The advance was again long enough to reach the Río del Plomo and the rock outcrop *Roca Pulida* on the east side of the valley (Figure 15) (Harrison et al., 2015). It was estimated that the total ice volume that was transferred from the upper part to the lower part was 83 x 10^6 m^3 (Ferri Hidalgo et al., 2012). This time, a lake of only 190 m in length and 45 m in width could be observed on the satellite image on November 14, 2007, however, nine days later it had already disappeared as the water could drain via a subglacial conduit preventing the formation of a sizeable lake (Ferri Hidalgo et al., 2012; Harrison et al., 2015; Pitte et al., 2016). According to Harrison et al., (2015) the valley was still covered with ice in the year 2013, but with a reduced volume and the debris-coverage was increasing.

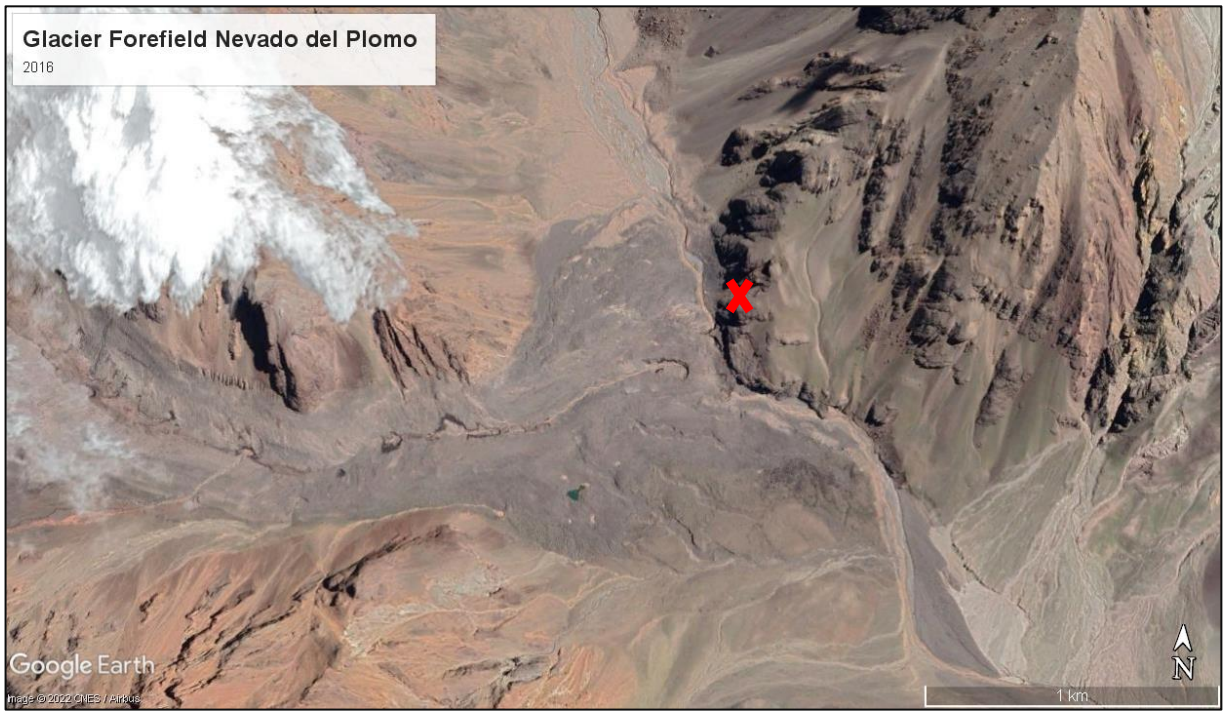

Figure 15: Screenshot of the Google Earth image of 23.02.2016 showing the Río del Plomo (flowing north to south), the Roca Pulida rock outcrop (red cross) and the debris covered ice remains of the surge in 2006-2007 (eye altitude 6.8 km).

3.6 Surges of Grande del Juncal Glacier and Horcones Inferior Glacier

Approximately 50 km to the north of the Nevado del Plomo glacier, the Horcones Inferior glacier flows down the southern slopes of the Cerro Aconcagua. It also belongs to the surge-type glaciers and at least two surges were observed in the last decades. The active phase of both surging events coincided with the active phases of the Nevado del Plomo glacier. The Horcones Inferior advanced 3.5 km from December 1984 to January 1990 (Happoldt and Schrott, 1993). The last surge happened in between January 2003 and February 2006 with an average velocity of 9.1 m / day, a maximum velocity of 14 m / day, an advance of 3.1 km and an active phase of 3.16 years. The volume of the transferred ice during the surge was estimated to be 10^8 m^3 (Pitte et al., 2016). In comparison to the Nevado del Plomo glacier, the velocity during the surging phase of the Horcones Inferior glacier was slower. According to Pitte et al. (2016) the reason for this is the different glacier geometry. The Nevado del Plomo has a smaller area and is shorter but has a steeper slope, all characteristics that support a faster flow. As the initiation of the surges of the Horcones Inferior glacier were in spring and the switches between the surging and quiescent phase occurred relatively fast, the glacier is categorized as an Alaska-type surging glacier, whereby the surge is initiated by a hydrological switch (Pitte et al., 2016). Besides the Nevado del Plomo and the Glaciar Horcones Inferior there are other glaciers in the Central Andes that show a surging behaviour, however, the investigations and reports were not as accurate and mostly not quantitative (Falaschi et al., 2018).

As stated by Helbling (1935), the Grande del Juncal glacier showed an unusual long advance between March and December 1910 and had a very chaotic surface comparable to the Nevado del Plomo glacier after the surge of 1933-1934 (Figure 16). According to the photographs taken, it is estimated that the advance was between 500-1000 m while the neighboring glaciers fronts were retreating (Espizúa, 1986). Following this, the glacier retreated again until 1934. In 1955 the glacier tongue was further down the valley than in 1934, which indicated an advance of approximately 140 m (Espizúa, 1986). Falaschi et al. (2018) describe a surge of the GGrande del Juncal between 1962 and 1974 with an average advance of 74 m per year and a total advance of approximately 0.9 km. The latest small surge of 224 m advance started simultaneously as the Nevado del Plomo surge in the year 2006 but continued until 2011 (Falaschi et al., 2018).

Figure 16: Photograph of the Juncal glaciers. 3) Oriental del Juncal, 4) Grande del Juncal, 5) Alfa and 6) Beta. Photograph taken by F. Reichert in 1910 (Espizua 1986: 322).

4 Data

In this chapter the used data for this thesis are shortly described. Firstly, the digitization process of the historical map is presented, followed by the description of the different digital elevation models and satellite images, and finally the National Glacier Inventory of Argentina is shortly described.

4.1 Historical Map of the Plomo Valley

The key source that enables the examination of the glaciological conditions of the Nevado del Plomo glacier before the surge in 1933 is the map created by the Swiss researcher and explorer Robert Helbling and his German friend Friedrich Reichert during the years 1908-1912. After climbing several mountains in the High Cordillera of Mendoza as the first people, both were overwhelmed by the big ice masses around the Juncal massif and decided to investigate the uncivilized and unexplored glacier area. Their goal was to show the extent of the ice masses between the Aconcagua and the Tupungato (Helbling, 1919). During their three expeditions between 1909 and 1912 they were supported by the *Pacific railway* and the company *Hotels Sud-americanos* with mules, helping hands, and cheap rail transport. The stereophotogrammetric recordings were carried out by Helbling with a heavy theodolite consisting of a camera with 194.4 mm focal length and glass plates of 18x13 cm for the easily accessible areas. With the lighter theodolite he completed the recordings up to the height of about 4500 m a.s.l. (Schellenberger, 2014). The basis of the topographical survey is a triangulation network of its own (Figure 17) and a base survey with approximately 900 m of Invar wire (Helbling, 1919; Schellenberger, 2014).

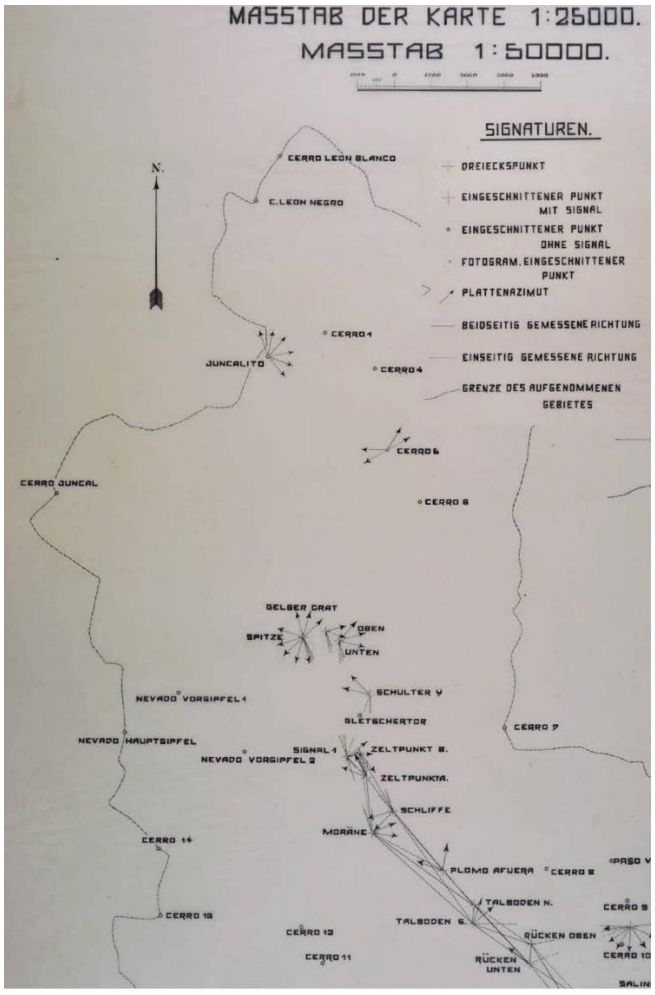

Figure 17: Part of the triangulation network plan which was the base of the "Mapa de los Ventisqueros en los Valles del Plomo" generated by Robert Helbling (1919). Image of Schellenberger (2014:18).

As there existed no precise elevation data and Helbling was not sufficiently equipped with meteorological instruments to carry out barometric measurements, Helbling determined with boiling thermometers the elevation of 3165 m a.s.l. at one point of the glacier tongue of the Plomo glacier. The altitudes are therefore only relatively accurate and are based on this one point. However, according to Helbling (1919), the heights are approximately in agreement with the Chilean map of the year 1898 and the discrepancy to the true sea level should not exceed 10 to 20 meters. In the historical map the altitude of the peak of the Nevado del Plomo is identified as 6050 m a.s.l. whereas in the glacial and periglacial inventory of the Río Mendoza basin the altitude is displayed as 6070 m a.s.l. (IANIGLA, 2018). The result of the three expeditions were three conjoined maps with a scale of 1:25'000 and an equidistance of 25 m, named *Mapa de los Ventisqueros en los Valles del Plomo* (Figure 18). The three maps combined cover the area of the Plomo glacier, important parts of the Taguas valley and the Toscas valley (Helbling, 1919).

Figure 18: Adjusted southern part of the map "Mapa de los ventisquerosen los valles del plomo – Parte meridional" drawn by Dr. Robert Helbling, Ing. Ed. Grubenmann, Kartographia Winterthur S.d.A. (1910-1914). In: Helbling (1919). The red crosses indicate the georeferencing points used for the digitalisation of the map (upper cross: rock outcrop, lower cross: Cerro Las Toscas).

4.2 Digital Elevation Models

To examine the temporal change of the Nevado del Plomo glacier using the GlabTop model and the DEM-differencing method, several DEMs were needed from different years. Following, the different types of DEMs are shortly described.

4.2.1 SRTM

The *Shuttle Radar Topographic Mission* (SRTM) was executed on a Space Shuttle Endeavour in February 2000 performed by a cooperation between the NASA, the U.S. National Geospatial-Intelligence Agency (NGA), the U.S. Department of Defense (DoD), the German Aerospace Center (DLR), and the Agenzia Spaziale Italiana (ASI). Within 11 days of recording, about 80% of the continental area of the earth was mapped in between 60° N and 56° S (Grohmann, 2018). The SRTM was provided with two synthetic aperture radars, one C-band (3.1 cm) and one X-band (5.6 cm) system (Farr et al., 2007). To cover the whole area of the Nevado del Plomo glacier, two tiles (S34W71, S34W70) of the SRTM Version 2 were acquired online from the Earth Explorer website (USGS, 2018). Both tiles (void filled) have a resolution of three arc-seconds and according to Farr et al. (2007) an absolute height error in South America of 6.2 m and an absolute geolocation error of 9.0 m. Steep terrain such as it is common in the Central Andes is responsible for the biggest errors. Voids can also be caused by radar shadowing.

4.2.2 TanDEM-X

For the analysis of the year 2010, the *TerraSAR-X add-on for Digital Elevation Measurement* (TanDEM-X) is used. Like the SRTM, it is a global DEM but with a better resolution ant not free of charges. It is a dataset generated by the German Aerospace Center (DLR). To produce the DEM the two satellites TerraSAR-X and TanDEM-X orbit the earth in 514 km height very closely to each other and thus enable contemporaneous records of different points of views. This results in a resolution of 12 m (0.4 arc-second) and a vertical accuracy of 2 m. The advantage of radar data (e.g. SRTM and TanDEM-X) is that cloud cover or darkness do not affect the recording, however, it is possible that the signal penetrates into dry snow and ice (Wessel, 2018). In order that the whole Plomo valley is covered, four tiles were merged (S33W070, S33W071, S34W070, S34W071) which were recorded on January 27, 2011 and February 23, 2011.

4.2.3 ASTER DEMs

ASTER is the abbreviation for the *Advanced Spaceborne Thermal Emission and Reflection Radiometer* which is on board of the Terra satellite of the NASA. This satellite was launched in December 1999 and generates high-resolution images of the earth which are freely available (Jet Propulsion Laboratory, 2004). The computed DEMs from the ASTER images have the advantage, that they are not relying on radar data but on an optical satellite and therefore are not affected by the problem of signal penetration through snow and ice. Nevertheless, the quality is negatively affected by cloud cover and low light conditions. The DEMs used in this thesis (of the years 2004-2018) originate from Inés Dussaillant and were used to assess the glacier mass loss along the Andes by examining a time-series of ASTER DEMs (Dussaillant et al., 2019). The DEMs were are already co-registered to the SRTM DEM and have a resolution of 30 m. As the Nevado del Plomo glacier is situated in the middle of two data tiles 1° by 1° (latitude by longitude) (S33W070 and S33W071) and the whole Plomo catchment area in the middle of four data tiles, the corresponding tiles were assorted according to the recording date and merged into one tile with the ArcGIS tool

mosaic. For many dates, however, there existed no neighboring tiles with the same date or there were too many voids, which limited the usable data for this thesis.

4.3 Satellite and Aerial Images

To determine the outline and glacier front position of the Nevado del Plomo glacier and its neighboring glaciers, several aerial images were used depending on the observation year. For the years 2014, 2018 2019 and 2020 the high-resolution *World Imagery* of ArcGIS Pro was downloaded from *arcgis.com* (ESRI). The image of 2014 has a resolution of 15 m, whereas the newer imagery have a resolution of 0.5 m. Additionally, for some closer examinations especially at the mountain ridges, the 3D view of Google Earth was used. For the determination of the glacier outlines of 2010 and earlier years Landsat-5 (30 m resolution) and ASTER satellite images were downloaded from USGS (earthexplorer.usgs.gov).

4.4 National Glacier Inventory of Argentina

In 2018 the *Inventario Nacional de Glaciares of Argentina* was published, which is the first National Glacier Inventory (NGI) of Argentina (IANIGLA, 2018). It is based on satellite images between 2004 and 2016 and for this thesis it is used as the base of the outlines for the observing dates. The inventory not only features the outlines of glaciers but also of rock glaciers and perennial snowfields. It distinguishes between clean ice and debris covered glaciers and active and inactive rock glaciers. As the glaciers in Argentina are an important source of water, the goal of the inventory was also to improve the understanding of the freshwater reservoirs of Argentina (Zalazar et al., 2020). It contains a total area of 5769 km^2 consisting of glaciers, rock glaciers and permanent snowfields and includes 16078 ice masses larger than 0.01 km^2, covering elevations between 200 and 6900 m a.s.l. The outlines of the Central Andes were drawn according to 28 ASTER scenes, 20 ALOS-AVNIR scenes and one Landsat-5 image between 2007 and 2011 and several field visits during 2012 to 2015 (Zalazar et al., 2020).

5 Methods

5.1 Digitizing Contour Lines of the Historical Map

To generate a digital elevation model of the Plomo area of the time before the surge in 1933 had happened, the scanned image of the historical map *Mapa de los ventisqueros en los valles del plomo – Parte Sud* of Helbling (1919) was opened in ArcGIS Pro which is a desktop geographic information system (GIS) application from Esri. First, the spatial reference was set to the projected coordinate system *WGS 1984 UTM Zone 19S* and then the outline of the glacier parts were retraced using the *editor* tool. As the Nevado del Plomo glacier is partly covered with debris, Helbling indicated the glacier ice below the debris by the continuing the blue colored contour lines in the brown (= debris) area. Therefore, the glacier outline is wider along the glacier tongue than the bright colored clean ice part (Figure 19). Subsequently to the outline, the contour lines of the Nevado del Plomo area were retraced and named with the corresponding height. In the lower part of the glacier area, where the contour lines with an equidistance of 25 m are far apart, it was easy to follow the contour line. Contrary, on the steep side slopes of the glacier it was difficult to identify the single contour lines due to the resolution. However, since per each two hundred meters of altitude the contour line is dashed and could be distinguished, the intermediate contour lines were just distributed in between.

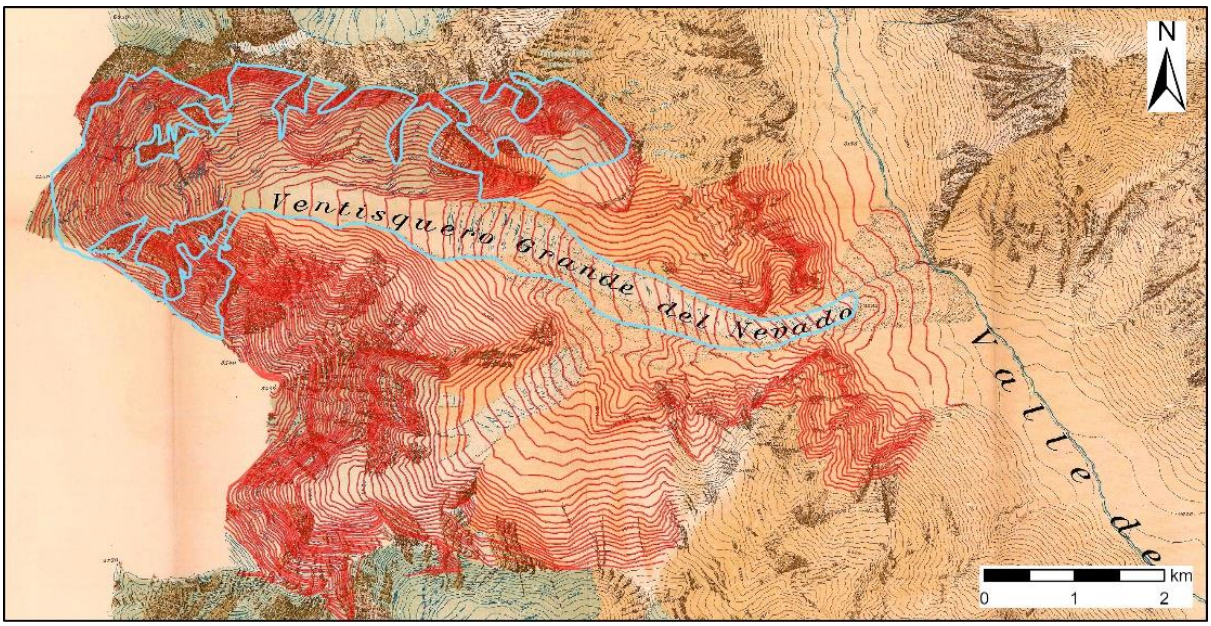

Figure 19: Retraced contour lines (red) and glacier outline (blue) of the Nevado del Plomo glacier using the underlying historical map of Helbling (1919).

To georeference the map with the digitized outline and contour lines, the base imagery of Arc GIS Pro of the year 2020 was used (Esri, 2020). To prevent the distortion of the map, only two georeferencing points were chosen to move the map and data to the right place and to scale it. According to the network plan of Helbling's measurements (Figure 17), the peak *Cerro Las Toscas,* which is situated in the south of the Nevado del Plomo glacier, was chosen as the first georeferencing point because Helbling conducted many measurements from this peak. Since the other points of the network plan e.g. *Signal 1, Moräne, Zeltpunkt A, …* could not be clearly determined on the satellite imagery and the historical map, a geomorphological, well recognizable element (rocky outcrop in the south-facing slope of the Nevado del Plomo glacier), which should have been stable over the time, was used as the second georeferencing point (red cross in Figure 18). After the

georeferencing it was measurable that the scale of the historical map is too small since one kilometer of the historical map corresponded to 1195 m on the satellite image, however, the elevation data coincided well with the measured altitude of the present. Furthermore, there were some discrepancies of the outline and contour lines to the valley which were corrected by rotating them slightly. As visible in Figure 21, it was difficult that all parts of the historical map matched perfectly with the topography of the recent satellite image. Either the glacier tongue was situated accurately or the upper part of the glacier. As the sidewalls of the glacier are very steep and the south facing slopes are distorted on the satellite image, the focus was set on the lower part. The upper edge of the glacier, in the west of the digitised glacier outline, had to be shortened as it was overlapping the ridge in the satellite image. It was difficult to recognize the ridge exactly and to define whether the snow field was already on the other side of the ridge or still flowing to the east side. Thus, the Google Earth 3D view was used to better examine the steep parts and to determine the snow fields that belonged to the east side and therefore supply the Nevado del Plomo glacier.

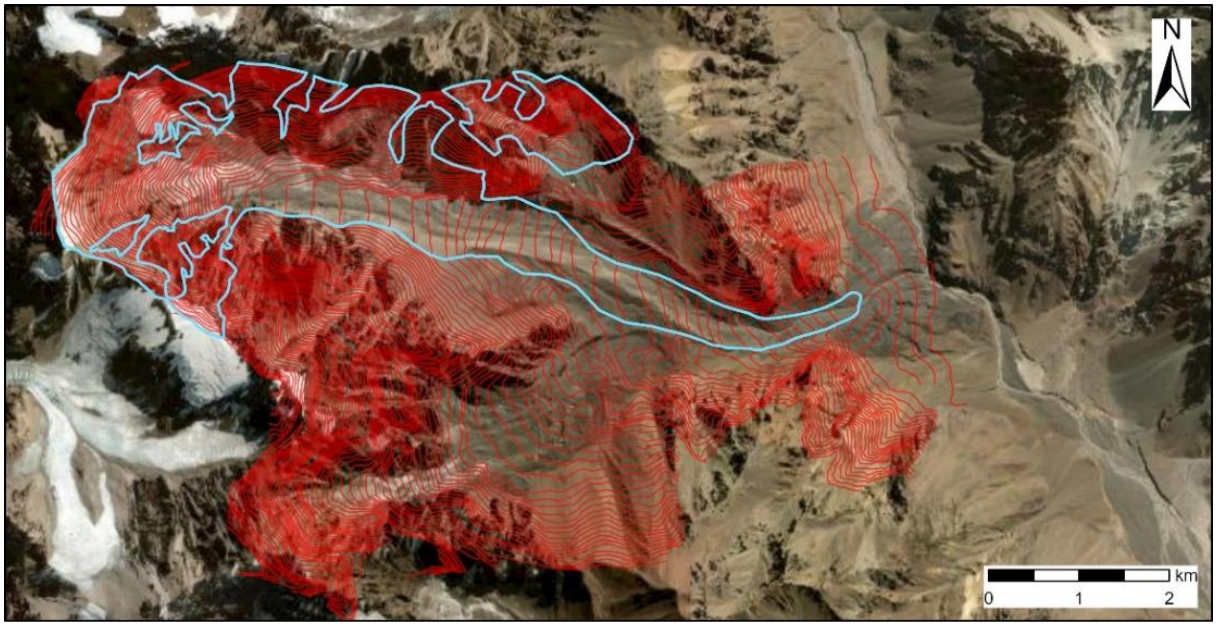

Figure 20: Digitized contour lines (red) and outline (blue) of the Nevado del Plomo glacier with the Esri World imagery of April 1, 2020, as background.

As soon as the contour lines and the outlines seemed to fit the actual topography, the ArcGIS Pro tool *Topo to raster* was applied to generate the digital elevation model. Additionally, a hillshade raster was created to examine the topography in more detail (Figure 21). Since the GlabTop model

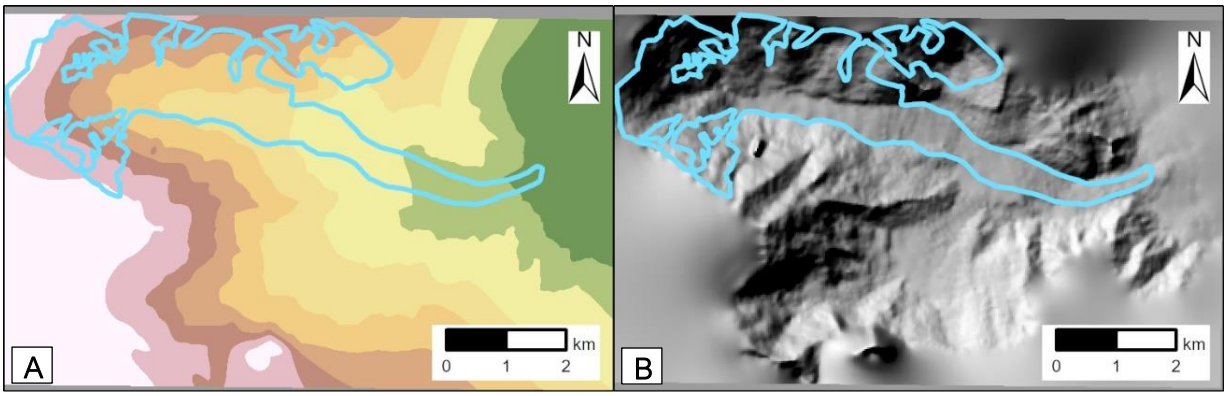

Figure 21: Output of A.Topo to raster B.Hillshade tool of ArcGIS Pro showing the Nevado del Plomo glacier area with the glacier outline in blue.

calculation only works for the whole glacier, when the extent of the digital elevation model surpasses the glacier outlines, the historical DEM was enlarged with the SRTM of the year 2000.

5.2 DEM-Differencing

To examine the surge process itself, several ASTER DEMs prior, during, and after the surge event of 2006-2007 were compared among each other. The DEM differencing method is widely used to calculate the elevation change and mass balance changes of glaciers and allows to identify the displacement of the ice masse due to the decrease and increase of the surface height. The output of the DEM differencing is a new raster with pixel values which correspond to the difference between the pixel elevation values of the two input datasets. Ferry et al. (2020) presented already an overview of the surface elevation change of the Plomo area for the years 2000-2018, 2000-2009, and 2009-2018 applying the ASTERIX method (Dussaillant et al., 2019). Therefore, the focus in this thesis is set to the time span shortly before, after and in between the active phase in 2006-2007. The DEM-differencing was done using the mathematical raster function tool *Minus* of ArcGIS Pro. The older DEM (t_1) was subtracted from the newer DEM (t_2) to get a negative value for the mass loss and a positive value for the mass gain. As input data, the ASTER DEMs of Dussaillant *et al.* (2019) were taken, which were already co-registered with the SRTM. Consequently, it was possible to visualize the surface height difference between the year 2000 (SRTM) and 2006 (ASTER DEM), shortly before the surge was initiated.

5.3 Glacier Flow Model

Another method applied for this thesis is the numerical glacier flow model (Vieli, 2021). It is used to reconstruct the surge extent of the Nevado del Plomo glacier of the year 2007 and to model a potential future surge extent with the glacier volume of the year 2020. More precisely, it is used to test, whether the mass transfer during the surge of 2006-2007 can be reconstructed by a surge forcing or a climate forcing. Afterwards, the same input parameters as used for the reconstruction of the surge in 2006-2007, are applied to the glacier extent of 2020, to see if the glacier volume is sufficient to advance down to the Río del Plomo during the surge phase.

5.3.1 Model Characteristics

The model is a 2-D numerical glacier flow model which runs on the software MATLAB. It calculates the surface elevation, the ice thickness and the glacier extent over a given bed topography and a prescribed mass balance forcing as described in more detail in Brown et al. (2013). The ice flow is calculated locally considering the surface slope and the ice thickness according to the Shallow Ice Approximation (Hutter, 1983) and depends on the ice softness parameter. In this version of the model, the sliding of the glacier is ignored but is indirectly simulated by the ice softness (personal communication A. Vieli, 30.08.22).

The surface mass balance *b* is parameterized by a linear function that depends on the surface elevation and the equilibrium line altitude:

$$b = m[S - ELA(t)]$$

S stands for the glacier surface altitude, *ELA* for the equilibrium line altitude and *m* for the mass-balance gradient. The model does not consider the redistribution of snow by avalanching or wind

and slopes steeper than 45° receive no accumulation in the model (Brown et al., 2013). The grid resolution of the model is 60 m.

To build up a glacier using a constant climate, the DEM of the glacier bed is needed as an input. Apart from this, several parameters of the model need to be prescribed such as the mass-balance gradient, the equilibrium line altitude and the rate factor *a* of the considered glacier. The rate factor describes the ice softness and corresponds in this version of the model to an ice temperature of 0°C (temperate ice) (Cuffey and Paterson, 2010). After the build-up of a glacier that is in balance with its climate (steady state) and therefore has a constant geometry, two forcing options are applied of which the type, magnitude and duration of the forcing can be varied. The first option is called the *surge-forcing option* in which the ice softness of the glacier is increased by a certain factor below a specified glacier bed elevation height. The glacier ice mass below this bed elevation starts surging due to a prescribed sudden increase in ice softness which increases the movement of the glacier. As soon as the forcing time elapsed, the ice softness switches to the normal value and is again homogeneous over the whole glacier. The other option, *the climate-forcing* affects the glacier evolution due to a shift of the equilibrium line altitude for a specified time. Through this, a climate warming or cooling phase can be simulated (personal communication A. Vieli, 30.08.22).

5.3.2 Application of the Model for the Nevado del Plomo Glacier

As above mentioned, the goal is to reconstruct the surge of 2006-2007 and to model a possible surge for the glacier extent in 2020. For this, firstly, two steady-state glaciers had to be built up for the pre-surge glacier extent of 2006 and the glacier extent of 2020 before the forcings could be applied. All model runs were conducted using the DEM of the glacier bed of the Nevado del Plomo glacier of February 2006, which resulted of the GlabTop model (Run 3, 2006) that will be discussed in chapter 5.4. The voids of the DEM were filled by interpolation.

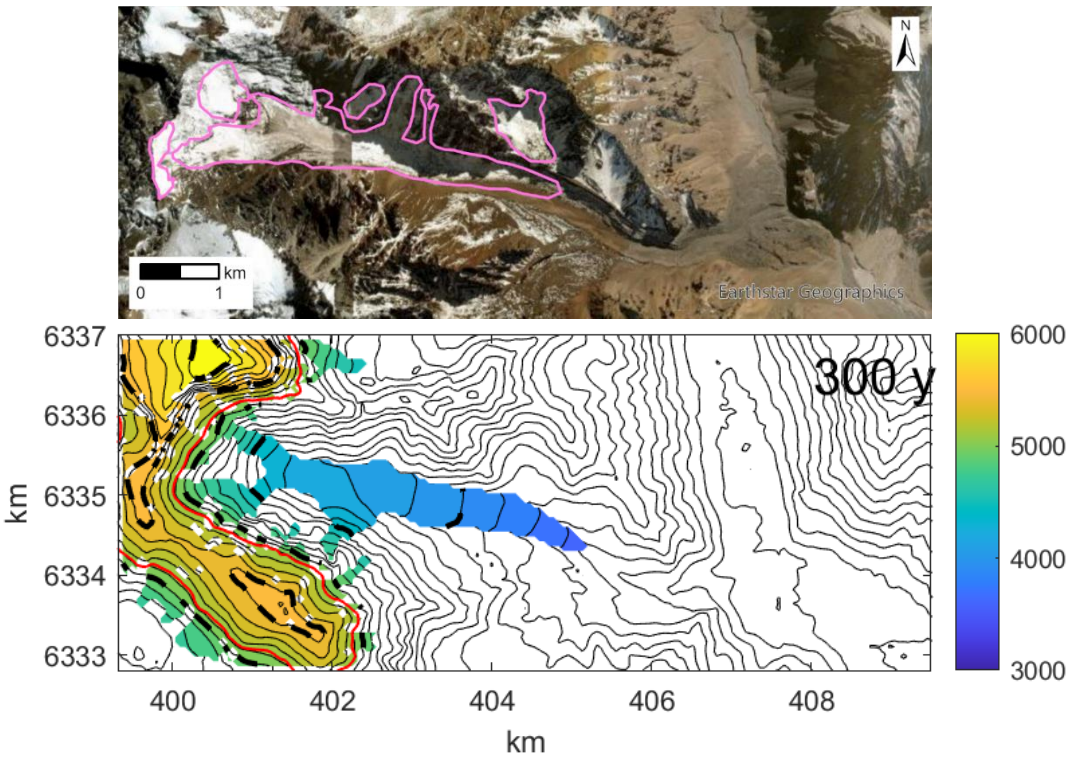

Figure 22: Comparison of the glacier flow model output and the glacier outline of the year 2006 of the Nevado del Plomo glacier. The ELA of the modelled glacier is set to 5100 m a.s.l (red line) and the build-up was stable after 300 years. The colors indicate the surface elevation. Background of the outline figure: Wayback imagery 2022 (Esri).

To reconstruct the pre-surge glacier geometry of the year 2006, the outlines drawn for the GlabTop model were taken as a guideline to find the glacier front position (Figure 22). Since data about the mass-balance gradient of the Nevado del Plomo glacier is lacking, a mass-balance gradient of 0.004 m was taken, which was the average gradient of the nearby Universidad Glacier (34°40' S, 70°20' W) during the years 2012-2014 (Kinnard et al., 2018). The ELA of the Nevado del Plomo glacier is also not defined as the glacier is supplied by avalanches and therefore does not show a clear accumulation area. Several ELAs were tried out to build up the glacier extent of the year 2006 and eventually the glacier geometry of the model run using an ELA of 5100 m a.s.l. was chosen for the forcing experiments.

Additionally, a second steady-state glacier geometry was built up for the year 2020 (Figure 23). The same mass-balance gradient of 0.004 was applied and again several ELAs were tested in different model runs. Eventually, an ELA of 5160 m a.s.l. showed the best result, even though the glacier tongue reaches slightly further compared to the satellite image of 2020. Experiments with a higher ELA resulted in a too short glacier tongue.

After the reconstruction of the pre-surge glacier conditions, the experiments with the two forcing options were conducted with the pre-surge glacier geometry of the year 2006. The climate step change was performed to assess if the past rapid advances (i.e. the surge events) could be explained by climatic forcings only and the surge step change to assess if the change of the ice rheology is the crucial factor for the initiation of a surge. The settings with the most accurate result were then eventually applied to the glacier conditions of 2020 to see whether the ice volume would be sufficient to reach the opposite valley wall and therefore possibly dam the Río del Plomo. Additionally to the active surge phase, the model enables to reconstruct the depletion phase during which the ice melts.

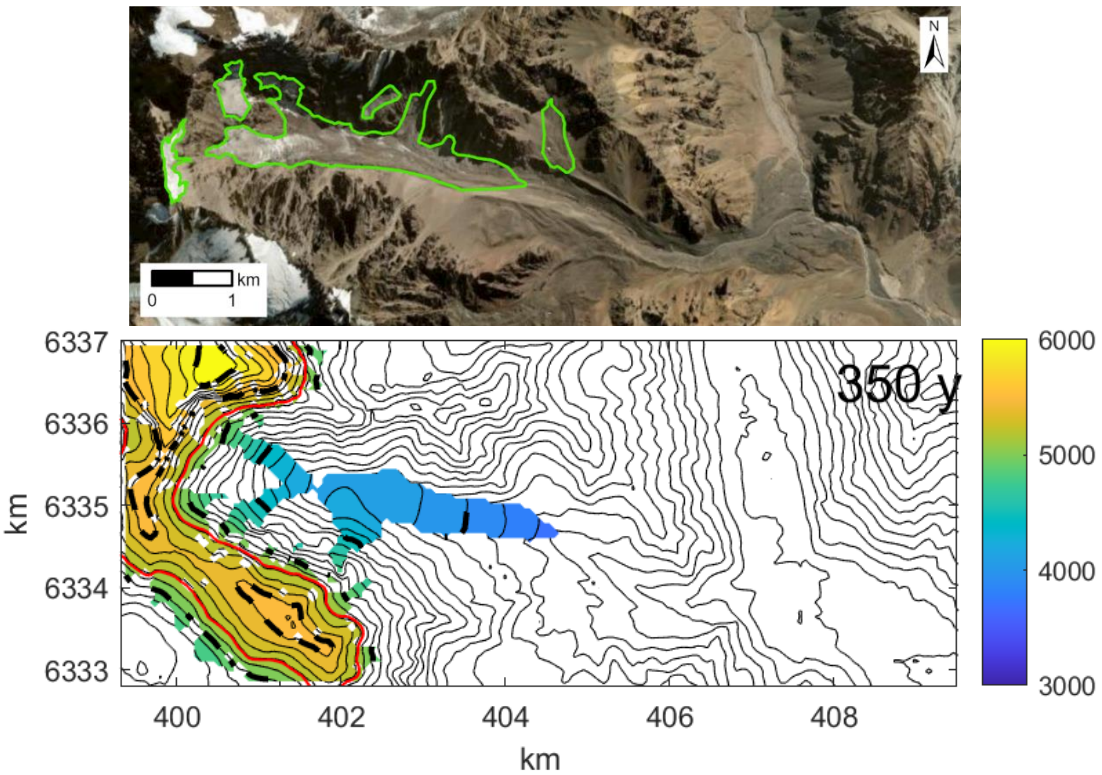

Figure 23: Comparison of the glacier flow model output and the glacier outline of the year 2020 of the Nevado del Plomo glacier. The ELA of the modelled glacier is set to 5160 m a.s.l (red line) and the build-up was stable after 300 years. The colors indicate the surface elevation. Background of the outline figure: Wayback imagery 2020 (Esri).

5.4 Glacier Bed Topography Model (GlabTop)

5.4.1 Model Characteristics

To estimate the ice thickness distribution of the Nevado del Plomo glacier and to evaluate the current ice volume of the glaciers in the catchment area, the Glacier Bed Topography (GlabTop) model of Paul and Linsbauer (2012) is applied. The model is suitable to determine the ice thickness distribution in remote areas for a large glacier sample as it only requires a digital elevation model, the glacier outline and the corresponding branch lines (Figure 24). Branch lines differ from flow lines as they do not have to cover the whole glacier from the top to the bottom but can also just indicate a side branch of a glacier and then end at a confluence point with a central branch line without touching it (Paul and Linsbauer, 2012). The model relies on the shallow ice approximation (SIA) by Paterson (1994) that assumes idealized glacier geometries and perfect plasticity and states that the ice thickness depends on the steepness of the glacier slope. The steeper the glacier surface, the thinner the ice and reverse. To calculate the ice thickness, the average basal shear stress is required. Therefore, for each glacier in the input dataset, an average value for the basal shear stress τ is calculated based on the vertical glacier extent ΔH (see Equation 1) by using an

$$\tau = 0.005 + 1.598\Delta H - 0.435\Delta \mathrm{H}^2$$
$$\tau = 150\ kPa\ for\ \Delta \mathrm{H} > 1600\ \mathrm{m} \quad (1)$$

$$h = \frac{\tau}{\rho * g * f * sin\alpha} \quad (2)$$

empirical relation between the basal shear stress and the vertical extent ΔH of the glacier (Maisch and Haeberli, 1982; Haeberli and Hoelzle, 1995). For glaciers with an elevation extent larger than 1600 m, a maximum average shear stress of 150 kPa is determined (Paul and Linsbauer, 2012; Maisch and Haeberli, 1982). Using the resulting basal shear stress value, the ice thickness h is then calculated by dividing the shear stress by the ice density ($\rho = 900\ kgm^{-3}$), the acceleration due to gravity ($\mathrm{g} = 9.81\ \mathrm{ms}^{-2}$), the glacier surface slope ($\alpha \neq 0$) and the shape factor ($f = 0.8$) (Paul and Linsbauer, 2012).

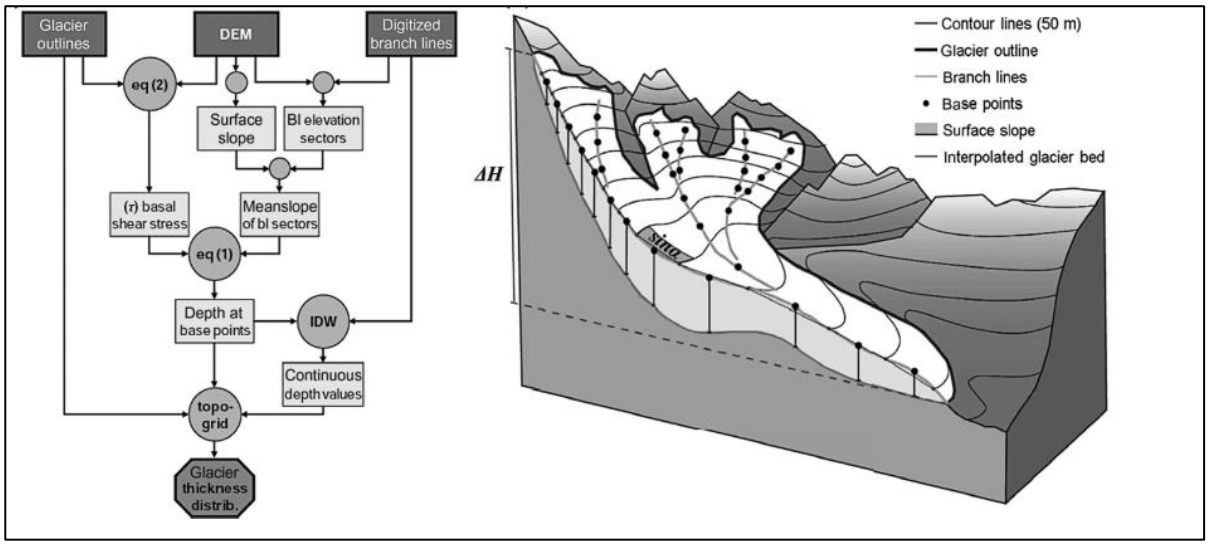

Figure 24: Schematic overview of the processing steps of the GlabTop model (circles represent calculations and the rectangles represent the datasets). Eq: equation, IDW: inverse distance weighting, bl: branch line. On the right side: Illustrated presentation of the parameters used in GlabTop. Figure by Linsbauer et al. (2009: 245).

Besides the ice thickness distribution from which the total ice volume of the considered glaciers is calculated, the model output also contains the glacier bed topography (i.e. the DEM without glaciers), a hillshade of the glacier bed topography, the calculated shear stress per glacier, and the potential overdeepenings. Glacier bed overdeepenings with an area of more than 1 hectare are converted into an additional layer of potential future lakes. Moreover, the bathymetry of all the lakes (= the 3D shape of the glacier bed overdeepenings) is presented in another layer. The potential future lakes are especially interesting in times of a glacier retreat, when the former glacier bed is becoming ice-free and the overdeepenings can be filled with meltwater (Linsbauer et al., 2012). The formation of new lakes can affect the hazard conditions as they are potential sources of future lake outburst floods (Frey et al., 2010).

5.4.2 Input Data Preparation

In the following, the data preparation for each of the examination periods is described. At the end of the sub-chapter a table with an overview of the runs and sources is given (Table 1).

The digitization of the historical map allows to examine the pre-surge conditions of the surge in 1933 even though no satellite data exist from this time. Contrary, at the time of the surge in 1984 satellites have been orbiting the earth already but the images have a very bad resolution which would make the outline determination fairly inaccurate. Additionally, no digital elevation model is available of this time and therefore no GlabTop run was planned to examine the surge in 1984. For the years 2010 and 2020 the ice thickness distribution of the whole catchment area was modelled additionally to the modelling of the Nevado del Plomo glacier ice thickness distribution. The selected satellite images for the analysis were recorded in austral summer when the snow coverage was reduced to a minimum.

5.4.2.1 Glacier Outlines

For the estimation of the pre-surge 1933 ice volume of the Nevado del Plomo glacier, the digitized outlines of the historical map (Helbling, 1919) are used (see chapter 5.1). To examine the ice volumes of the other years (2000, 2006, 2008, 2010 and 2020), the outlines of the Nevado del Plomo glacier were drawn as shapefiles in ArcGIS Pro using the *create* tool, and the corresponding satellite and aerial images as background (Figure 25). Owing to the pixel resolution of 30 x 30 m of the Landsat 5 satellite, it was difficult to determine the outlines of the year 2000. However, the

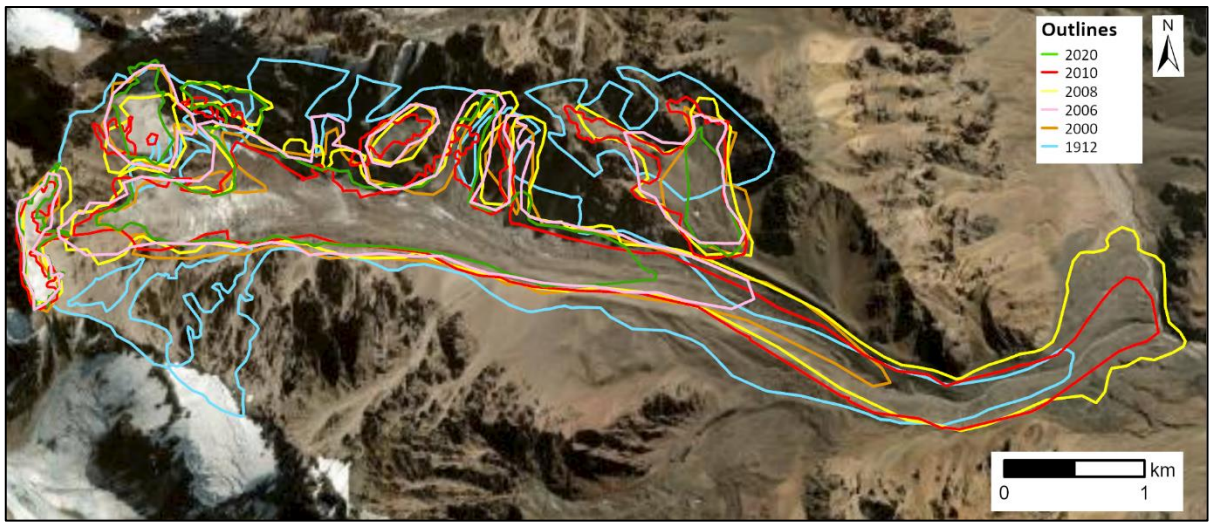

Figure 25: Outlines of the Nevado del Plomo glacier of the different years used as the input for the GlabTop model. Background: World Imaginary April 1, 2020 (Esri, 2020).

Landsat 5 images of February 29, 2000 and March 3, 2001 show the clean ice very well and in the austral winter image of July 27, 1999 the flowing structures of the glacier tongue could be recognized. Those outline assumptions were then slightly adapted to the NGI outlines of the year 2010.

For the pre-surge ice thickness modelling in 2006 the resolution of the Landsat 5 images again did not allow a precise definition of the glacier outlines, however, Pitte et al. (2016) show the surge evolution of the Nevado del Plomo glacier in their paper concerning the surges of the Horcones inferior. According to their analysis, the glacier tongue advanced 3 km during the surge event. The glacier tongue outlines were therefore drawn 3 km valley up and coincide well with the assumption of Pitte et al. (2016). To define the outlines in the upper, steep area of the Nevado del Plomo glacier, Landsat 5 images were examined and the *Wayback* imagery of February 23, 2018 (Esri, 2018) because the clean ice distribution seems very similar to the 2006 Landsat 5 images, but the resolution is better.

After the surge period in 2006-2007 the glacierized area increased. For the outline determination of 2008 the high-resolution world imagery *Wayback 2014-02-02* (Esri, 2014) was examined as the surge extent close to the Río del Plomo is clearly visible. The NGI outline was again taken as the base and was adapted to the ASTER image of March 3, 2008. Since the outlines of the glaciers in the whole area exist for the year 2010, it was decided to examine the ice volume of the Plomo catchment area additionally. However, the glacier outlines according to the NGI of Argentina (IANIGLA, 2018) are divided into clean ice, debris glacier and rock glacier as described in chapter 4.4. To use the outlines as a GlabTop input, the different outlines of one glacier were merged into a coherent polygon. The rock glaciers as well as the ice fields with a diameter less than 200 m were deleted. Additionally, the outlines were partly adjusted, e.g. when a glacier clearly did not coincide with the mountain range or when shadowing effects probably affected the NGI outline determination (Figure 26).

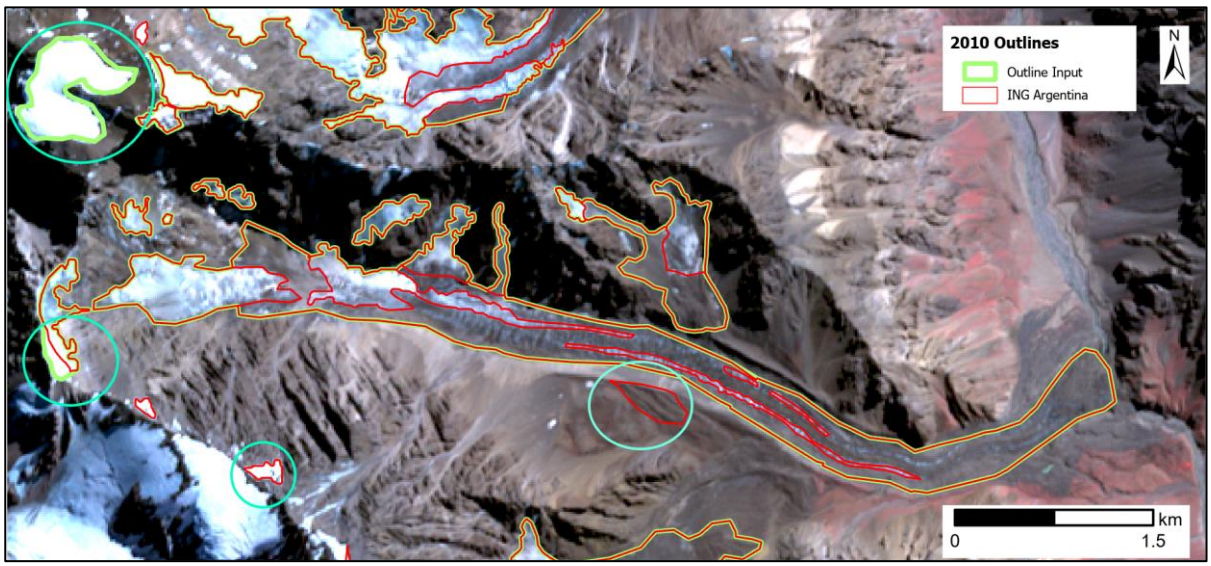

Figure 26: Comparison of the 2010 glacier outlines of the ING Argentina (red) and the adapted outlines used as the GlabTop input (green). The cyan blue circles indicate outlines that were adjusted or deleted. Background: ASTER 27.03.2010.

To compare the ice volume of the Plomo catchment area between the years 2010 and 2020, two GlabTop runs were planned for the year 2020. One run to model the ice thickness distribution of the Nevado del Plomo glacier individually and the other run to model all glaciers of the Plomo catchment area as in 2010. The outlines were drawn based on the *World Imaginary* of ArcGIS Pro

of April 1, 2020 (Esri, 2020) in consideration of the outlines of the *Inventario Nacional de Glaciares of Argentina* (IANIGLA, 2018). Similar to the drawing of the other outlines, it was difficult to identify glacier ice below the debris. If flow movement (crevasses, flow structures) are evident below the debris, the object was counted as part of the glacier. However, individual debris objects that are not adjected to a glacier and showed no clean ice parts were classified as rock glaciers and therefore not considered. If the bergschrund is visible in the accumulation area, it was marked as the upper border of the glacier.

5.4.2.2 Digital Elevation Model

To be able to compare the GlabTop results with each other, all DEMs were resampled to a 30 x 30 m pixel size using *the bilinear interpolation* method of ArcGIS Pro. This method is suitable for continuous data as it calculates the value for each 30 m pixel by averaging the values of the four closest input cells that were weighted according to their distance. The DEMs applied for only the Nevado del Plomo glacier were clipped to a 17 x 13 km raster and the DEMs used for the modelling of the catchment area to a 25 x 40 km raster. The spatial reference was set to the projected coordinate system *WGS 1984 UTM Zone 19s* for all DEMs. Since the observation dates are years apart, elevation models of different sources had to be taken. Table 1 shows an overview of the used DEMs for the GlabTop runs.

In 2006 the surging period started in February and since the ASTER DEMs of the time before February have too many voids or do not cover the whole glacier, the Aster DEM of February 21, 2006 was taken (Dussaillant et al., 2019). For the DEM input of the year 2010, the TanDEM-X 2011 (DLR) was prepared by setting the black areas (minus height) to *no value* using the *Set Null* tool and resampling the 12 m cells to 30 m cell size using the bilinear resampling method. This was necessary as all other input DEMs have a 30 m cell size.

5.4.2.3 Branch Lines

To keep the branch lines as similar as possible over the examination years, the base branch lines were drawn corresponding to the glacier extent in 2010 of the ING (IANIGLA, 2018) and the most recent imagery. Depending on the particular glacier extent of the other examination years, the branch lines were adjusted using the *editor* tool of ArcGIS Pro.

For the glacier condition according to the historical map of Helbling (1919), the branch lines were extended in the steep accumulation part as at this time the glacier was not separated yet. Furthermore, two additional branch lines were drawn to indicate the side branches from the steep slopes in the north. In comparison to the glacier extent of the year 2010, most branch lines needed

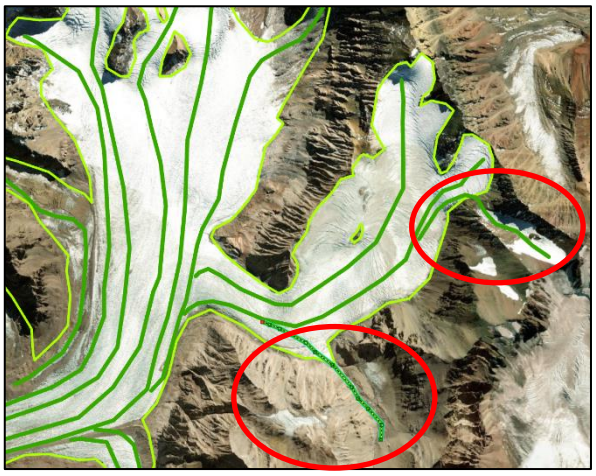

Figure 27: Screenshot of the ArcGIS Pro desktop showing the branch lines which needed adjustment to the glacier outline of 2020 (red circles).

to be shortened or even deleted to use them as the input data for the years 2000 and 2006, while the glacier branch lines needed no adaption for the year 2008. From 2010 to 2020 the glacierized area declined and therefore, most branch lines were shortened (see Figure 27).

5.4.3 Overview of the GlabTop Runs

To summarize the data preparation for the GlabTop model, Table 1 shows the different runs with the according sources and recording dates of the DEMs and the images which were considered while adjusting the outlines of the NGI and the branch lines. The results of run 9 and 10 are presented in the appendix.

Table 1: Overview of the GlabTop runs 1-6 of the Nevado del Plomo glacier (NdP) and the runs 7-10 for the Plomo catchment area, showing the sources of the used DEMs and images which were applied to draw the outlines. Years written in brackets in the column "Year" indicate that the year of the outline differs to the year of the DEM.

Run	Year	DEM	Sources to determine the outlines	NdP	Catchment Area
1	1910	**Digitized historical map of 1908-1912** R. Helbling (1919)	Map of Helbing (1919)	X	
2	2000	**SRTM (11-22 February 2000)** USGS (2018)	Landsat-5 images: 07.27.1999, 02.29.2000, 03.03.2001	X	
3	2006	**ASTER DEM (21 February 2006)** Dussaillant et al. (2019)	Landsat-5 images: 01.28.2006, 02.13.2006 Pitte et al. (2016: 121) World Imagery Wayback 23.02.2018 (Esri)	X	
4	2007	**ASTER DEM (23 November 2007)** Dussaillant et al. (2019)	World imagery Wayback 02.02.2014 (Esri) ASTER 30.03.2008 ASTER 27.03.2010 Landsat-5 10.07.2007	X	
5	2010	**TAN-DEM-X (2011-2014)** German Aerospace Center (DLR)	National Glacier Inventory of Argentina (IANIGLA, 2018) ASTER 27.03.2010	X	X (**Run 7**)
6	2020 (2017)	**ASTER DEM (December 20, 2017)** Dussaillant et al. (2019)	Adaption of National Glacier Inventory of Argentina (IANIGLA, 2018) World Imagery 01.04.2020	X	X (**Run 8**)
9 10	2022_20m 2022_2m (2020)	**Pléiades DEM (February 07, 2022)** Etienne Berthier (2022) (Results in the appendix)	Adaption of National Glacier Inventory of Argentina (IANIGLA, 2018) World Imagery 01.04.2020		X

6 Results

In this chapter the results of the applied methods are presented. To have a short and clear overview of the three main surge events of the Nevado del Plomo glacier, the events are firstly summarized in a table and compared with each other. Subsequently, the results of the DEM-differencing are displayed before the results of the GlabTop model runs are depicted. Finally, the results of the surge model are shown.

6.1 Comparison of the Past Surge Events and Temporal Lakes

Table 2 shows an overview of the reported characteristics in the literature of the three well documented surge events of the Nevado del Plomo glaciers. Considering only these events, the quiescence phase lasted 51 years between the surge in 1933 and 1984, and 22 years between the surge in 1984 to 2006. However, taking the possible surge event between1963 and 1973 in consideration, the quiescence periods between the surges would have been approximately 30 years, 21 years and 22 years, assuming a surge initiation in the year 1963.

Table 2: Overview of the three well documented surge events. Dashes mean no data. Sources according to the chapter 3.5.

Surge	Start	End	Advance [km]	Max Rate [m / day]	Dam Volume [m^3]	Lake Length / Width	Lake Volume [m^3]	Date of Flood	Primary Source
1933	-	~ Dez 1933	4.5	-	60 x 10^6	3 km / -	30-55 x 10^6	10. Jan 1934	Helbling, 1940
1984	16. Feb 1984	14. Nov 1985	2.7	16	27 x 10^6	2.8 / 1.1 km 1.5 / 0.7 km	55 x 10^6	14. / 22. Feb and 30. March 1985	Espizua and Bengochea, 1990 Bruce et al., 1986
2006	5. Feb 2006	16. Sept 2007	3.0	35	83 x 10^6	0.19 / 0.045 km	-	-	Pitte et al., 2016

The last two surges both started in February (austral summer) and had a similar duration of 19 to 20 months, but the ice volume of the dam is estimated to be more than three times higher in 2007 (83 x 10^6 m^3) than in the year 1985 (27 x 10^6 m^3) (Bruce et al., 1986) and it even exceeds the dam volume of the year 1933. However, it must be mentioned, that the sources did not mention how the dimension of the dam was defined. The maximum velocity of the glacier flow during the active phase in 2007 with 35 m / day was more than doubled in comparison with the maximum velocity of the surge in 1984-1985. In contrast, when comparing the lake volume, it is visible that the lake dimensions after the surge in 2007 are negligible in relation to the 3 km long lake in 1934 and the lake in 1985 with a length of 2.8 km. According to the sources, the terminus advance of 4.5 km during the active phase of the surge in 1933 was the longest of the three documented surges.

6.2 DEM-Differencing

To examine the ice displacement during the active phase of the last surge of the Nevado del Plomo glacier between February 5, 2006 to September 26, 2007, several ASTER DEMs of different dates were subtracted from each other. Looking at the DEMs of Difference (DoDs) of the Nevado del Plomo glacier, the elevation changes in the different phases are visible (Figure 28). Previous to the surge initiation in 2006 an increase in surface altitude is visible on the glacier tongue on the lower half of the glacier, whereas in the upper half of the glacier no striking elevation gain is observable. The mean elevation change between 2000 and 2006 (Figure 28A) of the lower half of the Nevado del Plomo glacier is a gain of 29 m. In the same area but during a two-year time span between 2004 and 2006 (Figure 28B) the mean elevation change is 11 m and the maximum increase of mass has shifted to the glacier terminus.

According to the DoD of February 2006 to December 2006 (Figure 28C) the surging phase is not obvious as no elevation gain is visible below the glacier terminus. However, in the DoD of the second part of the active phase from February 2007 to the end of the active phase in November 2007 (Figure 28D), an elevation gain with the shape of a glacier tongue is clearly visible, whereas in the upper part of the glacier, where previous to the surge an elevation gain was detected, a decrease of the surface elevation is recognizable. Comparing the DoD of the second part of the active phase with the DoD covering the whole time span of the surging phase from February 2006 to November 2007 (Figure 28E) the differences are minimal which indicate that ice mass transfer had happened mainly during the second half of the active phase. By separating the post-surge outline of the Nevado del Plomo glacier into two single polygons, delimited where the elevation change values switch from gain to loss, the volume change could be calculated. For the upper part of the Nevado del Plomo glacier a volume loss of -54'000'979 m^3 and for the enlarged glacier tongue a gain of 66'452'752 m^3 was calculated. The mean elevation changes in the upper area amounts to -18 m and in the lower area to 47 m. However, it must be noted that this is only a rough estimation as the ASTER DEMs are biased in the lower area, visible as a band which runs across the lower part of the glacier tongue of the Nevado del Plomo glacier. After the end of the active phase on September 26, 2007, a surface lowering on nearly the whole glacier area can be determined with an average elevation loss over the whole glacier of -5.4 m. The subsidence is even more evident in the DoD which compares the DEM of the end of the surge phase and the DEM of 2017 (Figure 28G) and shows an average elevation loss of -39 m in the lower part of the glacier. Nevertheless, an elevation gain is visible in the upper part of the glacier with values around 10-30 m.

Figure 29 shows the elevation changes of the Plomo valley glaciers during the time of the surge and the changes since the end of the active phase in 2007 until the year 2017. In the DoD of the time shortly before the surge started and after the surge (Figure 29A) it is visible that apart from the Nevado del Plomo glacier only the Grande del Juncal glacier shows a similar mass gain and mass loss pattern while on the other glaciers the mass loss mainly dominates, especially on the lower part of the glaciers. In between the time from 2007 to 2017 the Nevado del Plomo glacier, the Oriental del Juncal and the glaciers next to the Grande del Juncal show a negative elevation change (Figure 29B). At the terminus of the Grande del Juncal the surface elevation has increased while an elevation loss is displayed on the glacier tongue. The glacier in the south of the Nevado del Plomo glacier shows also an unusual elevation change with an elevation gain at the front of the glacier and a loss in the back.

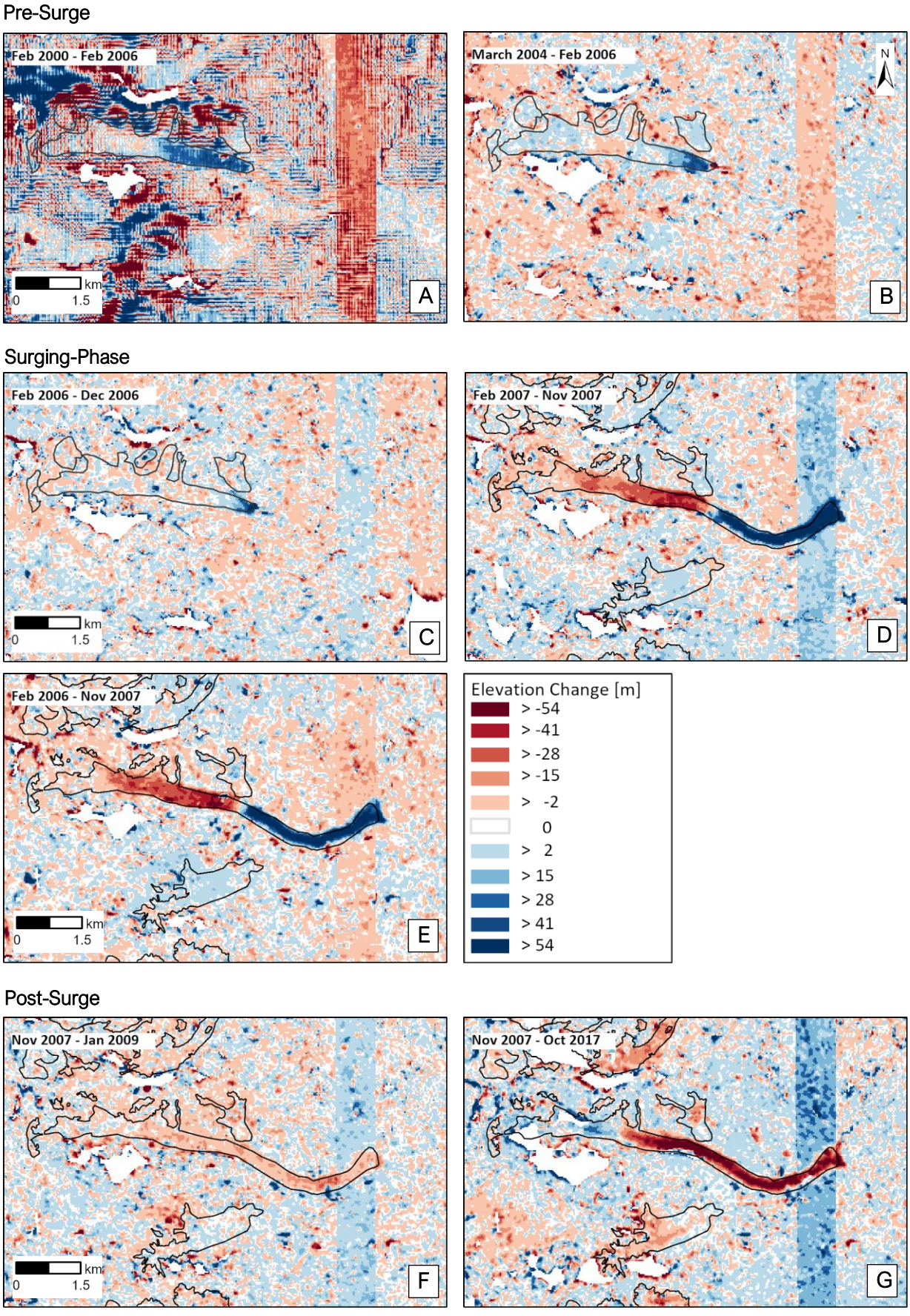

Figure 28: DEMs of difference of several dates before, during and after the surge of the Nevado del Plomo glacier in 2006-2007 showing the elevation change in meters. The glacier outlines in black correspond to the glacier level of the year 2006 (pre-surge) or 2010 (post-surge).

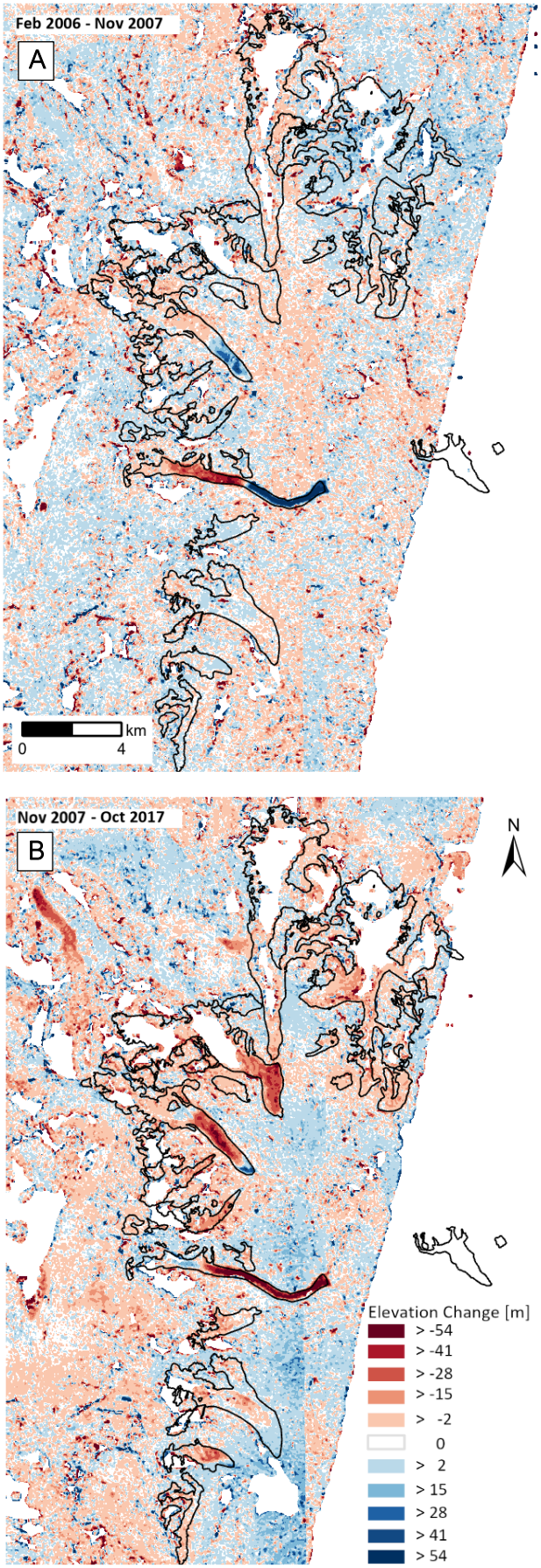

Figure 29: DEMs of difference of the Plomo valley showing the elevation gain and loss in meters of the period A) Feb 2006 to Nov 2007 and B) Nov 2007 to Oct 2017. The big white holes represent voids in the dataset and do not stand for zero elevation change.

6.3 Glacier Flow Model Experiments

6.3.1 Modelling Reconstruction of the Surge 2006-2007

To reconstruct the surge of 2006-2007, the pre-surge glacier geometry of 2006 is approximately built by running the model into a steady state (300 years) with an ELA of 5100 m a.s.l. (see Chapter 5.3.2 and Figure 22/1y). This initial geometry was then used to apply the different forcings with the glacier flow model. A surge with a similar extent as the 2006-2007 surge was reached by applying the surge forcing option for the duration of 2 years (model running time 1-3y) with an increase of the ice softness by a factor of 200 below the glacier bed elevation of 4300 m (red line in Figure 30). Figure 30 shows the advancing surging front which has already reached the Plomo valley after the first year of forcing. After switching off the surge forcing in year 3, the glacier stagnates and starts to slowly melt back.

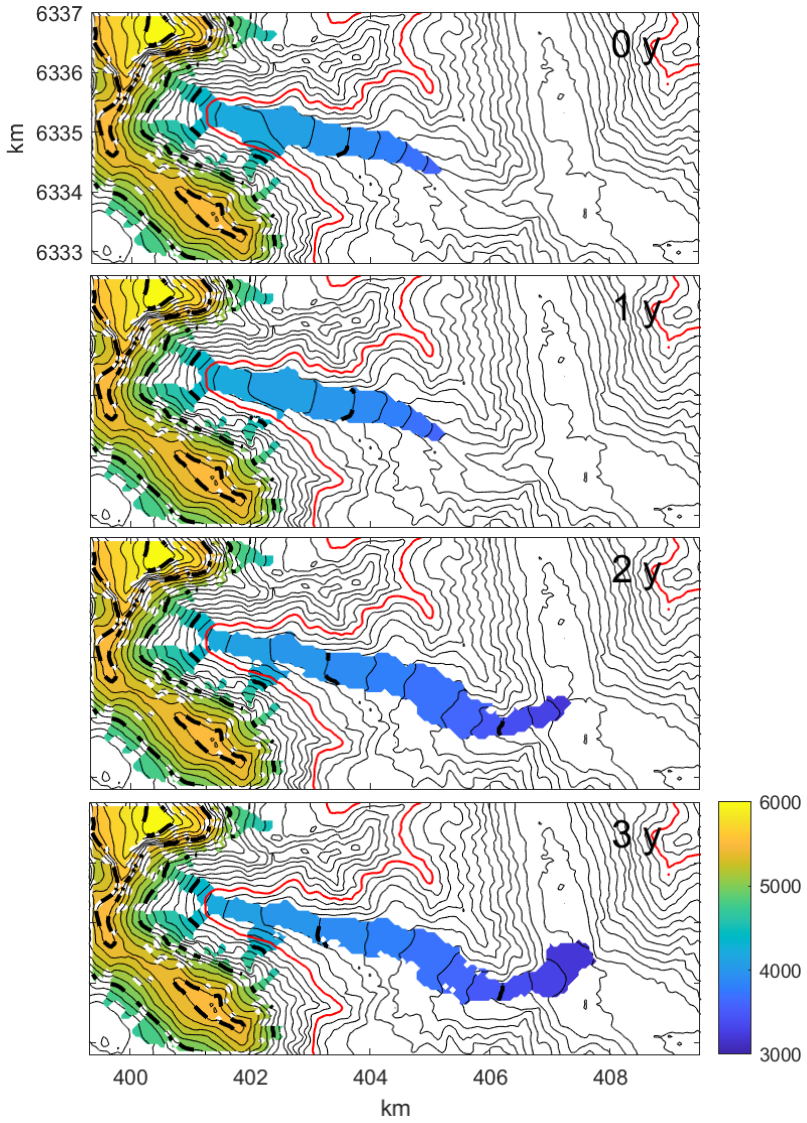

Figure 30: Modelling results of the surge step change of the Nevado del Plomo glacier. Figures of the year 1-3 show the advancing surge front and the figure of the year 4 the end of the active phase. The red line represents the altitude below which the increased ice softness was applied for 2 years (4300 m a.s.l.). The colors represent the surface height altitude. The ELA was set to 5100 and the mass-balance gradient to 0.004.

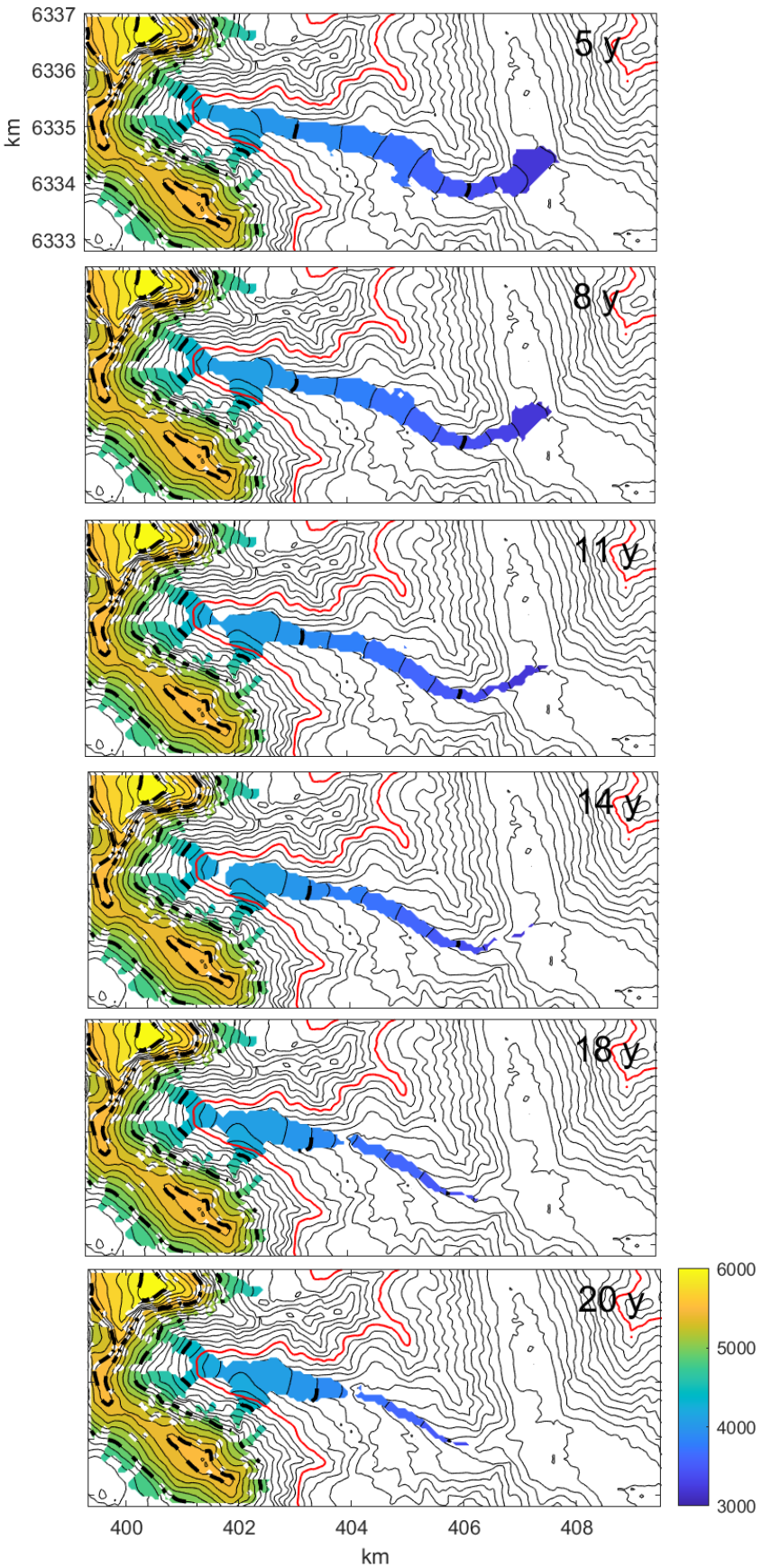

Figure 31: Continuation of Figure 30 showing the melt of the previously advanced glacier tongue of the Nevado del Plomo glacier. The red line represents the altitude below which the ice softness was increased for 2 years (4300 m a.s.l.). The colors represent the surface height altitude. The ELA was set to 5100 and the mass-balance gradient to 0.004.

In Figure 30 the mass transfer during the surging phase is evident as the upper part of the Nevado del Plomo glacier rapidly thins and loses in width and the glacier front advances and widens. According to the modelling results, the advance of the glacier front mainly occurs during the first year of the forcing because the glacier front already reaches the Plomo valley (Figure 30/2y). In the second year of the forcing, the glacier mass then mainly spreads in the Plomo valley and reaches the Río del Plomo. Figure 31 shows the depletion phase after the surge, in which the glacier tongue depletes from year to year until in the year 18 the tongue separates and the lower part of the tongue remains as dead-ice. Regarding the upper part of the glacier, it is visible that the recovery of the glacier mass is not yet finished in the year 20, as the mass is still smaller compared to the initial glacier geometry. Nevertheless, it is visible that in the year 18 the ice masses flowing down the steep glacier walls reach the main glacier again and supply it with new glacier ice.

6.3.2 Abrupt Cooling Event Experiment

The second forcing experiment which was tested was the climate step change (cooling event) and starts with the same 2006 initial geometry as the previous surge experiment. For this the ELA was shifted down from 5100 to 4300 m a.s.l. for 3 years to simulate a three-year phase with a high mass balance compared to the normal state of the glacier. The results show that the lower glacier slightly thickens and steadily advances but only slowly for 20 years (Figure 32). An abrupt mass

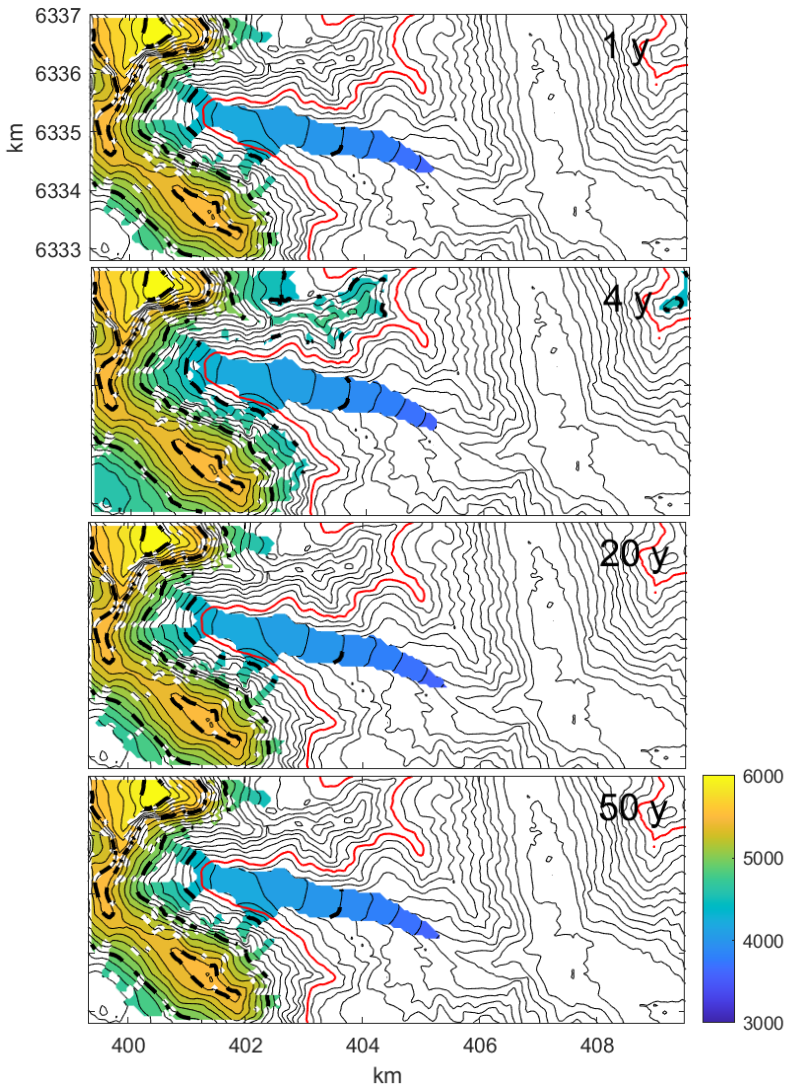

Figure 32: Glacier flow model output after an ELA lowering of 800 m for 3 years (year 1-4). The red line indicates the ELA position (4300 m a.s.l.) during the forcing period. Colors indicate the surface elevation in m a.s.l.

transfer down the valley does not occur. The glacier is in its initial position again after 50 years. Additional more extreme experiments showed that even a lowering of the ELA by 1000 m for 4 years did not show a remarkable glacier advance.

6.3.3 Modelling of a Surge with the 2020 Glacier Conditions

The identical surge parameters (ice softening and surge duration) as for the reconstruction of the 2006-2007 surge were used to model a surge with the approximate glacier geometry of the year 2020 (Figure 33/1y). The ice softness was again 200 times increased for the duration of 2 years (1-3y) below a surface altitude of 4300 m a.s.l. (red line in Figure 33). The only difference to the earlier surge experiment is the initial glacier geometry which in the year 2020 had a smaller area and a shorter glacier tongue length and therefore was modelled using an ELA of 5160 m a.s.l. instead of 5100 m a.s.l. The results, visible in Figure 33 and 34, show that the surging front also advances rapidly down the valley but not quite as fast and far as in the earlier experiment (Figure 30/2y). After the second year of the forcing (Figure 33/3y), the glacier front reaches the Plomo valley. However, this time the ice masses do not spread across the valley and do not reach the Río del Plomo.

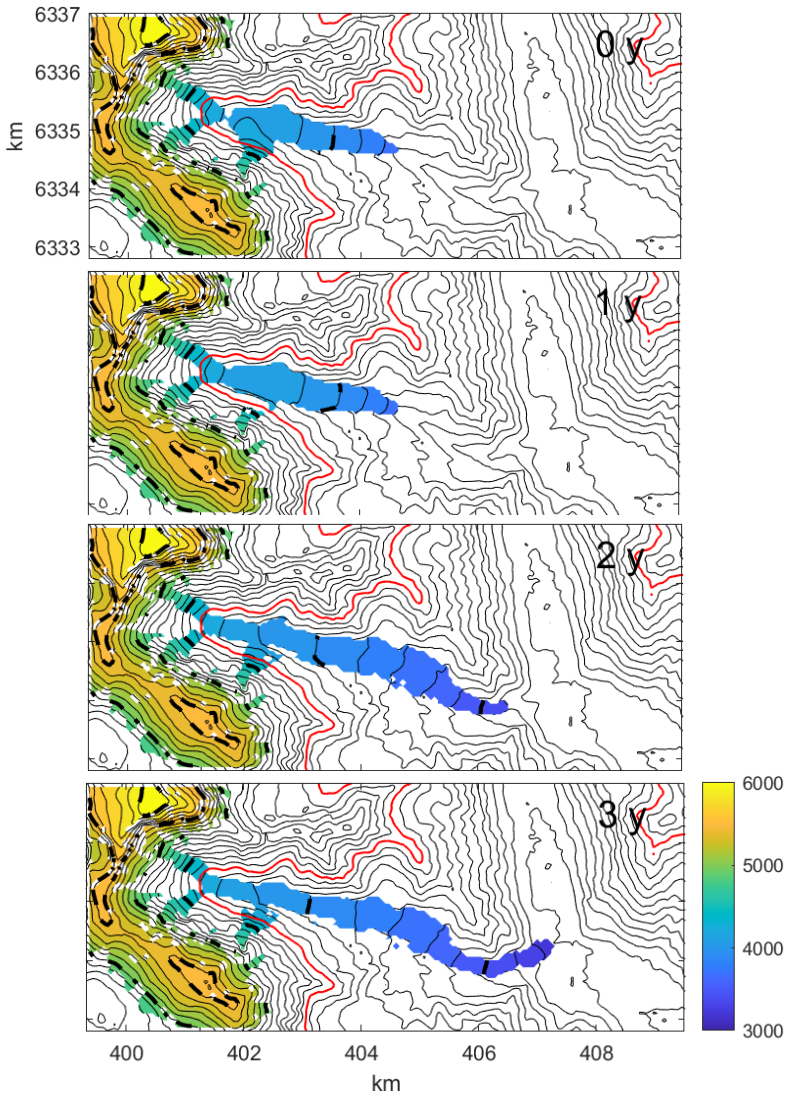

Figure 33: Modelling result of the first 3 years of the surge step change of the Nevado del Plomo corresponding to the glacier conditions of 2020. The red line represents the altitude below which the increased ice softness was applied for 2 years (4300 m a.s.l.). The colors represent the surface height altitude. The ELA was set to 5160 and the mass-balance gradient to 0.004.

As soon as the ice softness is set back to normal, the glacier tongue loses mass and starts retreating. After 15 years the glacier tongue is already separated until after 25 years the lower dead-ice part is melted completely, and the glacier is close to its initial geometry after 35 years.

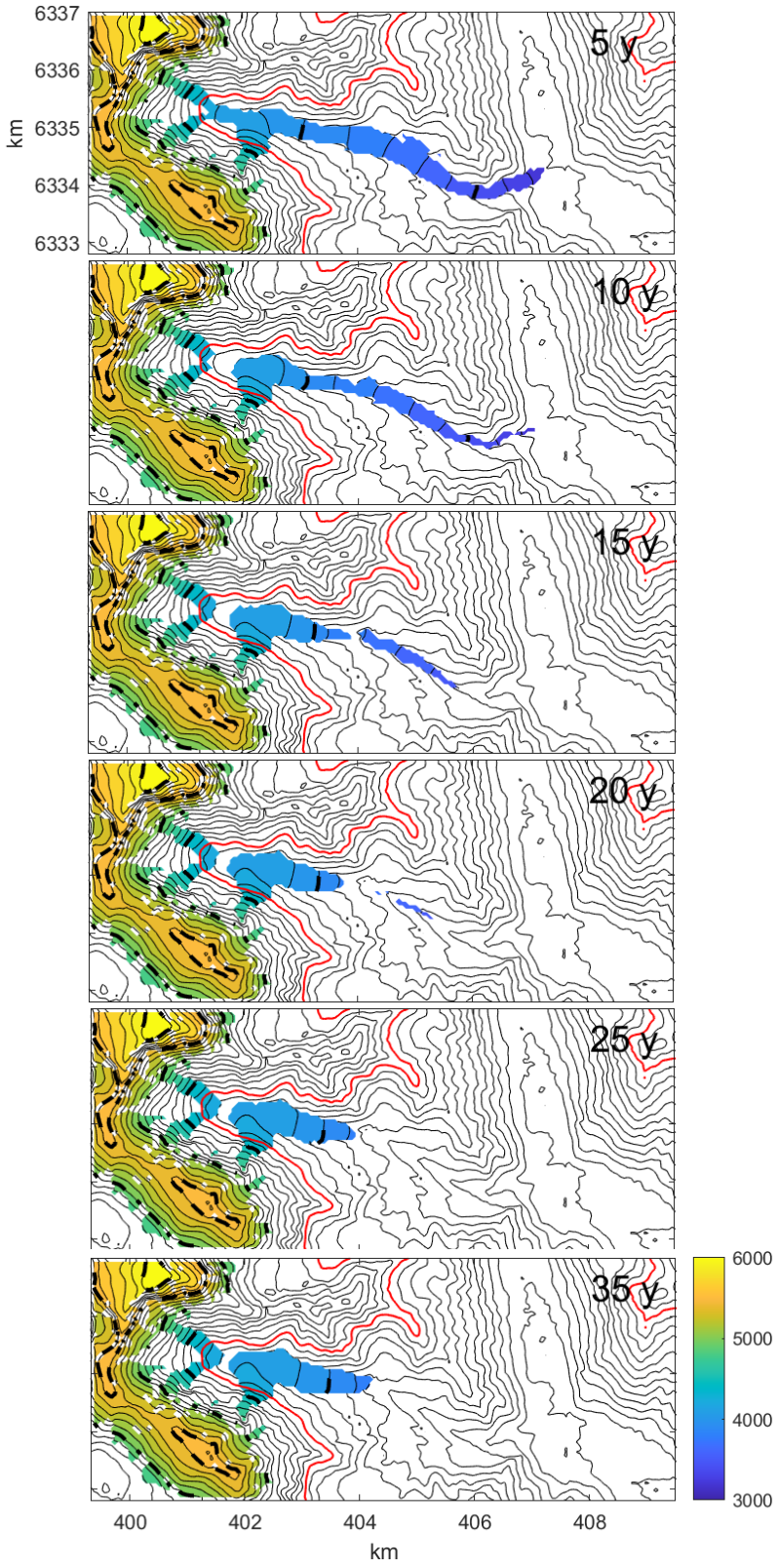

Figure 34: Continuation of the Figure 33 showing the melt of the previously advanced glacier tongue of the Nevado del Plomo glacier. The red line represents the altitude below which the ice softness was increased for 2 years (4300 m a.s.l.). The colors represent the surface height altitude. The ELA was set to 5160 and the mass-balance gradient to 0.004.

6.4 Results of the GlabTop Model

6.4.1 Ice Thickness Evolution of the Nevado del Plomo Glacier

The main results of the GlabTop model runs for each input year are shown in Table 3 and the corresponding figures, showing the ice thickness distribution, are depicted in Figure 35.

According to the output of the GlabTop model, considering the DEM and outlines of the digitised historical map of the year 1912, the Nevado del Plomo glacier has an area of 7.42 km^2 and an ice volume of 0.27 km^3. Contrary to the other examined years, there is still ice on the north facing slope in the upper glacier area (Figure 35). Additionally, the glacier is connected with all side branches apart from the ice mass in the north-east. The ice-volume of the main glacier tongue is 0.2578 km^3 and 0.0114 km^3 for the glacier part in the north-east. In the steep slopes (> 50°) of the upper part of the Nevado del Plomo glacier the ice thickness varies between 1 to 15 m close to the margin of the glacier and it increases downwards to approximately 45 m. Following the glacier flow direction, the ice thickness increases gradually until in the middle of the glacier the maximum thickness of 137 m is reached at a surface elevation of around 4050 m a.s.l. Further down, on the glacier tongue, the ice thickness increases from the sides to the middle where values of 50-75 m are reached. The separate part of the glacier in the north-east has a mean ice thickness of 13 m and a maximum ice thickness of 38 m.

Between the year 1912 and 2000 the Nevado del Plomo glacier surged at least twice and the glacierized area decreased from 7.42 km^2 to 3.79 km^2. Additionally, the glacier ice on the north facing slope vanished. The ice thickness distribution of the remaining ice is very similar to the year 1912 and the part with the most accumulated ice remains approximately at the same location as well as the point with the maximum ice thickness of 128 m.

Between 2000 to 2006 the decrease in the glacier area and ice volume was small but contrary to this decrease, the mean ice thickness increased to 52 m. The area with an ice thickness above 105 m enlarged compared to the year 2000. The maximum ice thickness value increased to 147 m and is shifted slightly upwards. The extent and volume of the separated ice masses remained similar to the year 2000. The input DEM of this model run was recorded in February 2006 when the surging phase had just started.

Table 3: Main results of the GlabTop runs calculation of the Nevado del Plomo glacier for the examination years 1912, 2000, 2006, 2008, 2010, and 2020. All disconnected glacier parts were taken into consideration for the calculation of the glacier area, ice volume and ice thickness maximum. However, for the mean ice thickness determination only the main glacier part was considered.

Year	Area [km²]	Ice Volume [km³]	Ice Thickness Maximum [m]	Mean Ice Thickness [m]**
1912	7.421	0.2693	137	39
2000	3.794	0.1550	128	50
2006	3.744	0.1520	147	52
2008	5.426	0.2650	132	57
2010	3.751	0.1420	156	40
2020*	2.540	0.0910	102	43

* Outlines according to the 2020 satellite image (Esri 2020) but ASTER DEM of the year 2017

** For the mean ice thickness only the connected valley glacier part of the Nevado del Plomo glacier was considered

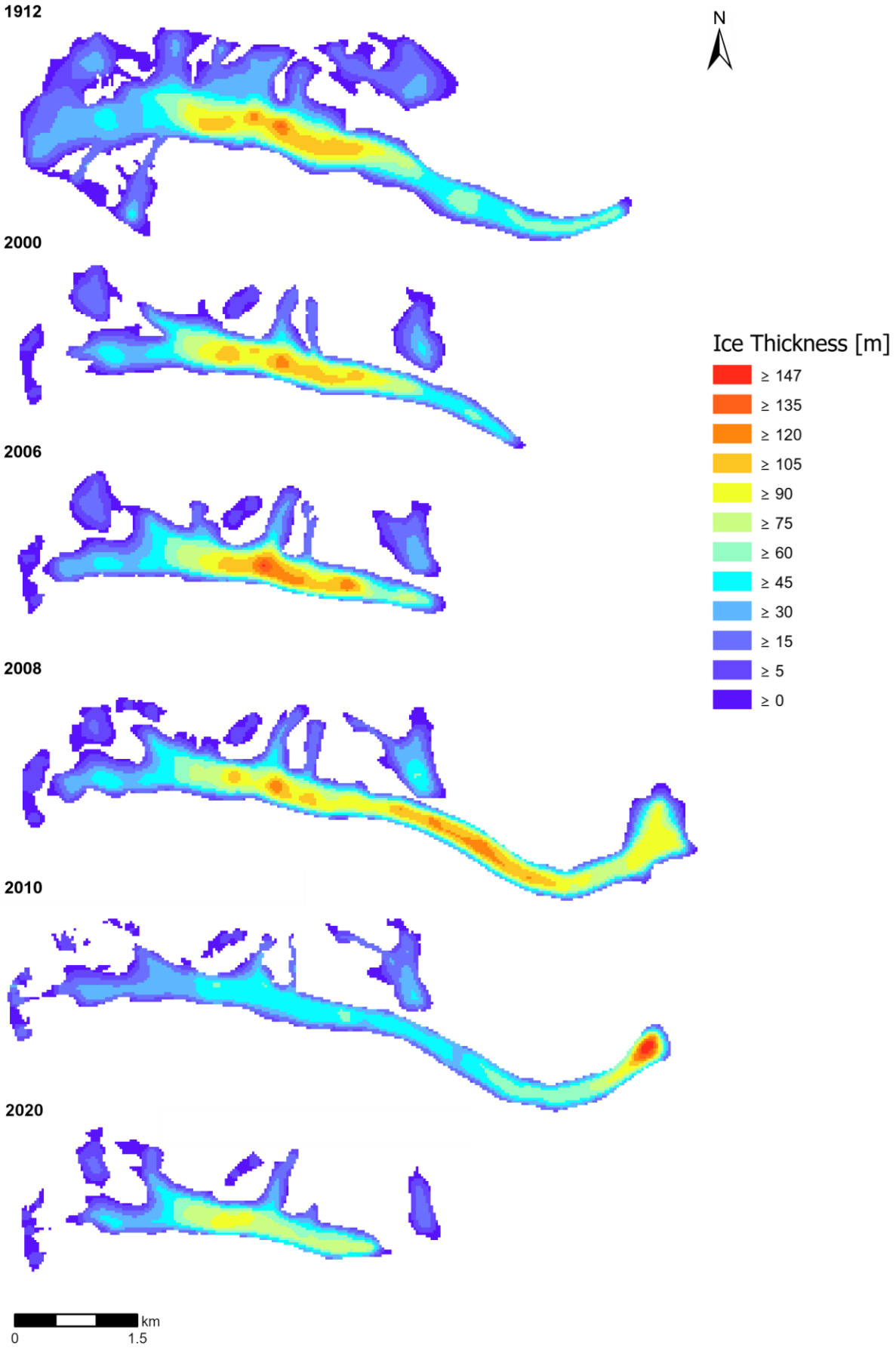

Figure 35: GlabTop model results showing the ice thickness distribution of the input years 1912, 2000, 2006, 2008 and 2020. The output of the year 2006 corresponds the date of the surge initiation and the figure of the year 2008 shows the glacier condition shortly after the surging phase ended.

After an active phase of 19 months, the surge ended in September 2007. The figure of the GlabTop output for the year after the surge in 2008 shows an elongation of the glacier tongue. The glacier terminus reaches the Río del Plomo and the width of the glacier front increases as the ice is piled up on the opposing valley wall. At the point where in the output of the earlier years the maximum ice depth was reached, an ice thickness of 132 m is still modelled but the whole part with an ice thickness of more than 105 m is moved downwards. The ice thickness in the middle of the glacier terminus, where the ice masses dam the Río del Plomo, is around 100 m.

Within the following two years the glacier area and volume declined, especially in the middle part of the glacier, where the ice thickness of the previous years was at least 75 m, it is in 2010 thinner than 60 m. Beside the main glacier tongue, the extent and volume of the separated ice masses are smaller as well. The glacierized part in the northeast has lost 0.0031 km^3 volume within two years but has still more ice volume than in the outputs of the years 2000 and 2006. Oppositional to the overall thinning, the lowest part of the glacier, where the ice masses were stopped due to the valley wall during the surge, the ice thickness increased up to 156 m according to the model output.

Since 2010, the Nevado del Plomo glacier has lost much of its area. For the year 2020 the GlabTop model run results in a glacier area of 2.54 km^2 and an ice volume of 0.0910 km^3. Comparing the glacier conditions of 2020 to the pre-surge glacier conditions of 2006, the glacier area diminished by 32.2% and the volume reduced by 40.1%. Since the first model output of the year 1912, the Nevado del Plomo glacier lost 65.7% of its area and 66.2% of its ice volume. The general ice thickness distribution remained somewhat the same, but the maximum ice thickness shrunk to 102 meters. In the highest area of the main glacier the ice thickness partly increased since the year 2010, but the area of the glacierized part in the northeast became smaller.

Summarized, it can be said that the ice thickness distribution remained relatively uniform, and the ice volume was gradually decreasing over the years except for the GlabTop model results of the years shortly before and after the surging phase of the Nevado del Plomo. Additional model results using a Pléiades DEM (2 m, 20 m) of 2022 as input are presented in the appendix.

6.4.2 Length Change of the Nevado del Plomo Glacier

Additional to the GlabTop runs, the glacier length was measured using the same outlines as for the GlabTop model run. For this purpose, a central flow line was drawn in ArcGIS Pro according to which all the lengths were measured. Even though the glacier is not fully connected anymore from the valley to the mountain ridge, the length was always measured from the top of the ridge downwards. This enables a comparison of the lengths and distances of the glacier terminus to the Río del Plomo. According to the digitised map of Helbling (1910-1914), the Nevado del Plomo glacier had a length of 7.85 km in 1912. The distance from the glacier terminus to the Río del Plomo was 0.65 km. This is the smallest distance measured apart from the examination years directly after the surge (2008 and 2010), when the glacier ice reached the Río del Plomo and the whole glacier had a length of 8.5 km. Between the years 2000 and 2006 the glacier length shortened from 6.40 km to 5.25 km, and the glacier terminus was approximately 3.25 km apart of the Río del Plomo shortly before the surge started in 2006. In 2010, the glacier front was still close to the Río del Plomo and hence the length was 8.5 km. Within the following 10 years, the glacier retreated to a length of 4.60 km.

6.4.3 Ice Thickness Distribution of the Plomo Area in 2010 and 2020

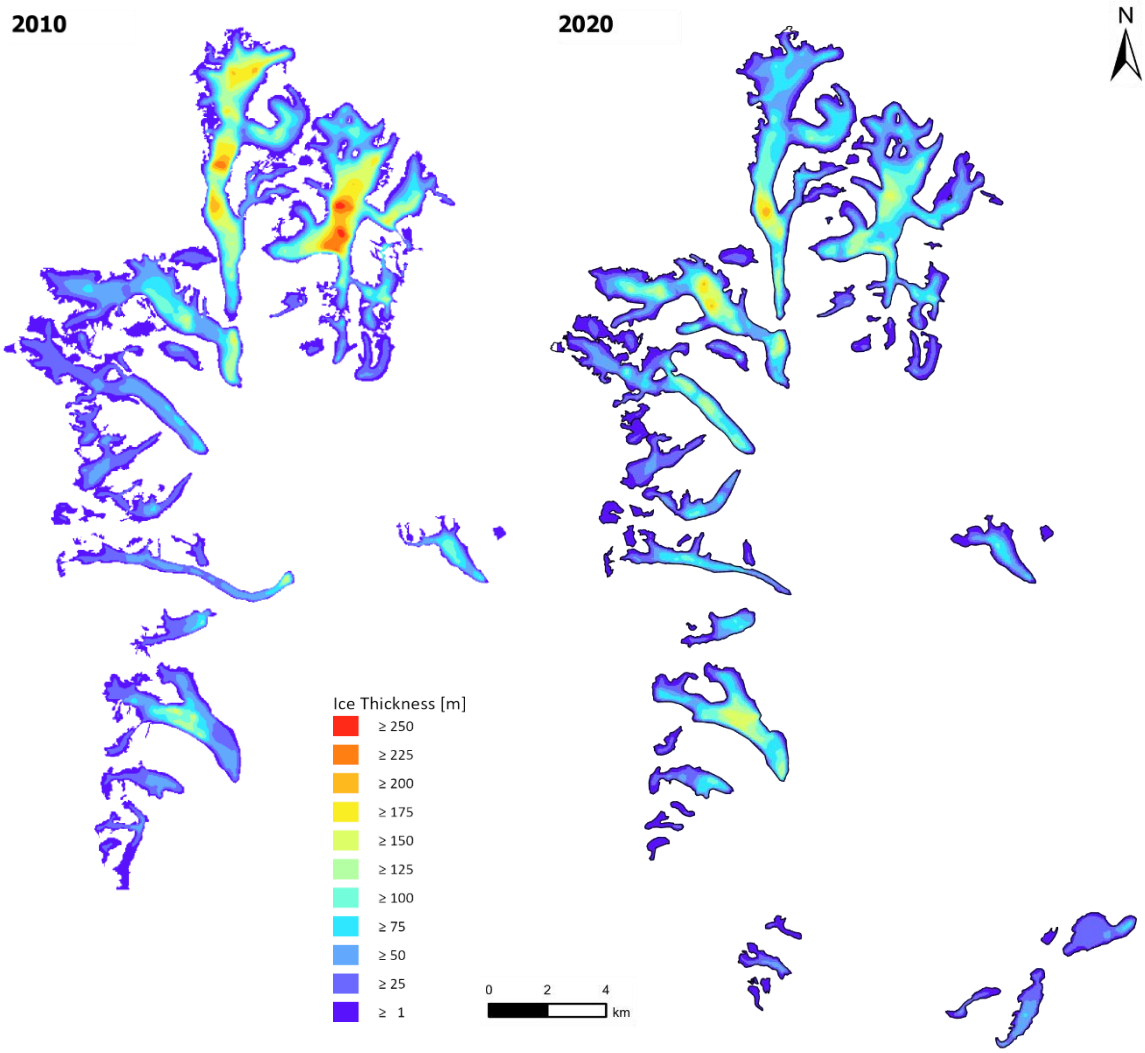

Figure 36: Comparison of the ice thickness distribution of the Plomo area of the years 2010 and 2020. For the figure of the year 2010 the glaciers in the south are missing as the DEM had voids.

To compare the ice volume of the Plomo valley between the years 2010 and 2020, two GlabTop model runs were conducted with the outlines of the Nevado del Plomo glacier and its neighboring glaciers. The ice thickness distribution is visible in Figure 36, however, it must be noted that the glacierized parts in the south of the Plomo valley (only visible in the 2020 part of Figure 36) are not considered in the calculations since the DEM of the year 2010 has a void in this area and therefore no result could be generated for these glaciers by the model. Overall, the glaciers covered an area of 82.116 km^2 in 2010 and an area of 69.178 km^2 in 2020 which results in a decrease of 12.938 km^2 (15.76%) within 10 years. The change of the ice volume shows a similar pattern. According to the GlabTop model results, the Plomo valley contained an ice volume of 4.56 km^3 in the year 2010 and 3.84 km^3 in the year 2020. The difference of -0.72 km^3 corresponds to an ice volume decline of 15.88%.

Regarding the glacier area in Figure 36, an overall ice thickness decrease is apparent comparing the output of the year 2010 to the year 2020. Nevertheless, the ice volume decrease is not as obvious. Visually, only for the two biggest glaciers in the north of the valley, the Alto del Plomo and the Bajo del Plomo glacier, the reduction of the area and ice thickness is evident. The Alto del Plomo glacier lost 0.4405 km^3 ice volume (-32%) during the years 2010 to 2020 and the Bajo del

Plomo glacier lost 0.5770 km^3 (-39%). Contrary to those two glaciers, the ice volume of the Oriental del Juncal and the Grande del Juncal increased by 21% and 44% to 0.6517 km^3 for the Oriental del Juncal and 0.3262 km^3 for the Grande del Juncal glacier. Despite the increasing ice thickness of those two glaciers, the area of the glaciers decreased similarly to the neighboring glaciers whereof the area loss of 6% of the Grande del Juncal was the smallest of all glaciers in the area. The Bajo del Plomo glacier experienced the largest area loss in the Plomo valley with an area reduction by 22%. The glacier in the south of the Nevado del Plomo glacier recorded an area loss of 18% but the ice volume increased by 33%. This glacier has no name but will be called Innominado glacier further on in this thesis.

In 2010 the maximum ice thickness was modelled for the Bajo del Plomo glacier with 280 m. The average ice thickness of the Bajo del Plomo glacier was 78 m. In 2020 the average diminished to 62 m and the maximum ice thickness decreased by 106 m to 174 m. In 2020 the maximum ice thickness of the modelled area resulted in 221 m for the Alto del Plomo glacier (249 m in 2010).

6.4.4 Potential Future Glacial Lakes

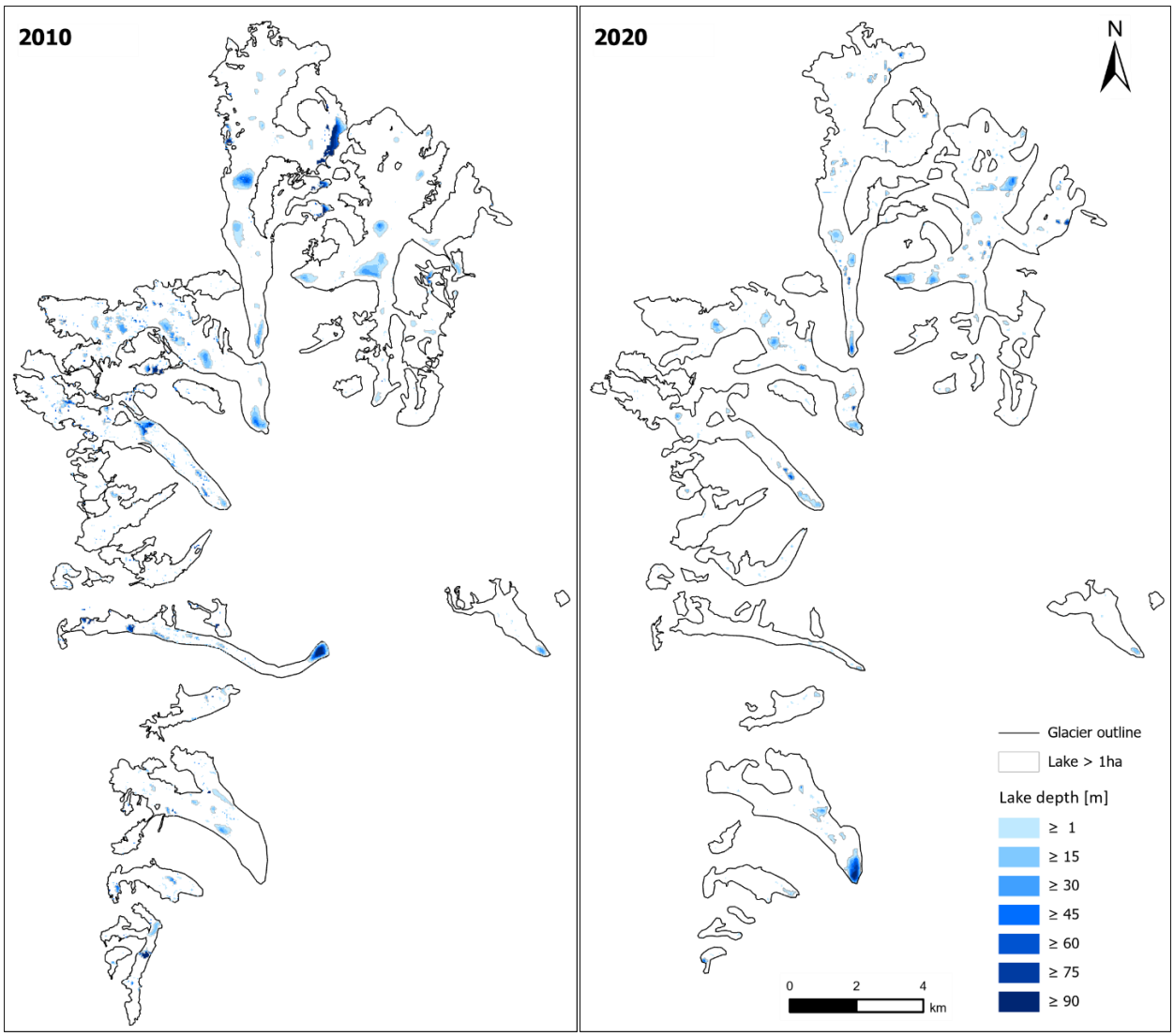

Figure 37: Glacier outlines of the Plomo valley of the years 2010 (left) and 2020 (right) with the modelled potential future lakes and their estimated depth in meter.

Figure 37 shows the potential future lakes according to the DEM and outlines of the year 2010 and 2020. The lakes are situated where overdeepenings of the glacier bed are modelled. Those overdeepenings are prone to fill with meltwater as soon as the glaciers retreat and the ice in the overdeepenings melts. For the inputs of the year 2010 the model calculates a total lake volume of 136 x 10^6 m^3 and a lake area of 4.598 km^2 of the defined Plomo catchment area. According to the output, a lake in the northeast of the Alto del Plomo glacier would be the one with the biggest volume, however, the formation of a lake in this area is unlikely and it is most probably an error in the DEM as the lake is not apparent anymore in the output of 2020. The lake with the second biggest volume (10.8 x 10^6 m^3) and a maximum depth of 115 m is modelled on the ice dam of the Nevado del Plomo glacier. The potential glacier lakes at the glacier tongue of the Oriental Juncal, Alto Plomo and Bajo del Plomo have a mean depth between 10-20 m and do not exceed a maximum depth of 65 m.

According to the GlabTop run with the input data representing the glacier extent of 2020, it is visible that overall the area of the predicted lakes is smaller than in the year 2010 with an area of 2.833 km^2. The total glacier volume of all potential future lakes according to the 2020 input is 51 x 10^6 m^3. Hence, in comparison with the output of 2010, the total area of the lakes has decreased by 1.764 km^2 and the total volume by 85 x 10^6 m^3.

Regarding the 2020 output (Figure 37/2020), some lakes are not modelled anymore such as for example the big lake in the middle of the Alto del Plomo glacier and the lake on the glacier tongue of the Nevado del Plomo glacier. Nonetheless, a new lake is modelled at the glacier tongue of the Innominado glacier in the south of the Nevado del Plomo glacier. The potential lake is estimated to have a volume of 13.390 x 10^6 m^3, a mean depth of 44 m and a maximum depth of 105 m. The predicted lake at the glacier tongue of the Bajo del Plomo is visible in both outputs and has a volume of 3.657 x 10^6 m^3 and a maximum depth of 47 m. Similar to the output of the year 2010, the mean depths of the lakes near the terminus of the glacier tongue in the north part of the Plomo valley are in between 10-20 m and the summed-up volume of those lakes is 7.888 x 10^6 m^3.

The individual GlabTop outputs of the Nevado del Plomo glacier for the years 1912, 2000, 2006, 2008, 2010 and 2020 show no additional big lakes compared to the area results. The lake in the upper part of the Nevado del Plomo glacier of the 2010 area output has a volume of 3.0 x 10^6 m but is not visible anymore in the 2020 output.

7 Discussion

In this chapter the results and methodological approach of the previous two chapters are critically analyzed and discussed. The methodological uncertainties are mentioned in the first part before in chapter 7.2 and 7.3 the results of the DEM-differencing, GlabTop model and the glacier flow model are discussed concerning the research questions. Finally, the focus is widened again by discussing the results regarding the ice volume and the possible future lakes of the whole Plomo valley.

7.1 Methodological Uncertainties and Input Data Quality

Several different input data for the three methods are used in this thesis. Therefore, to assess the quality of the results, the methodological uncertainties but also the quality of the input data must be considered.

One input data is the historical map of 1912 (Helbling, 1919), where the altitudes are based on one single measurement and therefore are not entirely accurate. However, the deviations are minor and for the GlabTop model only the relative accuracy is essential, since the ice thickness is calculated from the slope steepness. In addition, the comparison of the ice thickness distribution of the different years (see Figure 35) also shows that the model output of the year 1912 indicates a similar pattern across the Nevado del Plomo glacier as the outputs of the other years which are based on ASTER DEMs. Thus, the quality is comparable with the ASTER DEMs.

In addition to the the GlabTop runs, The ASTER DEMs with a resolution of 30 m, were also applied for the DEM-differencing method. Dussaillant et al. (2019) used the same ASTER DEMs but determined the surface elevation change of the pixels by fitting a linear regression through a time series of multiple ASTER DEMs, whereby the accuracy was increased. Since in this thesis, the DEM-differencing was applied to examine the ice displacement shortly before, during and after the surge, and only a few ASTER DEMs of the relevant dates were usable, single ASTER DEMs were compared with each other. In the results (Figure 28), a bias is visible as a band of increased or decreased elevation change on the east side of the figures. Moreover, stable and ice-free terrains, such as rock walls and the valley bottom, should show zero or only minimal elevation change in the DoD, since the DEMs are recorded in summer when no snow should have been on the stable terrain. However, this is not the case as it is visible that nearly the whole DEM extract seems to have undergone an elevation change. Therefore, the values derived from the DEM-differencing should be taken with caution. Nevertheless, the general pattern of increase and decrease of the surface elevation before, during and after the surge of the Nevado del Plomo glacier is clearly visible and can be taken to illustrate and analyze the surge process.

Another source of uncertainties are the glacier outlines which were used as an input for the GlabTop model. The outlines of the NGI of Argentina for 2010 are taken as a base, but it was difficult to determine the outlines of the year 2000 and 2006 due to the insufficient resolution of the satellite images. The clean ice parts are recognized well, but the outline of the debris-covered parts of the glacier had to be supposed by flow structures.

It is also noticeable that the GlabTop model is created for typical glaciers rather than surging glaciers. Figure 38 shows that the ice volume between 2006 and 2008 increased by 74%. The increase in the area can be explained by the fact that the glacier tongue enlarged due to the surge, during which the ice mass from the upper part of the glacier was shifted downwards. However, the ice volume should not have increased, as the existing ice mass was just distributed over a

larger area. This would also mean that the average ice thickness of the glacier must decrease in comparison to the pre-surge glacier conditions which is not the case according to the GlabTop output of the year 2008. Since the GlabTop model calculates the ice thickness based on the glacier slope, the surface would have to become much steeper to indicate a lower ice thickness. During a surge, however, the opposite is the case. The surface becomes flatter as the accumulated ice mass of the reservoir area advances and distributes downwards over a larger area. Therefore, applying the GlabTop model for a surging glacier is most probably limited to the quiescence phase. However, for using the model for the quiescence phase, the same question, whether the model estimates the ice thickness correctly, arises. According to theory, the glacier slope steepness increases during the build-up phase due to the accumulation in the reservoir area and the restricted glacier flow. The steepening would, in turn, lead to a decrease in ice thickness according to the model, but this does not correspond to the build-up phase. Thus, the GlabTop results for the time shortly before and during a surge must be interpreted with caution.

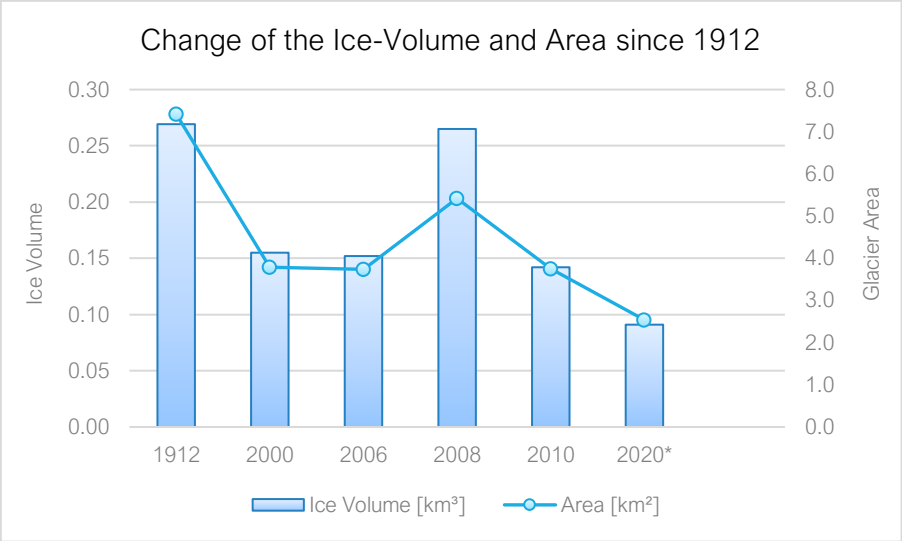

*Figure 38: Change of the ice volume and glacier area of the Nevado del Plomo from 1912 until 2020. *Outlines of the year 2020, but the input DEM of the year 2017.*

The quality of the results of the glacier flow model is mainly affected by the input file, which is the DEM of the glacier bed and the base for the model calculations. Additionally, knowledge of the accurate ELA and the mass balance gradient of the modelled glacier benefit the model's accuracy. However, as for the Nevado del Plomo glacier these data were lacking, different ELAs were tested out until the correct glacier length was reached. For the mass balance gradient an average value of the Echauerren Norte glacier was taken. Comparing the applied ELA of 5160 m a.s.l. for the steady state of the year 2020 with the modelled ELA of approximately 4500 m a.s.l. for glaciers situated at 33° S in the Central Chilean Andes (Barria et al., 2019), the ELA would be far too high. However, the goal of the model was to reconstruct the steady-state glacier geometry, which was only reached using this ELA height. Since the Nevado del Plomo glacier is surrounded by very steep slopes and is mainly fed by avalanches, it is difficult to reach the same glacier geometry with the model using the real ELA. Slopes steeper than 45° receive no accumulation in the model and avalanches are not considered as well. Thus, the focus was set on reaching the same glacier length as in 2006 and 2020, without scrutinising the ELA too much and experimenting with different forcings to initiate a surge.

7.2 Glaciological and Climatic Conditions of the Nevado del Plomo Glacier

7.2.1 Ice Volume of the Nevado del Plomo Glacier

The results of the GlabTop model indicate that the ice volume of the examined years of the Nevado del Plomo glacier reached its maximum in the year 1912, with a volume of 0.2693 km^3. It is not clear how the ice volume changed within the subsequent 21 years until the surge started in 1933. However, it can be assumed that the ice volume did not decline but rather increased, as the reconstructed mass balance of the Echaurren Norte glacier shows, on average, a positive mass balance in between the years 1912 to 1933 (Masiokas et al., 2016). Most ice of the Nevado del Plomo glacier is accumulated in the middle part of the glacier, below the steep walls where the glacier bed topography is flatter (see Figure 35). This makes sense since the steepness of the slopes prohibits a big snow accumulation, and the glacier is mainly fed by avalanches which flow down the steep slopes and pile up in the flatter glacier area. The ice thickness distribution showing the maximum value in the middle of the glacier, remained constant over the years. Six years before the last surge of the Nevado del Plomo glacier happened, the ice volume was 0.1550 km^3. Therefore, the ice volume of the glacier decreased by 42% within 88 years. Contrary to this decrease in volume, the mean ice thickness of the main glacier part increased by 11 m. This can be explained due to the glacier parts on the steep slopes with a small ice thickness which were still connected to the main glacier body in 1912 and therefore reduced the mean ice thickness of the Nevado del Plomo glacier. The biggest difference from the year 1912 to the year 2000 is the glacier area loss in the upper part of the glacier. The ice of the north-facing slope disappeared completely after 1912 due to the higher solar exposure, while the south-facing glacier parts became smaller or vanished as well. In comparison, the reconstructed cumulative mass balance of the Echaurren Norte glacier reveals a similar strong decrease of 40 m w.e. from the year 1940 to 2000 (Masiokas et al., 2016).

Shortly before the surge started in 2006, the ice volume of the Nevado del Plomo glacier was approximately 0.152 km^3. The glacier tongue has slightly retreated since the year 2000, but the mean ice thickness has increased, especially in the middle part of the glacier. This suits the general pattern of the build-up phase, which indicates that ice mass of the reservoir area increases while the glacier flow is still restricted, and the glacier tongue may even retreat (Pitte et al., 2016).

As mentioned before, the ice volume of the year 2008 cannot be accurate, since the ice volume should be similar to the volume of the glacier before the surge started. It is possible that there has been additional accumulation in this time period, but not to this extent. The distribution of the ice thickness seems also unrealistic as the ice thickness loss in the upper part is too small to build up the advanced glacier tongue. The output of 2010 is therefore more realistic since there has been a strong decrease in ice thickness in the upper part. The ice volume is even smaller than in the year 2006. Nevertheless, a thickness of more than 147 m at the glacier front seems unrealistic considering that the dam of 1933 was estimated to be 75 m (Helbling, 1935).

For the year 2020, thirteen years after the surge, an ice volume of 0.091 km^3 was modelled which is 40% less compared to the pre-surge ice volume of the year 2006. The loss of ice mass is also described by Ferri et al. (2020), according to whom the mass balance rate of the Nevado del Plomo glacier between the years 2000 and 2009 was only slightly negative with -0.07 ± 0.14 m w.e. yr^{-1} but then became even more negative during the period 2009-2018 with -0.97 ± 0.16 m w.e. yr^{-1}. Dussaillant et al. (2019) described that the average mass balance rate for the Desert Andes, Central Andes and North Patagonia are slightly positive from the year 2000 to 2009, while

the average mass balance rate between the years 2009 and 2018 was negative with -0.63 ± 0.18 m w.e. yr^{-1}. The reduction of the mass balance of the glaciers can be explained by the dry conditions due to the sustained drought in the Central Andes since 2010. The smaller ice volume of the glacier suggests that a current surge would not lead to the same length of glacier advance as in the previous surges when the Río del Plomo had been reached.

7.2.2 Ice Transfer During the Surge in 2006-2007

Whereas an alteration of the ice volume of a glacier usually takes a long time, the distribution of the ice mass can change in a less time, especially in the case of a surging glacier. To depict this, the comparison of the DEM-differencing results of the surge 2006-2007 enables to comprehend the ice displacement of the Nevado del Plomo glacier during the end of the build-up phase, the active phase and the depletion phase.

In Figure 28A and B, the glacier is still in the build-up phase, as the surface height increases strongly during the considered dates. Since the increase from 2000 to 2006 is much more extensive than during the last two years before the surge, it can be assumed that the build-up phase started before 2004 or even earlier. According to the theory (Jiskoot, 2011b), build-up phases can last decades, during which the glacier flow is restricted, and the glacier ice surface steepens.

Pitte et al. (2016) determined February 5, 2006 as the surge initiation, whereas Ferri Hidalgo et al. (2012) and Harrison et al. (2015) refer to September 25, 2006. According to the DEM-difference figure of February 2006 to December 2006 (Figure 28C), no surface increase below the pre-surge outlines of 2006 is evident. An increase in elevation is only visible close to the glacier front. Therefore, no surge activity can be detected according to the figure. In the DEM-difference figure of the second year of the active phase (February to November 2017), the glacier ice displacement from the upper part to the lower part is visible. The transition between the process of surface decrease to increase is located on the part of the glacier where before the surge the glacier front was positioned (Figure 28D). The more substantial advance during the second phase of the surge coincides with the measured maximum velocity of 35 m/d in May 2007 by Pitte et al. (2016). Since the DoD covering the surge period from February 2006 to November 2007 shows a similar surface elevation decrease and increase, the surge may have started later in 2006, as described by Ferri et al. (2012) and Harrison et al. (2015).

The ice volume that moved from the upper part down to the valley during the surge is approximately 54 x 10^6 m^3. For comparison, Helbling (1935) estimated a moving ice mass of 35 x 10^6 m^3 during the surge of 1933-1934 but mentioned that the calculated ice mass of 60 x 10^6 m^3, according to the field reports of the engineers Eliot and King, may also be possible. Considering that the glacier before the surge in 1933 was much longer than in 2006, but during both surge events the glacier masses reached the Río del Plomo, the calculated volume seems to be a good estimation. Pitte et al. (2016) estimated the displaced ice mass during the last surge of the Horcones Inferior glacier to 10^8 m^3, which is much more, yet explainable due to the larger area and length of the glacier compared to the Nevado del Plomo glacier.

After the active phase, the depletion phase follows, in which the displaced ice during the surge starts to melt. In the upper part of the Nevado del Plomo glacier, the reservoir slowly recovers, meaning that ice mass accumulates again. The surface lowering of the glacier tongue, formed during the surge, is visible in Figure 28G, showing the elevation change ten years after the surge

had stopped. Interestingly, the part where the surface increased before the surge has now also lost surface height, and only the glacier part in the west below the slopes of the Cerro Nevado del Plomo seems to have accumulated ice during this time. The same pattern is also visible in the study of Ferri et al. (2020), in which, based on the DEM-differencing results, a mass balance rate of -0.97 ± 0.16 m w.e. yr^{-1} was calculated for the Nevado del Plomo glacier during the period 2009-2018. The expansion of the ablation area compared to the pre-surge conditions is explainable since the mass balance rate of the years 2000-2009 was close to zero, and only afterwards became more negative as mentioned before.

7.2.3 Climatic Conditions Before the Surge Events

The build-up phase of a surging glacier is characterised by accumulation in the reservoir area. This would suggest that in the phase before a surge occurs, the climate should be favourable to accumulation with much precipitation in the form of snow.

To analyze the precipitation conditions of the last century in the Mendoza basin, the time series of Prieto et al. (2001) is used, which shows the annual amount of days with snowfall according to the documented snow days in the newspaper "Diario Los Andes". The snow conditions of four places in the upper Mendoza valley were reported daily by the Trans-Andean Railways Company to the newspaper (Gallego et al., 2008). Figure 39 shows the collected data of Prieto et al. (2001) as well as the active phases of the Nevado del Plomo glacier and the years of strong, warm El Niño-Southern Oscillation (ENSO) events since 1950, according to the Oceanic Niño Index (NOAA). The El Niño events are included since it is known that during the El Niño events above average snowfall anomalies can be observed in the Central Andes of Argentina and Chile (Masiokas et al., 2006; Rivera et al., 2017).

The most striking increase of precipitation before the surge of the Nevado del Plomo glacier is visible for the surge in 1984-1985 (Figure 39). In the two previous years to the surge a strong El Niño phase had been recorded and the amount of snow days is a lot higher than the average with 60 and 57 snow days. During the last eight years before the event, days with snowfall have steadily increased on average. A similar increase in snow days is evident between 1965 and 1972, a period

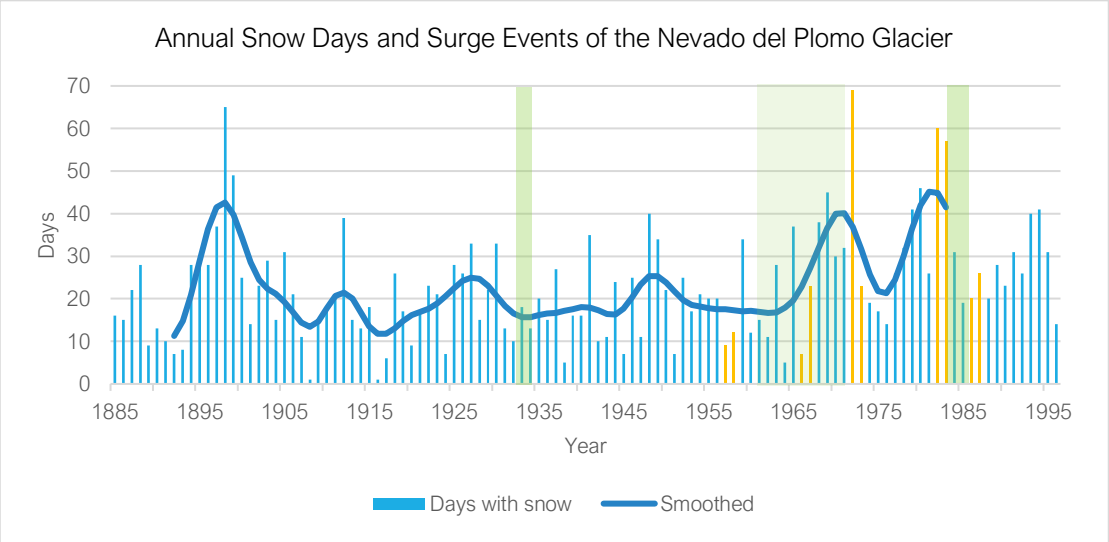

Figure 39: Adjusted timeline of Prieto et al. (2001) showing the annual frequency of snow days of the Mendoza basin. The surging phases of the Nevado del Plomo glacier are depicted with the green rectangle (potential surge between 1963-1973 in light green) and the strong El Niño years are marked in yellow.

in which the Nevado del Plomo glacier advanced as well. Prior to the 1933 surge event, a slight increase in the snow day frequency is apparent, yet the amount of snow days is comparatively low to the build-up phases of the other two events. The amount of annual snow days supports the assumption that the glacier extent could not have drastically decreased since the mapping of Helbling in 1912 as only two years (1916 and 1917) show less than 10 snow days. According to Pitte et al. (2016), the time between 1977 and 1987 was the wettest period in the Central Andes of Argentina since the recording of temperature and precipitation data. This is also noticeable in the frequency of the snow days which started to increase again in 1977 after some years of less than 20 annual snow days.

To continue the timeline with precipitation data, the snow cover area data for the Mendoza basin are shown in Figure 40 covering the years 2001-2021. The base data originates from the MODIS Terra and Aqua satellites and is processed and displayed on the website observatorioandino.com by the *Instituto Argentino de Nivología, Glaciología y Ciencias Ambientales* (IANIGLA-CONICET and CR[2].).

Figure 40 shows that every year between 2000-2009, except the year 2004, shows an above average snow coverage (Figure 40). During this time, the most recent surge of the Nevado del Plomo glacier happened (2006-2007). The impact of the dry conditions in the Central Andes since 2010 is also apparent as the area covered with snow was generally below average since the year 2010. 2015 and 2016 were the only two years with an above-average snow cover in the last decade and coincide with El Niño years.

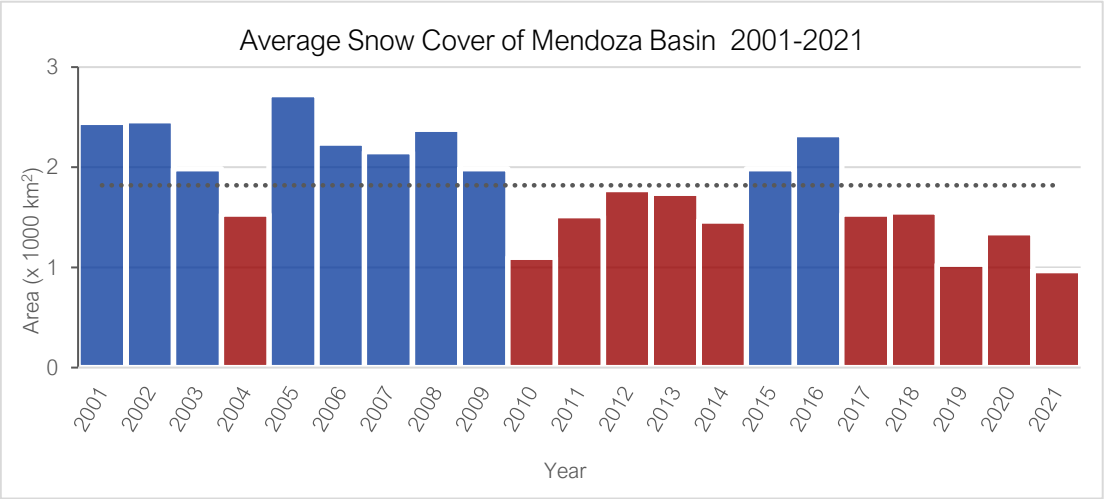

Figure 40: Adjusted figure showing the average snow cover area of the Mendoza basin between 2001 and 2021. The blue columns represent an above-average snow cover area while the below-average snow cover area years are depicted in red. The figure was downloaded from observatorioandino.com but the layout was adapted to match the other figures.

It is important to mention that this analysis of climate data is very superficial and was carried out without the determination of statistical values. The relationship between El Niño years and surge periods needs to be analyzed in more detail, but the increase in precipitation is clearly visible during the El Niño years 1986/1987 and 2015/2016. Moreover, it can be stated that the available precipitation data of the years before the surge events do not show a decrease over a longer period, but rather tend to be above average. This assumption is also shared by Pitte et al. (2016), who additionally observed below average temperatures in the periods before the surges of the Nevado del Plomo glacier and the Horcones Inferior glacier.

7.3 Potential Future Damming of the Plomo Valley due to a Surge

Even though the last surge of the Nevado del Plomo glacier in 2006-2007 did not cause any remarkable damage, the question of how the glacier will develop in the future and what has to be expected in case of a future surge remains. Falaschi et al. (2018) hypothesize a surge cycle of 20 to 30 years, in which the previous surge cycles fit, provided that the advance between 1963-1973 is considered. This means the next surge event of the Nevado del Plomo glacier can be expected between 2026-2036. Looking at the ice thickness distribution, it is evident that in the year 2020, the glacier's extent and ice thickness have been reduced compared to the pre-surge conditions of the year 2006, which suggests a smaller extent of a future surge.

The experiment with the glacier flow model, using the same surge forcing settings for the glacier extent in 2020 as for the reconstructed surge of 2006-2007, shows that the advance of the glacier front is shorter compared to the surge in 2007 and the ice masses do not spread in the Plomo valley (Figure 30 and 33). The glacier front does not reach the Río del Plomo, but the advance is still far enough to reach the main Plomo valley after two years of surging. The distance to the Río del Plomo is approximately 350 m. Since the initial geometry of the experiment was even a bit too big as it was in reality in the year 2020 and as it is in 2022, a surge at the moment would not lead to a damming of the Río del Plomo. Nevertheless, it is still impressive how far the glacier has advanced, even with the smaller glacier volume plus it cannot be conclusively said that the glacier will no longer reach the Río del Plomo. It depends on the future climatic developments which affect the mass balance of the glacier. A similar conclusion was drawn in the risk analysis of Correas-Gonzalez et al. (2020), surveying the Plomo and Mendoza valleys. According to them, the potential for a GLOF event caused by the Nevado del Plomo glacier tends to decrease since, due to the widespread glacier retreat in the Central Andes of Argentina, the elevation of the glacier front and the distance to the Río del Plomo increase. However, it is emphasized that the level of risk is mainly associated with land use in the valleys. The rise in tourism activities and the change in land use increase the vulnerability of the area close to the rivers.

Besides the damming of the Río del Plomo by a surge of the Nevado del Plomo glacier, its neighboring glacier, Glaciar Grande del Juncal must be examined and monitored as well, since the Río del Plomo flows along the glacier forefield of the Juncal Glacier. Moreover, landslides coming from the steep slopes need also to be considered in terms of a potential damming of the Río del Plomo.

Apart from the surge extent, the modelling experiments have also shown that a surge could be initiated by an increase in the ice softness, which should simulate the increase in the basal sliding of the glacier. To reach the surge extent of 2007, the ice softness was increased 200 times for two years below 4300 m a.s.l. This indicates that for the modelling of surges, very strong forcings must be applied. The second experiment, in which a climate-forcing was applied, showed that no surge could be triggered even by lowering the ELA by 800 m for three years. This is because the reaction time of the glacier is too slow. Therefore, a surge initiation due to a climate fluctuation is very unlikely.

7.4 Plomo Valley Glaciers

7.4.1 Volume and Surface Elevation Transformation of the Glaciers Since 2000

The DEM-differencing results and the overall GlabTop model results of the glaciers in the Plomo valley reflect the general ice mass loss of the last 10 years in the Central Andes of Argentina as reported by Dussaillant et al. (2019) and Ferri et al. (2020).

The results of the DEM-differencing are generally consistent with the results and figures of Ferri et al. (2020), who used the identical ASTER DEMs but calculated the elevation changes using a time series of multiple ASTER DEMs. Nevertheless, the pattern of increase and decrease of the surface elevation between the years 2007-2017 (2009-2018 in Ferri et al. (2020)) is very similar. In Figure 29A the ice transfer during the surge period of the Nevado del Plomo glacier is well visible as discussed in chapter 7.2.2. A similar but slightly extenuated pattern of surface lowering in the upper part of the glacier and a raise of the surface at the lower part of the glacier is also visible for the Grande del Juncal glacier. According to Falaschi et al. (2018), the initiation of the surging phase happened for both glaciers approximately at the same time in 2006, but the surging phase of the Grande del Juncal lasted until 2011. The longer duration of the active phase, combined with a shorter advance and an elevation change indicates that the Glacier Grande del Juncal has a slower flow velocity during the surging phase than the Nevado del Plomo glacier. While the two surging glaciers show this unusual reverse elevation change pattern, the other glaciers in the Plomo valley do not show any significant surface lowering or increase during this short period between February 2006 to November 2007. This is also consistent with the mass balance calculations of Ferri et al. (2020), who calculated a slight positive mass balance rate of 0.10 ± 0.22 m w.e. yr^{-1} for the glaciers of the Mendoza basin for the years 2000-2009. However, for the period 2009-2018 this changed to a negative value of -0.17 ± 0.20 m w.e. yr^{-1}. The negative mass balance coincides with the prevailing dry conditions and less snowfall in the Central Andes since the year 2010. Thus, most glaciers in the Plomo valley show a lowering of the surface elevation on the lower part of the glacier between the years 2007-2017 (Figure 29B). At the front of the Grande del Juncal glacier, an increase in the surface elevation is apparent which is explainable by the surging activity of the glacier until the year 2011. The increase of the ice surface was most probably not yet compensated by the ablation until the year 2017, the reason why the elevation change is still positive. Apart from the Grande del Juncal glacier, the Innominado glacier in the south of the Nevado del Plomo glacier also shows a converse pattern with a slight increase of the surface in the lowest part of the glacier. The reason for this could be the extended debris coverage, especially on the lower glacier tongue visible on satellite images of this glacier. Debris coverage can lead to an insulating effect above a certain thickness and therefore a reduced ablation (Mattson et al., 1993). However, to proof if the debris cover is thick enough to insulate, in situ measurements are necessary.

Contrary to the DEM-differencing results, the ice volume calculations of the GlabTop model show an increase of the ice volume for some glaciers, which are not congruent with the DEM-differencing results and the reported ice mass loss of the glaciers in the Central Andes of Argentina. According to the GlabTop model, the glaciers of the Plomo valley lost 15.88% of the glacier volume and glacierized area between 2010 and 2020. The two largest glaciers in the area, the Bajo del Plomo and the Alto del Plomo experienced a relatively high decrease of their ice volume, while the ice volume of the large glaciers flowing from west to southeast (Grande del Juncal, Oriental del

Juncal and Innominado) increased from 2010 to 2020, except the Nevado del Plomo glacier (Figure 36 and 41). This volume increase is not consistent with the DEM-differencing results and the mass balance calculations of Ferri et al. (2020), according to which all glaciers of the Plomo area had a negative balance in the period 2009-2018. This result is even more conspicuous considering the fact that the area of these glaciers decreased during this period. The reason for this discrepancy is difficult to determine. In the case of the Grande del Juncal glacier, a possible explanation could be that the glacier was still surging until 2011 and the GlabTop model is not made for surging glaciers. The ice-volume increase of the Oriental del Juncal and Innominado glacier are highly questionable too. As mentioned before, the Innominado glacier is covered by debris to a large extent. However, according to satellite images no significant gain of the debris or general obvious change of the glacier surface and extent is apparent. The reason for the overestimation of the ice thickness can therefore only be caused by the input ASTER DEM and the GlabTop model itself. Certain deviations were to be expected due to the 30 m resolution of the DEM and some small voids in the DEM, but not to this extent.

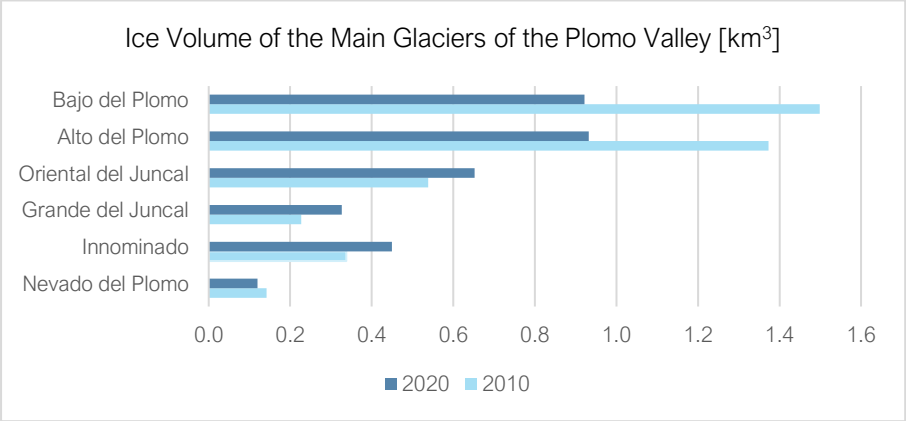

Figure 41: Corresponding Figure to the Table 6 showing the ice volume change of the glaciers in between the years 2010 to 2020.

7.4.2 Potential Future Lakes in the Plomo Valley

The analysis of the potential future lakes of the Plomo valley glaciers shows that the area and volume of the potential lakes decreased drastically from 2010 to 2020. However, the lakes at the glacier front of the Bajo del Plomo, Alto del Plomo and Oriental del Juncal glaciers remained. These lakes and the potential lake at the glacier front of the Innominado glacier are the first lakes that could be filled with meltwater when the retreating behaviour of the glaciers continues. The total sum of the volume of these lakes is negligible compared to the estimated lake volumes of the past lakes caused by the Nevado del Plomo surges. Moreover, it must be mentioned that the volume calculation of the GlabTop model assumes that the overdeepening is filled all the way to the top with water, so the volume of the lakes is even overestimated. Since most glacier tongues are partly covered with debris, apart from the Bajo del Plomo glacier, it can also be assumed that the overdeepenings will be filled with debris as soon as the ice melts and no lake will develop.

According to the GlabTop model, there are no extensive overdeepenings evident in the upper parts of the glaciers. This is particularly surprising in the case of the Nevado del Plomo glacier, where the ice thickness modelling results displayed a punctual maximum of the ice thickness in the middle of the glacier. However, no lake is modelled in this area.

Although the glacier retreat due to climate warming has exposed more glacial lakes globally, the formation of new glacial lakes in the Central Andes of Argentina and Chile is declining (Emmer and Vilímek, 2013; Wilson et al., 2018).The reason for this is the retreat of the glacier fronts to higher elevations and consequently in steeper areas, where the formation of a big, threatening lake is limited (Wilson et al., 2018).

In summary, small glacial lakes may evolve in the Plomo Valley in the future, but the water volume stored in these lakes is not comparable to the lake volume of the GLOF event in 1934. Consequently, the biggest hazard related to a flood event in the Plomo valley remains the damming of the Río del Plomo by an unexpected glacier advance or landslide. A similar conclusion was reached by Wilson et al. (2018). They stated that the potential hazard caused by a future GLOF is low for the lowlands of the Central Andes because the glacial lakes are generally small, and the growth in size is limited.

8 Conclusion and Outlook

8.1 Conclusion

The main goal of this thesis was to investigate the historical surges of the Nevado del Plomo with the focus on the surge events of 1933 and 2006-2007. Using the obtained results, it was the aim to assess the present glacier condition in consideration of a future surge event. Apart from the collocation of the characteristics of the past surge events, three methods were applied. The DEM-differencing of the ASTER DEMs enabled to see the elevation changes of the glacier during the surge of 2006-2007. By the use of the GlabTop model, the ice thickness distribution, potential future lakes and the ice volumes of the glaciers in the Plomo valley were explored. As a third method, the glacier flow model was applied to model a possible future surge extent. The following part summarises the results of the research questions.

1. Which are the glaciological and environmental conditions before and after the past surge events in the Plomo valley?

a) What is the ice volume of the Nevado del Plomo glacier in its quiescent phase?

According to the investigated years, the biggest ice volume of the Nevado del Plomo glacier was measured in 1912 with 0.2693 km^3, according to the digitized historical map. This volume decreased within 88 years by 42% to 0.1550 km^3. Six years later, just before the most recent surge started in 2006, the ice volume was 0.1520 km^2. Even though the volume decreased drastically since 1912, it was still sufficient that the glacier front reached the Río del Plomo during the surging phase in 2006-2007. The dry conditions over the last 10 years have led to another sharp decline in glacier volume, with a volume of 0.091 km^3 calculated for the year 2020.

b) How much ice volume is moved around by a surge?

During the last surge of the Nevado del Plomo glacier in 2006-2007 an ice volume of approximately 54 x 10^6 m^3 moved from the upper glacier part in the west down to the Plomo valley in the east. Compared to the ice volume of the glacier shortly before the surge had started, 36% of the glacier ice was shifted. The ice volume of the surge of 1984-1985 is not known but for the surge in 1933 a moving ice mass of 35-60 x 10^6 m^3 was estimated according to reports of this time.

c) What were the climatic conditions before the surge events? Can we deduce some characteristics for glacier surging in general?

Generally, for the years prior to the surge initiation a slight increase of precipitation in the Mendoza basin is observable and no sustained periods with less precipitation compared to the previous and subsequent years. During the El Niño events, the precipitation usually increases to above-average values, which is especially visible before the surge in 1984-1985. The first decade of the 21st century was characterized by mass balance rates close to zero for the glaciers in the Central Andes but changed to more negative values due to the prevailing megadrought since 2010.

The reason for the surge initiation is still unclear, however, the experiments of the glacier flow model showed that a surge could not be initiated due to a climate forcing because the glacier reacts too slowly to the change of the mass balance. Nonetheless, alterations in the glacier rheology such as the ice softness could successfully initiate a surge.

2. **Can these results give insight to expect a future damming of the Plomo valley related to a surge of the Nevado del Plomo glacier?**

According to the glacier extent of the year 2020, it can be assumed that a current surge would not lead to the damming of the Río del Plomo, since the modelling experiments have shown that the glacier advance would not be far enough to reach the Río del Plomo. However, the glacier front would still reach the Plomo valley. The input geometry of the Nevado del Plomo glacier was slightly overestimated. In the future, according to climate projections, the glacier will most likely continue to lose mass, which is why a smaller advance length than modelled can be assumed.

Nevertheless, it cannot be conclusively said that no further damming of the Río del Plomo is to be expected. The experiment was carried out with a simplified model and the glaciers are constantly changing due to the climate. Moreover, knowledge about the exact mechanism and processes during a surge are still lacking, which makes it impossible to predict if a surge occurs again and when. Regarding the damming of the Río del Plomo, it is important to mention that a damming of the Río del Plomo due to landslides must as well be considered for the risk assessment.

8.2 Outlook

In this thesis, several new findings about the glaciological conditions of the Nevado del Plomo glacier in the past are presented. However, to assess the possibility of a future surge and GLOF event in more detail in the Plomo valley, additional knowledge about the general surge mechanism is needed and further investigations of surging glaciers are required. Very little is known about the second surging glacier in the Plomo valley, the Grande del Juncal glacier, which according to its glacier volume, would also have the potential to advance down to the Río del Plomo. Correas-Gonzalez et al. (2020) already analyzed the ice-dammed lake outburst flood risk in the Plomo basin, but the potential damming of the Río del Plomo due to landslides was not yet considered.

Since the glaciers of the Plomo valley are essential for the water supply of the lowlands during the dry summer season, monitoring the glaciers is even more crucial in times of global warming. Therefore, weather stations as well as mass balance measurements of the glaciers in the Plomo Valley would undoubtedly be helpful to analyze the development of the remaining ice masses and to study the impacts of the climate on surging glaciers. Moreover, it would allow to research the impacts of El Niño events on the cycle length of surging glaciers.

9 Acknowledgement

I would like to express many thanks to my two supervisors Dr. Samuel Nussbaumer and Dr. Holger Frey for introducing me to the impressive world of the Central Andes and sharing their experience with valuable suggestions. It was a pleasure for me to get supported by you.

I would also like to express my gratitude to Prof. Dr. Andreas Vieli for preparing the glacier flow model with annotations for me and taking his time to explain the model and helping when problems arose.

Furthermore, I would like to thank Dr. Andreas Linsbauer for giving me the possibility to work with the GlabTop model, the explanations, advice, and the final conduction of the GlabTop runs with my input data while it did not work on my laptop.

Thank you, Dr. Inés Dussaillant, for giving me the ASTER DEM tiles and the very helpful and kind advice.

Many thanks to Dr. Etienne Berthier for providing the Pléiades DEMs, which enabled the modelling of the ice volumes for the year 2022.

Many thanks to all those who gave me helpful tips throughout the master thesis and who shared their knowledge about the Nevado del Plomo glacier and its environment with me.

Finally, I would like to thank my family and Jan for always supporting and believing in me and especially my sister Désiré for proofreading the thesis.

10 References

Alean, J. (1987). Surge-Gletscher. *Die Alpen* 63, 30–41.

Barcaza, G., Nussbaumer, S. U., Tapia, G., Valdés, J., García, J. L., Videla, Y., et al. (2017). Glacier inventory and recent glacier variations in the Andes of Chile, South America. *Ann. Glaciol.* 58, 166–180. doi: 10.1017/aog.2017.28.

Barria, I., Carrasco, J., Casassa, G., and Barria, P. (2019). Simulation of Long-Term Changes of the Equilibrium Line Altitude in the Central Chilean Andes Mountains Derived From Atmospheric Variables During the 1958–2018 Period. *Front. Environ. Sci.* 7. doi: 10.3389/fenvs.2019.00161.

Benn, D. I. (2021). Surging glaciers in Scotland. *Scottish Geogr. J.* 137, 1–40. doi: 10.1080/14702541.2021.1922738.

Benn, D. I., and Evans, D. J. A. (2010). *Glaciers & Glaciation*. 2nd ed. London: Hodder Eduaction.

Benn, D. I., Fowler, A. C., Hewitt, I., and Sevestre, H. (2019). A general theory of glacier surges. *J. Glaciol.* 65, 701–716. doi: 10.1017/jog.2019.62.

Björnsson, H., Pálsson, F., and Sigurðsson, O. (2003). Surges of glaciers in Iceland. *Ann. Glaciol.* 36, 82–90.

Boisier, J. P., Alvarez-garreton, C., Cordero, R. R., Damiani, A., Gallardo, L., Garreaud, R. D., et al. (2018). Anthropogenic drying in central-southern Chile evidenced by long-term observations and climate model simulations. *Elem. Sci. Anthr.* 6.

Braun, M. H., Malz, P., Sommer, C., Farías-Barahona, D., Sauter, T., Casassa, G., et al. (2019). Constraining glacier elevation and mass changes in South America. *Nat. Clim. Chang.* 9, 130–136. doi: 10.1038/s41558-018-0375-7.

Brown, V. H., Evans, D. J. A., Vieli, A., and Evans, I. S. (2013). The Younger Dryas in the English Lake District: Reconciling geomorphological evidence with numerical model outputs. *Boreas* 42, 1022–1042. doi: 10.1111/bor.12020.

Bruce, R. H., Cabrera, G. A., Leiva, J. C., and Lenzano, L. E. (1986). The 1985 surge and ice dam of Glaciar Grande del Nevado del Plomo, Argentina. *J. Glaciol.*, 131–132.

Carvallo y Goyeneche, V. (1889). Descripción histórico-geográfica del Reino del Chile, 2da. parte. *Col. Hist. Chile*.

Clague, J. J., and Evans, S. G. (2000). A review of catastrophic drainage of moraine-dammed lakes in British Columbia. *Quat. Sci. Rev.* 19, 1763–1783. doi: 10.1016/S0277-3791(00)00090-1.

Clarke, G. K. C. (1987). Fast glacier flow: ice streams, surging, and tidewater glaciers. *J. Geophys. Res.* 92, 8835–8841. doi: 10.1029/JB092iB09p08835.

Correas-Gonzalez, M., Moreira, S. M., Jomelli, V., and Arnaud-Fassetta, G. (2020). Ice-dammed lake outburst flood risk in the Plomo basin, Central Andes (33° S): Perspectives from historical events. *Cuad. Investig. Geográfica* 46, 223–249.

Cuffey, K., and Paterson, W. S. B. (2010). *The Physics of Glaciers*. Butterworth-Heinemann/Elsevier.

Darwin, C. (1916). *The voyage of the Beagle*. New York: J. M. Sons & Co., London; E. P. Dutton & Co.

De Geer, G. (1910). Guide de l'excursion au Spitzberg. *Stock. XIe Congrès Géologique Int.*

Del Rosario Prieto, M. (1986). The glacier dam on the Rio Plomo: a cyclic phenomenon? *Zeitschrift für Gletscherkd. und Glazialgeol.* 22, 73–78.

Diario Los Andes (1934). Proporciones de catástrofe adquirió el aluvión. 1.

Dunse, T., Schellenberger, T., Hagen, J. O., Kääb, A., Schuler, T. V., and Reijmer, C. H. (2015). Glacier-surge mechanisms promoted by a hydro-thermodynamic feedback to summer melt. *Cryosphere* 9, 197–215. doi: 10.5194/tc-9-197-2015.

Dussaillant, I., Berthier, E., Brun, F., Masiokas, M., Hugonnet, R., Favier, V., et al. (2019). Two decades of glacier mass loss along the Andes. *Nat. Geosci.* 12, 802–808. doi: 10.1038/s41561-019-0432-5.

Eisen, O., Harrison, W. D., Raymond, C. F., Echelmeyer, K. A., Bender, G. A., and Gorda, J. L. D. (2005). Variegated Glacier, Alaska, USA: A century of surges. *J. Glaciol.* 51, 399–406. doi: 10.3189/172756505781829250.

Emmer, A., Harrison, S., Mergili, M., Allen, S., Frey, H., and Huggel, C. (2020). 70 years of lake evolution and glacial lake outburst floods in the Cordillera Blanca (Peru) and implications for the future. *Geomorphology* 365, 107178. doi: 10.1016/j.geomorph.2020.107178.

Emmer, A., and Vilímek, V. (2013). Review article: Lake and breach hazard assessment for moraine-dammed lakes: An example from the Cordillera Blanca. *Nat. Hazards Earth Syst. Sci.* 13, 1551–1565. doi: 10.5194/nhess-13-1551-2013.

Espizúa, L. E. (1986). Fluctuations of the Rio del Plomo Glaciers. *Geogr. Ann. Ser. A Phys. Geogr.* 68, 317–327.

Espizúa, L. E., and Bengochea, J. D. (1990). Surge of Grande del Nevado Glacier (Mendoza , Argentina) in 1984 : Its Evolution through Satellite Images. *Geogr. Ann. Ser. A, Phys. Geogr.* 72, 255–259.

Esri World Imagery Wayback of 2020-04-01, 2018-02-23, 2014-02-20. Available at: https://livingatlas.arcgis.com/wayback/#active=47471&ext=-69.85037,-32.96639,-69.61553,-32.78589.

Falaschi, D., Bolch, T., Lenzano, M. G., Tadono, T., Lo Vecchio, A., and Lenzano, L. (2018). New evidence of glacier surges in the Central Andes of Argentina and Chile. *Prog. Phys. Geogr.* 42, 792–825. doi: 10.1177/0309133318803014.

Farr, T. G., Rosen, P. A., Caro, E., Crippen, R., Duren, R., Hensley, S., et al. (2007). The Shuttle Radar Topography Mission. *Rev. Geophyisics* 45. doi: 10.1029/2005RG000183.

Fellmann, H., and Studer, B. (2020). Transandino. Erinnerungen an die kühnste amerikanische Zahnradbahn. *Eisenbahn-Kurier* 6, 68–73.

Ferri Hidalgo, L., Espizúa, L. E., and Pitte, P. (2012). 'Grande del Nevado del Plomo (AR3304)', in *Fluctuations of Glaciers 2005-2010 (Vol. X)*, eds. M. Zemp, H. Frey, I. Gärtner-Roer, S. U. Nussbaumer, M. Hoelzle, F. Paul, et al. (Zurich: World Glacier Monitoring Service (WGMS)), 49–50. doi: d10.5904/wgms- fog-2012-11.

Ferri, L., Dussaillant, I., Zalazar, L., Masiokas, M. H., Ruiz, L., Pitte, P., et al. (2020). Ice Mass Loss in the Central Andes of Argentina Between 2000 and 2018 Derived From a New Glacier Inventory and Satellite Stereo-Imagery. *Front. Earth Sci.* 8, 1–16. doi: 10.3389/feart.2020.530997.

Flores-Aqueveque, V., Rojas, M., Aguirre, C., Arias, P. A., and González, C. (2020). South Pacific Subtropical High from the late Holocene to the end of the 21st century : insights from climate proxies and general circulation models. *Clim. Past* 16, 79–99. doi: 10.5194/cp-16-79-2020.

Frey, H., Haeberli, W., Linsbauer, A., Huggel, C., and Paul, F. (2010). A multi-level strategy for anticipating future glacier lake formation and associated hazard potentials. *Nat. Hazards Earth Syst. Sci.* 10, 339–352. doi: 10.5194/nhess-10-339-2010.

Gallego, D., García-Herrera, R., Prieto, R., and Peña-Ortiz, C. (2008). On the quality of climate proxies derived from newspaper reports - A case study. *Clim. Past* 4, 11–18. doi: 10.5194/cp-4-11-2008.

Garreaud, R. D. (2009). The Andes climate and weather. *Adv. Geosci.* 22, 3–11. doi: 10.5194/adgeo-22-3-2009.

Garreaud, R. D., Boisier, J. P., Rondanelli, R., Montecinos, A., and Veloso-aguila, H. H. S. D. (2019). The Central Chile Mega Drought (2010-2018): A climate dynamics perspective. *Int. J. Climatol.* 40, 421–439. doi: 10.1002/joc.6219.

Grohmann, C. H. (2018). Evaluation of TanDEM-X DEMs on selected Brazilian sites: Comparison with SRTM, ASTER GDEM and ALOS AW3D30. *Remote Sens. Environ.* 212, 121–133. doi: 10.1016/j.rse.2018.04.043.

Haeberli, W. (1983). Frequency and Characteristics of Glacier Floods in the Swiss Alps. *Ann. Glaciol.* 4, 85–90.

Haeberli, W., and Hoelzle, M. (1995). Application of inventory data for estimating characteristics of and regional climate-change effects on mountain glaciers: A pilot study with the European Alps. *Ann.*

Glaciol. 21, 206–212.

Haenke, T. (1943). Viaje por el Virreinato del Río Plomi ice-dam. *Geogr. J.* 8, 41–49.

Happoldt, H., and Schrott, L. (1993). 'Horcones Inferior—Glacier surge', in *Fluctuations of Glaciers 1985-1990* (Zurich, Switzerland: IAHS (ICSI)/UNEP/ UNESCO), 70.

Harrison, S., Kargel, J. S., Huggel, C., Reynolds, J., Shugar, D. H., Betts, R. A., et al. (2018). Climate change and the global pattern of moraine-dammed glacial lake outburst floods. *Cryosphere* 12, 1195–1209. doi: 10.5194/tc-12-1195-2018.

Harrison, W. D., Osipova, G. B., Nosenko, G. A., Espizua, L., Kääb, A., Fischer, L., et al. (2015). 'Glacier Surges', in *Snow and Ice-Related Hazards, Risks, and Disasters* (Elsevier Inc.), 437–485. doi: 10.1016/B978-0-12-394849-6.00013-5.

Helbling, D. R. (1919). 'Beiträge zur Topographischen Erschliessung der Cordilleras de los Andes zwischen Aconcagua und Tupungato', in *Jahresbericht des Akademischen Alpenclub Zürich 1918* (Buchdruckerei Jacques Bollmann), 5–36.

Helbling, R. (1935). The Origin of the Rio Plomo Ice-Dam. *Geogr. J.* 85, 41–49.

Helbling, R. (1940). Ausbruch eines Gletschersees in den Argentinischen Anden und aussergewöhnliche Gletscherschwankungen im Allgemeinen. *Schweizerische Bauzeitung* 115, 121–128.

Herreid, S., and Truffer, M. (2016). Automated detection of unstable glacier flow and a spectrum of speedup behavior in the Alaska Range. *J. Geophys. Res. F Earth Surf.* 121, 64–81. doi: 10.1002/2015JF003502.

Hoinkes, H. C. (1969). Surges ofthe Vernagtferner in the Ötztal Alps since 1599. *Can. J. ofEarth Sci.* 6, 853–860.

How, P., Messerli, A., Mätzler, E., Santoro, M., Wiesmann, A., Caduff, R., et al. (2021). Greenland-wide inventory of ice marginal lakes using a multi-method approach. *Sci. Rep.* 11, 1–13. doi: 10.1038/s41598-021-83509-1.

Huss, M., Bauder, A., Werder, M., Funk, M., and Hock, R. (2009). Glacier-dammed lake outburst events of Gornersee, Switzerland. *Mitteilungen der Versuchsanstalt fur Wasserbau, Hydrol. und Glaziologie an der Eidgenoss. Tech. Hochschule Zurich* 53, 65–84.

Hutter, K. (1983). *Theoretical Glaciology: Material Science oflce and the Mechanics of Glaciers and Ice Sheets*. Tokyo: D. Reidel Publishing Company and Terra Scientific Publishing Company.

IANIGLA-CONICET, and CR^2. Datos provenientes de los sensores MODIS Terra & Aqua, procesados por el Observatorio de Nieve en los Andes de Argentina y Chile. Available at: https://www.observatorioandino.com [Accessed September 10, 2022].

IANIGLA (2018). 'Inventario Nacional de Glaciares: Informe de la subcuenca del río Tupungato, Cuenca del río Mendoza, Cuenca del río Mendoza', in, ed. IANIGLA-COINCET (Mendoza: Ministerio de Ambiente y Desarrollo Sustentable de la Nación), 60.

Iribarren Anacona, P., Mackintosh, A., and Norton, K. P. (2015). Hazardous processes and events from glacier and permafrost areas: Lessons from the Chilean and Argentinean Andes. *Earth Surf. Process. Landforms* 40, 2–21. doi: 10.1002/esp.3524.

Iturrizaga, L. (2011). 'Glacier Lake Outburst Floods', in *Encyclopedia of Snow, Ice and Glaciers*, eds. R. Armstrong, He. Bishop, W. Haberli, J. Oerlemans, J. F. Shroder, and M. Tranter, 381–399. doi: 10.1007/978-90-481-2642-2.

Jiskoot, H. (2011a). Dynamics of Glaciers. *Encycl. Snow, Ice Glaciers*, 245–256.

Jiskoot, H. (2011b). Glacier Surging. *Encycl. Snow, Ice Glaciers*, 415–427.

Jiskoot, H., Boyle, P., and Murray, T. (1998). The incidence of glacier surging in Svalbard: evidence from multivariate statistics. *Comput. Geosci.* 24, 387–399. doi: 10.1016/S0098-3004(98)00033-8.

Jiskoot, H., and Juhlin, D. T. (2009). Surge of a small East Greenland glacier, 2001–2007, suggests Svalbard-type surge mechanism. *Jounal Glaciol.* 55, 31–52. doi: 10.7135/upo9781843318927.003.

Kamb, B., Raymond, C. F., Harrison, W. D., Engelhardt, H., Echelmeyer, K. A., Humphrey, N., et al. (1985).

Glacier Surge Mechanism: 1982-1983 Surge of Variegated Glacier, Alaska. *Science (80-.).* 227, 469–479. doi: 10.1126/science.227.4686.469.

Kienholz, C., Hock, R., Truffer, M., Bieniek, P., and Lader, R. (2017). Mass balance evolution of black rapids glacier, Alaska, 1980–2100, and its implications for surge recurrence. *Front. Earth Sci.* 5. doi: 10.3389/feart.2017.00056.

King, W. D. V. . (1934). The Mendoza River Flood of 10-11 January 1934-Argentina. *Geogr. J.* 84, 321–326.

King, W. D. V. O. (1935). A Further Report on the Plomo Valley Ice-Dam, Argentina. *R. Geogr. Soc.* 86, 441–444.

Kinnard, C., MacDonell, S., Petlicki, M., Mendoza Martinez, C., Abermann, J., and Urrutia, R. (2018). Mass Balance and Meteorological Conditions at Universidad Glacier, Central Chile. *Andean Hydrol.*, 102–123. doi: 10.1201/9781315155982-5.

Linsbauer, A., Paul, F., and Haeberli, W. (2012). Modeling glacier thickness distribution and bed topography over entire mountain ranges with glabtop: Application of a fast and robust approach. *J. Geophys. Res. Earth Surf.* 117, 1–17. doi: 10.1029/2011JF002313.

Linsbauer, A., Paul, F., Hoelzle, M., Frey, H., and Haeberli, W. (2009). The Swiss Alps without glaciers - A GIS-based Modelling Approach for Reconstruction of glacier beds. *Proc. Geomorphometry 2009*, 243–247. doi: 10.5167/uzh-27834.

Lv, M., Guo, H., Yan, J., Wu, K., Liu, G., Lu, X., et al. (2020). Distinguishing Glaciers between Surging and Advancing by Remote Sensing : A Case Study in the Eastern Karakoram. *Remote Sens.* 12, 1–18. doi: 10.3390/rs12142297.

Maisch, M., and Haeberli, W. (1982). Interpretation geometrischer Parameter von Spätglazialgletschern im Gebiet Mittelbünden, Schweizer Alpen. *Beiträge zur Quartärforsch. der Schweiz*, 111–126.

Masikoas, M. H., Villalbam, R., Luckman, B. H., and Mauget, S. (2010). Intra- to Multidecadal Variations of Snowpack and Streamflow Records in the Andes of Chile and Argentina between 30 8 and 37 8 S. *J. Hydrometeorol.* 11, 822–831. doi: 10.1175/2010JHM1191.1.

Masiokas, M. H., Christie, D. A., Le Quesne, C., Pitte, P., Ruiz, L., Villalba, R., et al. (2016). Reconstructing the annual mass balance of the Echaurren Norte glacier (Central Andes, 33.5° S) using local and regional hydroclimatic data. *Cryosphere* 10, 927–940. doi: 10.5194/tc-10-927-2016.

Masiokas, M. H., Rabatel, A., Rivera, A., Ruiz, L., Pitte, P., Ceballos, J. L., et al. (2020). A Review of the Current State and Recent Changes of the Andean Cryosphere. *Front. Earth Sci.* 8. doi: 10.3389/feart.2020.00099.

Masiokas, M. H., Villalba, R., Luckman, B. H., Le Quesne, C., and Aravena, J. C. (2006). Snowpack variations in the central Andes of Argentina and Chile, 1951-2005: Large-scale atmospheric influences and implications for water resources in the region. *J. Clim.* 19, 6334–6352. doi: 10.1175/JCLI3969.1.

Mattson, L. E., Gardner, J. S., and Young, G. J. (1993). Ablation on Debris Covered Glaciers: An Example from the Rakhiot Glacier, Punjab, Himalaya. *IAHS Publ.*, 289–296.

Meier, M. F., and Post, A. (1969). What are glacier surges? *Can. J. Earth Sci.* 6, 807–817.

Mergili, M., Pudasaini, S. P., Emmer, A., Fischer, J. T., Cochachin, A., and Frey, H. (2020). Reconstruction of the 1941 GLOF process chain at Lake Palcacocha (Cordillera Blanca, Peru). *Hydrol. Earth Syst. Sci.* 24, 93–114. doi: 10.5194/hess-24-93-2020.

Minchew, B. M., and Meyer, C. R. (2020). Dilation of subglacial sediment governs incipient surge motion in glaciers with deformable beds. *Proc. R. Soc. A Math. Phys. Eng. Sci.* 476. doi: 10.1098/rspa.2020.0033rspa20200033.

Moreiras, S. M. (2005). Climatic effect of ENSO associated with landslide occurrence in the Central Andes, Mendoza Province, Argentina. *Landslides* 2, 53–59. doi: 10.1007/s10346-005-0046-4.

Murray, T., and Drewry, D. (1998). Geometric evolution and ice dynamics during a surge of Bakaninbreen, Svalbard. *J. Glaciol.* 44, 263–272. doi: 10.1017/S0022143000002604.

Murray, T., Strozzi, T., Luckman, A., Jiskoot, H., and Christakos, P. (2003). Is there a single surge

mechanism? Contrasts in dynamics between glacier surges in Svalbard and other regions. *J. Geophys. Res. Solid Earth* 108, 1–15. doi: 10.1029/2002jb001906.

NOAA Historical El Niño/La Niña Episodes (1950–Present). Available at: https://origin.cpc.ncep.noaa.gov/products/analysis_monitoring/ensostuff/ONI_v5.php [Accessed September 20, 2022].

Paterson, W. (1994). *The Physics of Glaciers*. Tarrytown, N.Y.

Paul, F., and Linsbauer, A. (2012). Modeling of glacier bed topography from glacier outlines, central branch lines, and a DEM. *Int. J. Geogr. Inf. Sci.* 26, 1173–1190. doi: 10.1080/13658816.2011.627859.

Paul, F., Piermattei, L., Treichler, D., Gilbert, L., Girod, L., Kääb, A., et al. (2022). Three different glacier surges at a spot: what satellites observe and what not. *Cryosph.* 16, 2505–2526. doi: 10.5194/tc-16-2505-2022.

Pitte, P., Berthier, E., Masiokas, M. H., Cabot, V., Ruiz, L., Ferri Hidalgo, L., et al. (2016). Geometric evolution of the Horcones Inferior Glacier (Mount Aconcagua, Central Andes) during the 2002-2006 surge. *J. Geophys. Res. Earth Surf.* 121, 111–127. doi: 10.1002/2015JF003522.

Prieto, M. R., Herrera, R., Castrillejo, T., and Dussel, P. (2001). Variaciones climáticas recientes y disponibilidad hídrica en los Andes Centrales Argentino–Chilenos (1885-1996). El uso de datos periodísticos para la reconstitución del clima. *Meteorológica* 25, 27–43.

Reynolds, J. M. (2006). The role of geophysics in glacial hazard assessment. *First Break* 24, 61–66.

Richardson, S. D., and Reynolds, J. M. (2000a). An overview of glacial hazards in the Himalayas. *Quat. Int.* 65–66, 31–47. doi: 10.1016/S1040-6182(99)00035-X.

Richardson, S. D., and Reynolds, J. M. (2000b). 'Degradation of ice-cored moraine dams: implications for hazard development', in *Debris-Covered Glaciers*, 187–197.

Rivera, J. A., Otta, S., Lauro, C., and Zazulie, N. (2021). A Decade of Hydrological Drought in Central-Western Argentina. *Front. Water* 3. doi: 10.3389/frwa.2021.640544.

Rivera, J. A., Penalba, O. C., Villalba, R., and Araneo, D. C. (2017). Spatio-Temporal Patterns of the 2010 – 2015 Extreme Hydrological Drought across the Central Andes , Argentina. *Water* 9, 1–18. doi: 10.3390/w9090652.

Ruetz, B. (2022). *Robert Helbling. Alpinist, Vermessungspionier, Firmengründer*.

Sagredo, E. A., and Lowell, T. V (2012). Climatology of Andean glaciers : A framework to understand glacier response to climate change. *Glob. Planet. Change* 86–87, 101–109. doi: 10.1016/j.gloplacha.2012.02.010.

Schellenberger, A. (2014). Robert Helbling : Pionier der Stereophotogrammetrie in den argentinischen Anden und in der Schweiz. *Cartogr. Helv. Fachzeitschrift für Kartengeschichte*, 15–26.

Secretaría de Ambiente y Desarrollo Sustentable de la Nación (2019). *Atlas de glaciares de la Argentina*. 1ra edició. , eds. L. G. Silva, M. L. Jover, A. Nahas, L. Ferri Hidalgo, R. Villalba, Z. Laura, et al. Ciudad Autónoma de Buenos Aires.

Sevestre, H., and Benn, D. I. (2015). Climatic and geometric controls on the global distribution of surge-type glaciers: Implications for a unifying model of surging. *J. Glaciol.* 61, 646–662. doi: 10.3189/2015JoG14J136.

Shugar, D. H., Burr, A., Haritashya, U. K., Kargel, J. S., Watson, C. S., Kennedy, M. C., et al. (2020). Rapid worldwide growth of glacial lakes since 1990. *Nat. Clim. Chang.* 10, 939–945. doi: 10.1038/s41558-020-0855-4.

Stuart-Smith, R. F., Roe, G. H., Li, S., and Allen, M. R. (2021). Increased outburst flood hazard from Lake Palcacocha due to human-induced glacier retreat. *Nat. Geosci.* 14, 85–90. doi: 10.1038/s41561-021-00686-4.

Tarr, R. S., and Martin, L. (1914). Alaskan Glacier Studies of the NGS, Prince William Sound and Lower Copper River Regions. Washington, DC. *Geogr. Soc.*, 498.

Thorarinsson, S. (1969). Glacier surges in Iceland with special refer- ence to the surges of Bruárjökull. *Can. J. ofEarth Sci.* 6, 875–882.

Tweed, F. S., and Carrivick, J. L. (2015). Deglaciation and proglacial lakes. *Geol. Today* 31, 96–102. doi: 10.1111/gto.12094.

USGS (2018). Earth Resources Observation and Science (EROS) Center: USGS EROS Archive – Digital Elevation – Shuttle Radar Topography Mission (SRTM), Void Filled, 3 Arc-Second Global. doi: 10.5066/F71835S6.

Vieli, A. (2021). Numerical modelling assessment of glacier surge impact on observed elevation change signals. 14874.

Walder, J. S., and Costa, J. E. (1996). Outburst floods from glacier-dammed lakes: The effect of mode of lake drainage on flood magnitude. *Earth Surf. Process. Landforms* 21, 701–723.

Weidick, A. (1988). Surging glaciers in Greenland - a Status. *Rapp. Grønlands Geol. Undersøgelse* 140, 106–110.

Wessel, B. (2018). TanDEM-X Ground Segment DEM Products Specification Document. Oberpfaffenhofen, Germany.

Westoby, M. J., Glasser, N. F., Brasington, J., Hambrey, M. J., Quincey, D. J., and Reynolds, J. M. (2014). Modelling outburst floods from moraine-dammed glacial lakes. *Earth-Science Rev.* 134, 137–159. doi: 10.1016/j.earscirev.2014.03.009.

Wilson, R., Glasser, N. F., Reynolds, J. M., Harrison, S., Anacona, P. I., Schaefer, M., et al. (2018). Glacial lakes of the Central and Patagonian Andes. *Glob. Planet. Change* 162, 275–291. doi: 10.1016/j.gloplacha.2018.01.004.

Zalazar, L., Ferri, L., Castro, M., Gargantini, H., Gimenez, M., Pitte, P., et al. (2020). Spatial distribution and characteristics of Andean ice masses in Argentina: Results from the first National Glacier Inventory. *J. Glaciol.* 66, 938–949. doi: 10.1017/jog.2020.55.

Zalazar, L., Ferri, L., Castro, M., Gargantini, H., Giménez, M., Pitte, P., et al. (2017). Glaciares de Argentina: Resultados Preliminares del Inventario Nacional de Glaciares. *Rev. Glaciares y Ecosistemas Montaña* 2, 13–22. doi: 10.36580/rgem.i2.13-22.

Zemp, M., Frey, H., Gärtner-Roer, I., Nussbaumer, S. U., Hoelzle, M., Paul, F., et al. (2015). Historically unprecedented global glacier decline in the early 21st century. *J. Glaciol.* 61, 745–762. doi: 10.3189/2015JoG15J017.

Appendix

A. Additional Information to the GlabTop Model Runs 7 and 8

Table 4: Change of the area and ice volume of the glaciers of the Plomo valley without the glaciers situated in the south (only visible in the 2020 output).

Year	Area [km²]	Ice Volume [km³]
2010	82.116	4.56
2020	69.178	3.84
Δ	-12.938	-0.72
%	-15.76%	-15.88%

Table 5: Ice volume [km^3] of the main glaciers of the Plomo valley of the years 2010 and 2020.

Ice Volume [km³]						
Year	Nevado del Plomo	Innominado	Grande del Juncal	Oriental del Juncal	Alto del Plomo	Bajo del Plomo
2010	0.142031	0.337444	0.226931	0.538995	1.372918	1.498149
2020	0.120196	0.449526	0.326154	0.651692	0.932426	0.921126
Δ	-0.021834	0.112083	0.099223	0.112697	-0.440492	-0.577023
%	-15%	33%	44%	21%	-32%	-39%

Table 6: Area [km^2] of the main glaciers of the Plomo valley of the years 2010 and 2020.

Area [km²]						
Year	Nevado del Plomo	Innominado	Grande del Juncal	Oriental del Juncal	Alto del Plomo	Bajo del Plomo
2010	3.750761	3.750761	7.616329	10.236970	16.959171	19.092223
2020	2.915711	2.915711	7.165305	9.015300	14.157000	14.877900
Δ	-0.835051	-0.835051	-0.451025	-1.221670	-2.802171	-4.214323
%	-22%	-22%	-6%	-12%	-17%	-22%

B. Additional Data Retrieved from Pléiades Satellite Image

The last two GlabTop runs (9/10) were executed using the Pléiades image from February 07, 2022, which were kindly provided by Etienne Berthier, LEGOS Toulouse. Apart from the DEM input, the input data (outlines, branchlines) did not change except for the Nevado del Plomo glacier. For the Nevado del Plomo glacier, the shorter oulines and branchlines were used, like in the individual output. First the results of the model run with the 20m resolution Pléiades DEM are presented, followed by the results of the 2m resolution Pléiades DEM.

Pléiades DEM (20 m)

Comparison of the ice thickness distribution resulting of the ASTER DEM and the Pléiades DEM

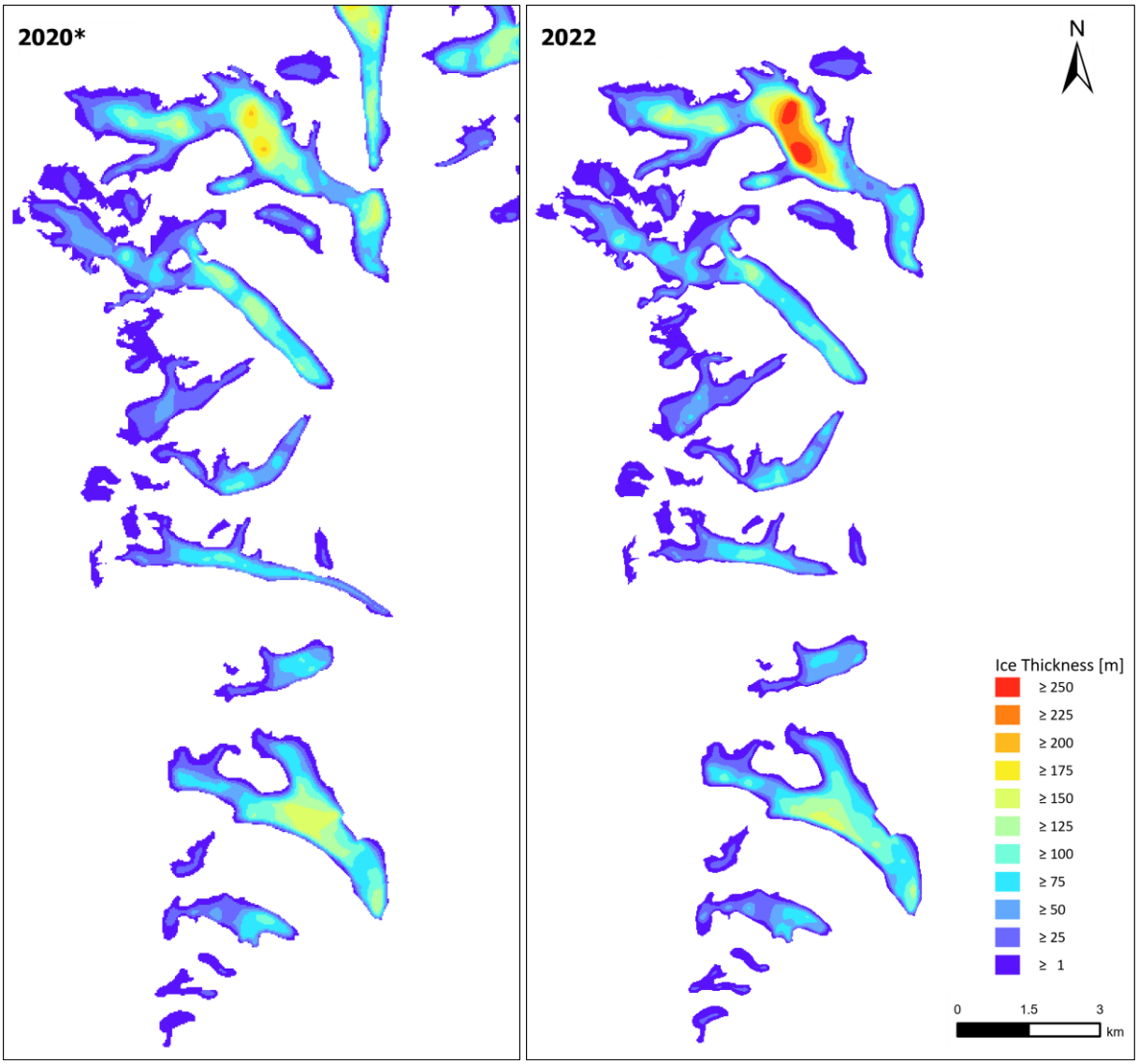

Figure 42: Comparison of the GlabTop results of the runs using the ASTER DEM (30 m) as input (left) and the Pléiades DEM (20 m). The 2022 output shows slightly decreased ice thickness values for all glaciers, except the Oriental Juncal which has, according to the Pléiades DEM a comparatively high ice thickness in the middle of the glacier.

Comparison of the Ice Volume

Table 7: Comparison of the ice volume GlabTop results of the 2020 run using the ASTER DEM (30 m) as input and the 2022_20 run using the Pléiades (20 m) as input. The volume of the Nevado glacier for the year 2020 originates of the individual output (run 6) for which the same outlines were used.

Ice Volume [km³]				
Year	Nevado del Plomo	Innominado	Grande del Juncal	Oriental del Juncal
2020	0.091000	0.449526	0.326154	0.651692
2022_20	0.093278	0.418227	0.314891	0.779665
Δ	0.002278	-0.031299	-0.011263	0.127973
%	3%	-7%	-3%	20%

Potential Future Glacial Lakes according to the 20 m Pléiades DEM

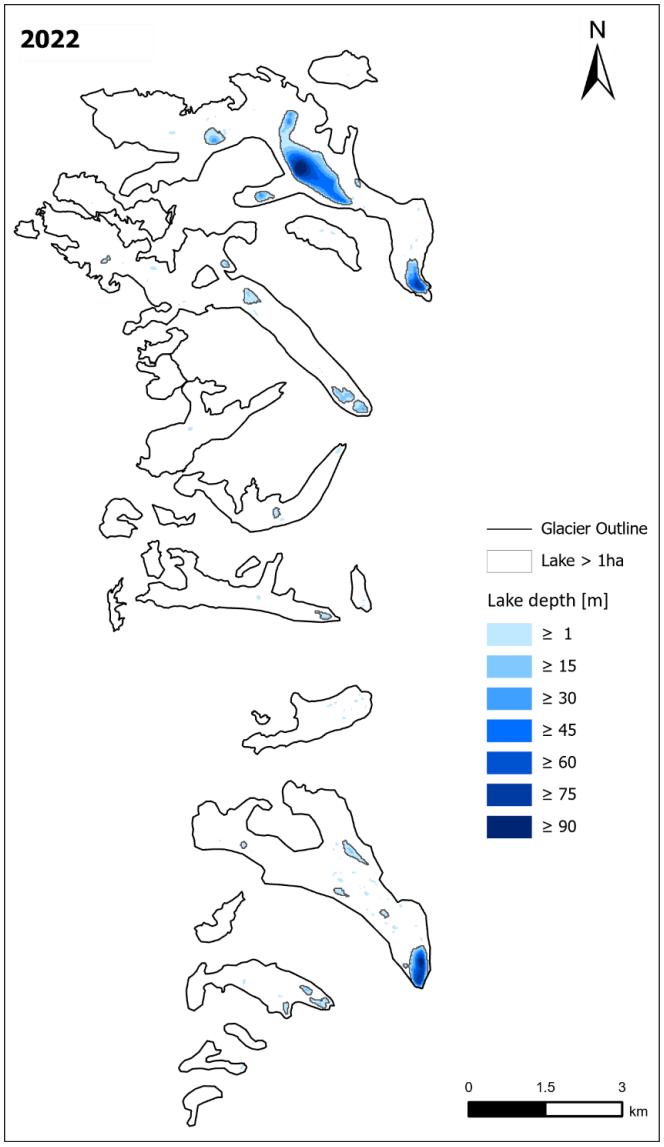

Figure 43: Future potential lakes according to the GlabTop model, using the 20 m Pléiades DEM as input. Showing a big potential lake in the middle of the Oriental del Juncal glacier and one the glacier front. Smaller lakes are modelled below the tongue of the Juncal glacier, the Nevado del Plomo glacier and the Innominado glacier.

Pléiades DEM (2 m)

Comparison of the Ice Thickness Distribution of the 2 m Pléiades and the 20 m Pléiades

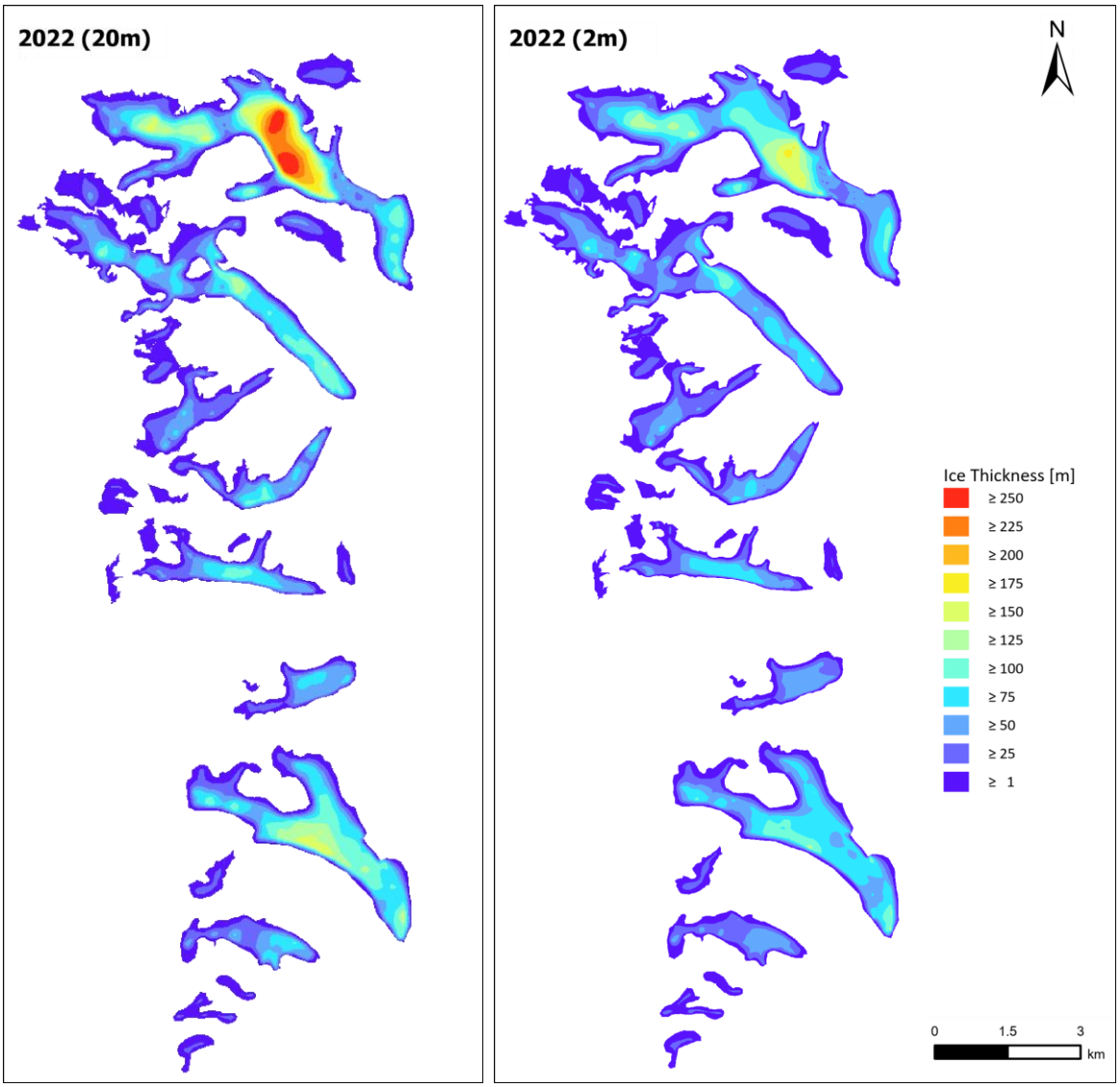

Figure 44: Comparison of the results of the ice thickness distribution of the 20 m resolution DEM (left) and the 2 m resolution DEM (right). The ice thickness values are nearly similar for the Nevado del Plomo glacier but differ strongly for the other glaciers, especially the Oriental Juncal glacier in the north.

Comparison of the ice volume results between the 2 m and 20 m Pléiades DEM

Table 8: Comparison of the ice volumes of the glaciers in the Plomo valley according to the results of the GlabTop run with the 20 m resolution Pléiades DEM and the 2 m resolution Pléiades DEM. It is evident that the ice volume calculations according to the 20 m DEM are smaller than the 20 m DEM.

Ice Volume [km³]				
Year	Nevado del Plomo	Innominado	Grande del Juncal	Oriental del Juncal
2022_20m	0.093278	0.418227	0.314891	0.779665
2022_2m	0.083948	0.334025	0.258358	0.571720
Δ	-0.009330	-0.084202	-0.056533	-0.207945
%	-10%	-20%	-18%	-27%

Potential Future Glacial Lakes according to the 2 m Pléiades DEM

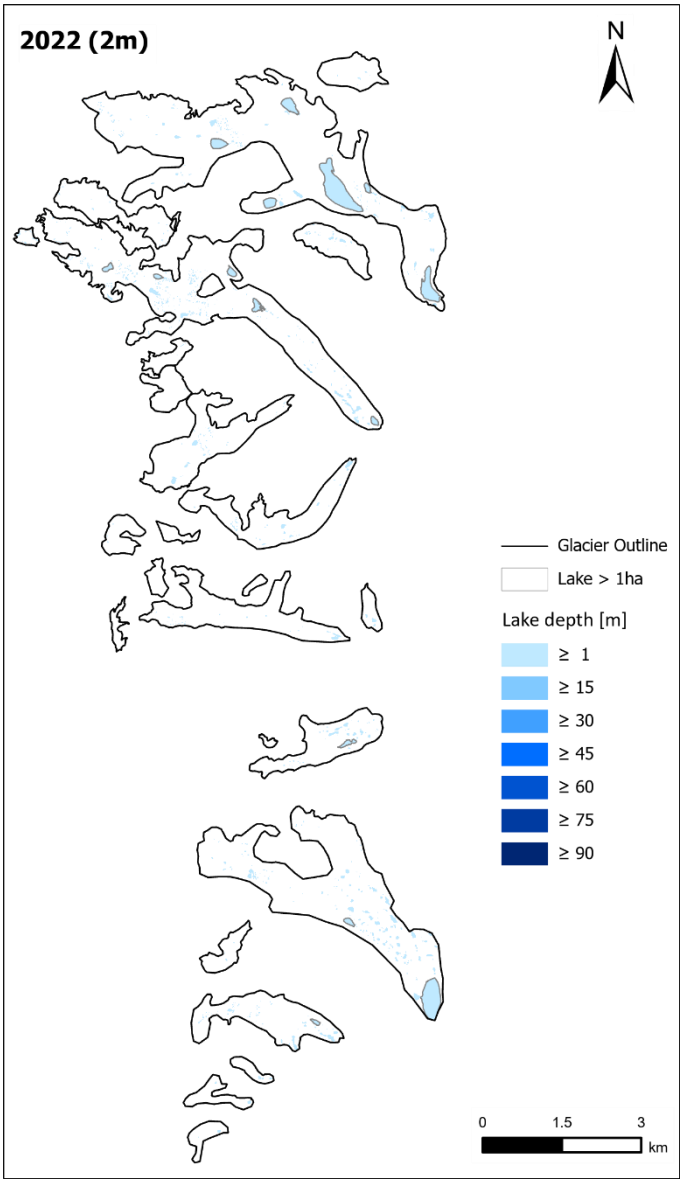

Figure 45: Future potential lakes according to the GlabTop model using the 2 m Pléiades as input. No lakes deeper than 15 m are modelled.

C. Slope of the Environment of the Nevado del Plomo Glacier

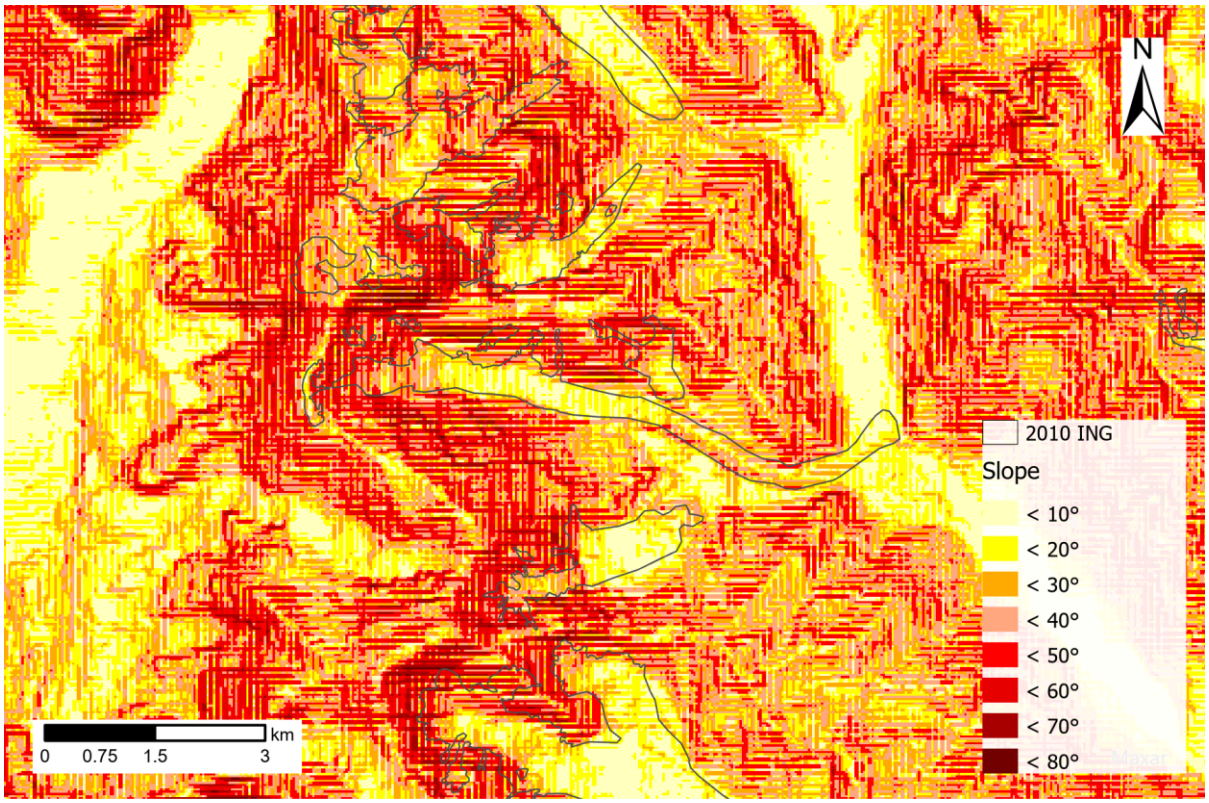

Figure 46: Slope of the Nevado del Plomo glacier area and glacier outlines of the NGI 2010, calculated in ArcGIS Pro using the SRTM 2000 as an input.

Personal Declaration

I hereby declare that the submitted thesis is the result of my own, independent work. All external sources are explicitly acknowledged in the thesis.

Valerie Widmer

Chur, 30.09.2022